NAVAL POSTGRADUATE SCHOOL
Monterey, California

THESIS

MESOSCALE FORCING OF OCEAN WAVES DURING GULF STREAM NORTH WALL EVENTS

by

John A. Okon

March 2003

Thesis Advisor:	Wendell A. Nuss
Second Reader:	David S. Brown

Approved for public release; distribution is unlimited

THIS PAGE INTENTIONALLY LEFT BLANK

REPORT DOCUMENTATION PAGE			*Form Approved OMB No. 0704-0188*

Public reporting burden for this collection of information is estimated to average 1 hour per response, including the time for reviewing instruction, searching existing data sources, gathering and maintaining the data needed, and completing and reviewing the collection of information. Send comments regarding this burden estimate or any other aspect of this collection of information, including suggestions for reducing this burden, to Washington headquarters Services, Directorate for Information Operations and Reports, 1215 Jefferson Davis Highway, Suite 1204, Arlington, VA 22202-4302, and to the Office of Management and Budget, Paperwork Reduction Project (0704-0188) Washington DC 20503.

1. AGENCY USE ONLY *(Leave blank)*	2. REPORT DATE March 2003	3. REPORT TYPE AND DATES COVERED Master's Thesis	
4. TITLE AND SUBTITLE: Mesoscale Forcing on Ocean Waves During Gulf Stream North Wall Events		5. FUNDING NUMBERS	
6. AUTHOR(S) John A. Okon			

7. PERFORMING ORGANIZATION NAME(S) AND ADDRESS(ES)
    Naval Postgraduate School
    Monterey, CA 93943-5000
		8. PERFORMING ORGANIZATION REPORT NUMBER	

9. SPONSORING /MONITORING AGENCY NAME(S) AND ADDRESS(ES) N/A		10. SPONSORING/MONITORING AGENCY REPORT NUMBER	

11. SUPPLEMENTARY NOTES The views expressed in this thesis are those of the author and do not reflect the official policy or position of the Department of Defense or the U.S. Government.			
12a. DISTRIBUTION / AVAILABILITY STATEMENT Approved for public release; Distribution is unlimited		12b. DISTRIBUTION CODE	

13. ABSTRACT *(maximum 200 words)*

Under meteorological conditions associated with extreme cold air outbreaks (CAO) off the U.S. East Coast, large ocean waves sometimes develop along the North Wall of the Gulf Stream. These wave events produce wave heights above those expected given the short fetch and moderate winds. The highest waves are often very localized, which suggests localized forcing by the atmosphere. In this study, results from four cases are examined to characterize the role of high resolution, mesoscale wind forcing in generating localized regions of large ocean waves during events with large air-sea temperature differences. A known "true" atmosphere is simulated through the use of the Navy's Coupled Oceanographic and Atmospheric Mesoscale Prediction System (COAMPS). Model surface wind output from COAMPS is used to generate a wave field using Wavewatch Three (WW3), which is then compared to buoy observations and ship reports. Results of these cases show the mesoscale wind forcing of ocean waves during CAO and the importance of mesoscale atmospheric modeling in localized generation of ocean wind waves. Additionally, empirical wave forecast techniques are compared to WW3 model output for these cases to further reinforce the mesoscale atmospheric forcing during rapid growth of wind wave events in fetch limited environments.

14. SUBJECT TERMS Mesoscale effects, North Wall, Gulf Stream, Cold-Air Outbreak, Near-shore wave growth			15. NUMBER OF PAGES 115
			16. PRICE CODE
17. SECURITY CLASSIFICATION OF REPORT Unclassified	18. SECURITY CLASSIFICATION OF THIS PAGE Unclassified	19. SECURITY CLASSIFICATION OF ABSTRACT Unclassified	20. LIMITATION OF ABSTRACT UL

THIS PAGE INTENTIONALLY LEFT BLANK

**MESOSCALE FORCING ON OCEAN WAVES
DURING GULF STREAM NORTH WALL EVENTS**

John A. Okon
Lieutenant Commander, United States Navy
B.S., State University of New York, Maritime College, 1991

Submitted in partial fulfillment of the
requirements for the degree of

**MASTER OF SCIENCE IN METEOROLOGY
AND PHYSICAL OCEANOGRAPHY**

from the

**NAVAL POSTGRADUATE SCHOOL
March 2003**

Author: John A. Okon

Approved by: Wendell A. Nuss
                 Thesis Advisor

                 David S. Brown
                 Second Reader

                 Carlyle H. Wash
                 Chairman, Department of Meteorology

THIS PAGE INTENTIONALLY LEFT BLANK

ABSTRACT

Under meteorological conditions associated with extreme cold air outbreaks (CAO) off the U.S. East Coast, rapid growth of large ocean waves sometimes develop along the North Wall of the Gulf Stream. These wave events produce wave heights above those expected given the short fetch and moderate winds. The highest waves are often very localized, which suggests localized forcing by the atmosphere.

In this study, results from three cases are examined to characterize the role of high-resolution mesoscale wind forcing in generating localized regions of rapid ocean wave growth during events with large air-sea temperature differences. Analysis of 4 buoys, located in the western Atlantic and coastal waters of North Carolina, were compared to 48 hour atmospheric and ocean model simulations. The Navy's, Coupled Oceanographic and Atmospheric Mesoscale Prediction System (COAMPS) and National Oceanic and Atmospheric Administration's, Wavewatch Three (WW3), were used for atmospheric and ocean wave simulations (respectively) with additional observations from land based stations and ship reports utilized to established model simulation validity. Results of these cases show how mesoscale atmospheric forcing effects rapid growth of ocean waves during CAO and the importance of mesoscale atmospheric modeling in localized generation of ocean wind waves.

Additionally, near-shore uniformed observed wind fields were used to generate simulated wave fields then compared to WW3 model output for these cases to further reinforce the rapid and highly non-linear wave growth under strong mesoscale atmospheric forcing during wind wave events in fetch limited environments.

THIS PAGE INTENTIONALLY LEFT BLANK

TABLE OF CONTENTS

ACKNOWLEDGEMENT

The accomplishment of this thesis research has been aided greatly in different ways by a number of specific individuals. Specifically, I would like to thank Dr. Wendell A. Nuss for his keen academic leadership and dedication in accepting this un-funded research project. His understanding of operational applied marine meteorology is unparalled. He truly understands the limitations and conditions in which we environmentally support operational forces, and his service and dedication to educating our Navy's future leaders in meteorology should be commended. His consistent devotion of time and encouragement to this research in coastal meteorology and oceanography were invaluable and inspiring. I also thank Dave Brown, for his early guidance and partnership in the development of this research. Without the help and work of Mr. Bob Creasey and Dr. Doug Miller, there is no doubt this research, which is so heavily relied upon atmospheric and ocean modeling, would not have been possible, and for your specific work I thank you. For the help in understanding ocean wave spectra and wave propagation I would like to thank Dr. Thomas Herbers and Mr. Paul Jessen, who's computer programming technical assistance was greatly appreciated. To Dr. Wash and Captain Clark at SPAWAR for providing the opportunity to present this research at the annual American Meteorology Society meeting, further advancing my professional and scientific background

I would like to specifically thank my friend and wife, Valerie, for whose support and constant devotion to me provided the personal foundation for the accomplishment of this work. For all that she has been through in the past two years and for the fourteen years we have spent together she has constantly been by my side with support and encouragement, I love you.

To those whom I have accidentally left out in this formal acknowledgement, and for the many professors and military staff that have contributed and assisted in the education I received at the Naval Post Graduate School in Monterey, CA, I thank you.

THIS PAGE INTENTIONALLY LEFT BLANK

I. INTRODUCTION

High wind and seas events in coastal regions during a strong dynamic Cold Air Outbreak (CAO) off the eastern United States provide evidence of strong ocean-atmosphere interaction. This strong interaction is a difficult problem to capture and model, but such feedback plays a significant role in near-shore wave forcing during these events. Wave model guidance in coastal regions often fail to adequately capture the rapid wave growth.

Over the last decade numerous advances in mesoscale atmospheric modeling have been made. Through finer resolution grids, increased observations and data assimilation from numerous sources, the prediction capability of mesoscale models have significantly improved. The Navy's Coupled Ocean Atmosphere Mesoscale Prediction System (COAMPS), utilizing high-resolution sea surface temperatures for it's ocean forcing is leading the way toward truly coupling the ocean and atmospheric in an operational model. However, the ability of this model or others to properly forecast near-shore waves in extreme CAO's is not known. While atmospheric fields may be well predicted, their forcing of waves, either empirically or numerically, is an open question.

A.   THE OPERATIONAL SIGNIFICANCE

The operational significance of this research is to provide insight to ocean and atmospheric modelers on the mesoscale forcing of near-shore wave processes during intense air-sea interactions associated with CAO. The Department of Defense has and will continue to operate naval forces in the littoral to support interests around the world. While operating in the littoral has its own challenges with oceanographic parameter forecasting, the role of atmospheric forcing from the ocean is crucial to the successful modeling of the littoral environment. In the cases analyzed, the forcing of the air-sea interaction is predominately the western boundary current, the Gulf Stream. While the discussion in this research is limited to these cases, this air-sea interaction problem could easily be adapted to cold outbreaks in the Gulf of Genoa or in the Gulf of Tuanapec,

where strong synoptic forcing induces mesoscale features over the land-ocean transition where near-shore wave forecasting is effected.

In the future, operational forecasting units will be called upon to make rapid environmental assessments of the littoral battle space utilizing high resolution ocean and atmospheric models. As advances are made in computer technology to process higher resolution models, it is important to also advance our understanding of boundary layer interactions in order to properly gauge their performance. It is the goal of this research to provide insight into mesoscale atmospheric forcing of ocean wave fields and to stimulate ocean and atmospheric modelers to continue to work together to improve the prediction capabilities of the littoral environment.

B.   ENVIRONMENTAL FORCING

During the months from late Fall to early Spring strong polar and arctic air masses move from the north and central regions of Canada southeast to the mid-Atlantic coast of the United States. These air masses bring near freezing temperatures to the eastern United States seaboard and adjacent coastal waters. The CAO produces rapidly increasing strong winds and high near-shore seas posing hazards to coastal regions, mariners and naval operations. These events know to mariners and coastal meteorologists as "North Wall" events are typically poorly modeled by atmospheric global spectral models and deep ocean wave models as a result of multiple sub grid point atmospheric scale interactions, strong ocean forcing on the atmosphere, and their duration. These events can produce localized regions of relatively high waves near-shore inspite of obvious fetch limitations described through empirical wave theory.

As strong polar and artic air masses move southeast from north central Canada they bring cold offshore directed northwest winds to the mid-Atlantic coast. North Wall events occur as a result of the strong air-sea temperature difference between the cold air mass and warm waters of the Atlantic western boundary current. The large air-sea temperature difference results in intense upward heat fluxes and downward momentum fluxes which work in tandem to destabilize the boundary layer and induce boundary layer mesoscale circulations embedded in the synoptic pattern. The introduction of mesoscale

circulations enhances the offshore synoptic flow to produce localized regions of strong surface winds, particularly in the vicinity of the North Wall of the Gulf Stream, where seas rapidly build as a result of the strong air-sea temperature discontinuity and associated strong winds.

C.   HYPOTHESES

The possible role of mesoscale atmospheric forcing in generating high waves during strong coastal air-sea interaction events, such as east coast CAO, is the focus of this study. It is relatively well understood through research from Vukovich (1991), Konrad and Colucci (1989) and Boyle (1986) that the magnitude and duration of CAO are influenced by three main factors:

1. Air mass characteristics (predominately temperature and moisture)
2. Off-shore wind trajectory
3. Location, temperature, and area of the Gulf Stream Core

All three factors work together and must be present to force an embedded mesoscale circulation in the synoptic pattern, which in turn forces a localized high wind region in the vicinity of the North Wall. However, based on current wave theory, the above factors do not explain the rapid growth of high wind waves in an obvious fetch limited region. Our specific hypotheses are that

1. Mesoscale atmospheric features that are captured well by mesoscale atmospheric models and forced by the local ocean environment, provide rapid forcing to the ocean wave field, which are not captured well by the deep ocean wave model, Wave watch three.
2. In a CAO regime, rapid growth in ocean wave fields are directly linked to specific changes in air-sea temperature differences, wind speed and wind direction.

D.   EXPECTED RESULTS

The expected results of this thesis are to better understand the dynamic atmospheric forcing and the atmospheric feedback to the ocean that results in rapid growth of near-shore wave fields during strong air-sea interaction events.   Through analysis and comparison of wave model output to observations, we attempt to gain insight into how the variability in the atmospheric models effect dynamic wave model output during short period rapid growth wave fields in a fetch-limited area.

Finally, knowing the limited availability of over ocean observations, we expect the research to stimulate:

(1) The scientific community to develop forward thinking sensors capable of sampling the boundary layer in order to capture surface fluxes

(2) The modelers that would assimilate high-resolution boundary layer air-sea fluxes into an operational coupled ocean atmospheric models.

II. PROCEDURE

A.   THE ATLANTIC OCEAN

One of the most volatile areas for wintertime weather in the northern hemisphere is over the United States mid-atlantic seaboard and adjacent coastal waters. This area experiences occasional strong polar and artic air masses from late fall to early spring. With the proximity of a warm offshore ocean current (Gulf Stream) to cold air masses, these two features provide the ingredients for intense wind and wave interaction through a two-way feedback of mesoscale momentum and energetic processes. Other areas around the world, such as coastal waters of Japan and the Kuroshio Current, would also be prone to this type of intense wind wave interaction. However, U.S. coastal waters were chosen for this research due to the abundance of atmospheric and oceanographic observations, model availability, and intensity of air-sea interactions during CAO.

B.   REQUIRED ATMOSPHERIC CONDITIONS

Conditions for intense wind-wave interaction are very sensitive to atmospheric and oceanographic parameters. A deep upper level (500 millibars (mb)) trough over the central and eastern U.S. propagating south and/or east is crucial (Figures 1-3). This upper level trough allows cold air from central Canada, a source region for continental polar air masses, to push south across the Great Lakes and east of the Appalachian Mountains. Speed of the upper level trough is critical to the timing and duration of the event. A fast moving 500mb trough may not allow cold air enough time to interact with the warm ocean to force mesoscale atmospheric processes responsible for large wind increases and wave growth. It is not the goal of this research to develop time scales of these interactions, but for the case selection described below, the movement of the upper level trough axis was approximately 30 knots (kts). While this speed seems a bit fast for such dynamic processes to occur at the surface, it is not only the speed of the upper level trough that play into the equation, it is also the speed in which the downstream ridge

builds over the eastern U.S. In the cases discussed in section three, all had fast moving upper level troughs that slowed over the Western Atlantic, allowing a prolonged northwest flow aloft to bring cold air from central Canada to the Mid-Atlantic States. Strong upstream ridging did not occur in the case studies, this prolonged the upper level northwest flow over the mid-atlantic coast. At the surface, a developing low-pressure system typically in the middle to latter stages of development moves off the coast of the eastern U.S., with cold frontal passage bringing gale force northwesterly winds across the Gulf Stream (Figures 4-6). As the front moves offshore, cold high pressure moving out of southern Canada/Northern Plain states slowly builds southeast across the Mississippi River Valley and into the southeast U.S., prolonging the cold northwest winds and the destabilization of the boundary layer over the eastern seaboard and coastal waters. Figure 7 shows a cross section along longitude 75 west of equivalent potential temperature. The surface to 925mb layer is absolutely unstable east of the 36th parallel and is characterized by strong winds. The movement of the surface high and interaction with the offshore low-pressure system plays an important role in the duration and trajectory of the gale force winds and cold temperatures over the Gulf Stream. As will be seen in the discussion of the case studies in section III, the offshore trajectory of the wind is one of the major determining factors for the duration of the North Wall event. If the wind continues to veer quickly to the north following cold frontal passage the cold air quickly modifies over the coastal waters, reducing the heat, moisture and momentum fluxes that are the primary mechanisms for inducing mesoscale atmospheric processes. This leads to a decrease in the wind stress on the ocean and growth rate of the coastal wind-wave field.

Oceanographic conditions and their variability are less restrictive on the North Wall events than the atmospheric conditions, as the Gulf Stream is a permanent feature along the shores of the Southeast U.S. Temperature of the current's core, width of the current and distance of the current from the coast (Figure 8) are all important factors in the intensity of the North Wall event. The Gulf Stream core temperature and width of the current provide the necessary ocean surface for the upward heat and moisture fluxes into the atmosphere, which results in intense mesoscale circulations embedded in the synoptic flow during CAO. Cooler ocean current temperatures, narrower currents and location of the gulf stream well offshore all lead to a reduction in the air-sea interactions causing

North wall events. There was not a minimum Gulf stream temperature, width or distance offshore chosen for this study. However, based on research by Konrad and Colucci (1989) and Boyle (1986), a minimum threshold of negative 6 to 15 degree Celsius air-sea temperature difference was set for case selection to ensure that there were adequate heat, moisture and momentum fluxes to initiate mesoscale atmospheric processes.

All cases chosen for this research had the above synoptic atmospheric and oceanographic conditions. Additional requirements in case selection included the 5400 meter 1000-500mb thickness line located south of frying pan shoals buoy (FPSN7) (Figure 10). The southern extent of the 5400m thickness location ensured cold air-warm ocean current interaction. Additionally, a minimum of 12 hours of offshore NW flow with the 5400m thickness line located south of Frying Pan shoals, allowing adequate time for mesoscale processes to be induced in the boundary layer as a result of air-sea interaction.

C.   CASE STUDIES

North wall events rapidly develop and require small time step modeling to ensure adequate representation of the driving processes. With the typical event duration of between 12-30 hours, a minimum time threshold of mesoscale processes forcing ocean waves of 12 hours was set. During case study selection, strong wind-wave forcing was present during numerous North wall events, however the identification of mesoscale processes in model simulations was not present in all cases reviewed. For this reason, these cases were rejected from the study. For all three cases discussed in section III, embedded mesoscale circulations are present in the synoptic pattern, as analyzed through buoy reports and model analysis, and were present in the boundary layer circulation from 12 hours to 24 hours. 18 cases of CAO over the last 5 years were reviewed. Most cases were rejected due to the weak intensity of CAO, causing weak synoptic and mesoscale forcing, and short duration of the event. Three cases, February 3-5, 2002, March 5-7, 2001, and March 31-April 2, 1997 were chosen for their completeness of the data set, availability of observations and for the reasons discussed above.

D.   COAMPS MODEL SIMULATIONS

The model used for atmospheric simulations was the U.S. Navy's Coupled Ocean and Atmosphere Mesoscale Prediction System (COAMPS). COAMPS, a non-hydrostatic model, was chosen for the simulations because it is capable of capturing both the induced mesoscale circulations as well as the background synoptic flow. COAMPS boundary conditions were initialized through the analysis of the U.S. Navy's Operational Global Atmosphere Prediction System (NOGAPS) at one-degree resolution.   Additional observations, not available during the real-time model run of NOGAPS, obtained from the U.S. Navy's detachment at the National Climate Data Center in Ashville, N.C., were assimilated into the initialization scheme. Numerical simulations of the atmosphere were generated (COAMPS version 2.0.15) on three nested grids of 81, 27, and 9 kilometers (km) (Figure 9) from analysis to 48 hours with output every 3 hours. Finally, a static analyzed 10km sea surface temperature field, obtained from the U.S. Navy's Naval Oceanographic Office, Stennis Space Center, MS, was meshed under the grid domain to provide mesoscale ocean forcing.

To ensure proper wave field forecasts, discussed below, an initial 36-hour COAMPS simulation was conducted at the start of the CAO. Additionally, a 48-hour COAMPS simulation was initialized 12 (T-00) hours prior to the onset of the CAO (T-12 to T-48). The initial 36-hour simulation was compared with the 48-hour simulation, yielding insignificant and minor variations. As a result, the 48-hour model run was used as the forcing for the wave field simulations to allow adequate wave spin-up prior to the primary wave growth period.

E.   WAVE WATCH III AND BUOY-WIND WAVE MODEL SIMULATIONS

The model used for wave field simulation was the U.S. National Oceanographic and Atmospheric Administration's, National Center for Environmental Prediction Wave watch III (WW3). WW3 (version 2.20) was chosen for wave model simulations, as it is a full spectra wave model that includes nonlinear effects occurring during rapid wave growth, conditions that are prevalent along the North wall during CAO. WW3 was

initialized under simulated weak atmospheric synoptic conditions 12 hours prior to the onset of the CAO then meshed under the COAMPS run with the 10 meter atmospheric wind component as the primary driver and no input from ocean currents.

To help validate the hypothesis that accurate atmospheric mesoscale forcing plays a significant role in the rapid development of near-shore wave fields, observed buoy wind fields for DSLN7 (2002, 1997) and FPSN7 (2001) were used to simulate a near-shore wave field. These wave fields were then compared with WW3 model output and observed significant wave heights to test a state of the art wave model and current wave theory's ability to capture the rapid wave growth under highly non-linear processes of strong air-sea interaction.

F.   MODEL DATA ANALYSIS PROCESS

As discussed above, 3 CAO cases over the last 5 years were chosen for this study. COAMPS model runs were conducted from analysis (T00) through 48 hours (T48), at 3-hour time steps. Analysis of the 500mb, 850mb and 925mb pressure levels as well as the mean sea level pressure fields were conducted to ensure the quality of the simulation through comparison of upper-air, synoptic and buoy observations. Specific attention was paid to the distribution of temperature and humidity as well as wind speed and direction. While each case is somewhat different in duration and magnitude, over the mid-atlantic region and coastal waters all four cases had errors in the model simulation of, temperature less than 4° Celsius, wind speeds of less 10 kts and direction of less than $20^{o.}$ The COAMPS model run time steps T-00 to T-48 were used for WW3 initializations as discussed above.

G.   COMPARISON OF SYNOPTIC OBSERVATIONS TO MODEL OUTPUT

Along the coastal waters of N.C. lie 5 reporting stations operated by NOAA's National Data Buoy Center (Figure 10). Two of the stations (41001, 41002) are offshore buoys while the other three are C-MAN stations (DSLN7, CLKN7, FPSN7). Four of the locations are equipped with accelerometers or inclinometers, which, through the use of

fast fourier transforms, calculate wave spectral data. Spectral data, as well as standard atmospheric data such as wind speed, wind direction, air temperature and sea surface temperature from these four locations were analyzed and compared with point spectral output from WW3 and atmospheric output from COAMPS.

Data comparison of observed and modeled spectral wave data was conducted to determine wave growth characteristics and possible deficiencies in WW3 model output. Additionally, an attempt was made to determine a critical offshore wind angle, through the correlation of wind angle to wave growth, where the offshore fetch variation impacts air-sea interaction and wave spectral frequencies. Spectral data was also used to calculate significant wave height and analyzed to determine wave generation locations outside of strong air-sea gradients. This analyzed data was then compared to WW3 model output for signal correlation. Comparison of this data was conducted along side the calculation of the critical wind angle to attempt to determine where the rapid wave growth caused by mesoscale atmospheric processes, in a fetch limited environment, transitions to a wave field generated in a more fetch favorable environment.

III. ATMOSPHERIC ANALYSIS

A.   CASE I - FEBRUARY 4 – 6, 2002

A CAO occurred over the eastern U.S. in early February 2002 surging freezing temperatures across the outer banks and coastal waters of North Carolina and northern coastal South Carolina. Over the coastal waters, rapidly increasing gale force winds and a developing wave field quickly followed frontal passage in response to intense air-sea interaction. The event lasted approximately 18 hours with wind reports of near 50kts and seas in the protected waters of 12-15 feet (ft).

1.   Synoptic Forcing

a.   Upper Level (500mb) Synoptic Flow

A strong polar airmass originated north of Hudson Bay and moved southeast over eastern Canada and the Northeast U.S. under a developing 500mb trough. A 5100m closed 500mb low was located over north-central Quebec at 04/00Z with a positively tilted 500mb trough axis oriented northeast-southwest, from James Bay across the eastern Great Lakes and into the central plains (Figure 11). This low slowly filled to 5120m by 05/00Z (Figure 12) and became indiscernible after 05/12Z. A new closed 5160m low formed over Nova Scotia by 05/12Z and the trough axis reoriented itself into a negative tilt over the western Atlantic. This low formed along the axis of the negatively tilted trough in response to strong upper level dynamics including a 120kt 500mb jet maximum to the south and strong vorticity advection. Weak ridging, with moderate northwest flow aloft dominated the Mid-Atlantic States following the passing of the trough axis and continued through 06/00Z (Figure 13).

b.   Mid Level (850mb) Synoptic Flow

Weak west-northwest flow and mild temperatures at 850mb dominated the mid-Atlantic coastal waters at 04/12Z (not shown) as the trough axis is draped just to the east over the eastern shelf waters. Mid level flow continued to gradually veer to the north through 06/00Z while potential temperatures dropped nearly fifteen degrees as the cold

surge from Canada made its way southeast under deep northwesterly flow to the mid-Atlantic region.

Mid level winds gradually increased along the mid-Atlantic coastal waters from 20kts at 04/12Z to 35kts at 05/00Z then decreased to 20kts from the NNW by 05/12Z as the vertical mixing of momentum (a secondary circulation resulting from air-sea temperature contrast) and synoptic pressure gradient weakened.

c.   *Surface Flow*

A 1007mb low located over southern Quebec at 04/00Z (Figure 14) moved east and deepened to 997mb over the western Atlantic at 04/12Z. The low then moved northeast and deepened to 976mb at 05/12Z east of Sable Island (Figure 15). This low began to fill as it became stacked with the upper level low after 05/12Z, and slowly tracked northeast to south of Newfoundland by 06/00Z (Figure 16). The associated developing occluded front continued to strengthen over the western Atlantic and moved east into the central Atlantic.

West to North winds dominated the mid-Atlantic region following cold frontal passage (FROPA) on 03FEB. Strong cold air advection lagged 12 hours behind FROPA as the developing offshore low enhanced advections along the coast. The 5400m 1000-500mb thickness line moved across Hampton Roads, VA by 04/00Z then slowly pushed south across Elizabeth City, N.C. at 04/12Z then became oriented Northeast-Southwest and continued south and east over coastal waters of N.C. and extreme Northern waters of S.C. by 04/18Z. The 5400m thickness line gradually moved north, and reoriented east-west, after 05/12Z as the air mass began to modify over the eastern U.S. and coastal waters and high pressure built across the region.

Strong cold air advection occurred under strong northwesterly winds over the Northwall of the Gulf Stream from 04/12Z through 05/18Z, with a max at 05/03Z as the 5190m thickness line briefly draped south of the northwall. Over the Gulf Stream, westerly 15-20kt surface winds at 04/12Z gradually veered northwest and increased to gale by 05/00Z further increasing to strong gale, as a result an induced mesoscale circulation forced from strong vertical mixing as a result of intense negative air-sea temperature differences through 05/06Z. After 05/12Z winds decreased to sub-gale and veered northerly through 06/00Z.

d.   Coastal Wave Field

Along the coast of N.C., near-shore buoy (FPSN7 and DSLN7) wave heights of 1.25-1.5 meters at 04/12Z decreased slightly to 1.0-1.25 meters through 04/18Z. Near-shore buoy wave fields rapidly grew after 04/18Z to 3.2-3.5 meters by 05/04Z then gradually decreased through the period (Figures 17-18). Ship observations along coastal N.C. waters, further offshore than the buoys, and in the vicinity of the northwall of the Gulf Stream indicated waves building to 8 meters at 05/06Z, with 25nmi. of fetch, then slowly decreased to 6 meters by 05/12Z.

In the northern N.C. coastal areas, buoy wave periods (calculated from wave spectra Figures 13-14, as period = 1/frequency of the peak energy) of 5 seconds at 04/12Z gradually grew to 10 seconds by 05/12Z then continued through 06/00Z as the energy in the wave field decreased. In the southern N.C. coastal areas, wave periods of 4.7 seconds at 04/12Z increased to 6 seconds by 05/00Z, at peak wave energy, then continued to increase to 7 seconds as the wave energy decreased (Figures 19-20).

2.   Mesoscale Atmospheric Influences in Observational Data

a.   Off-shore Observations

Buoy 41001, located about 150nmi offshore at 34.68^o north latitude and 72.66^o west longitude, experienced weak wave height growth from 3 to 3.5 meters from 04/12Z through 05/00Z (Figure 21). This small wave growth occurred under westerly winds at 26kts (Figures 22-23). Over this period Figure 24 shows a slow decrease of air-sea temperature difference from $–7.5^oC$ to $–10^oC$. While decreasing air-sea temperature differences tend to favor wave growth, this decrease showed little effect on the wave growth time series. From 05/00Z through 05/12Z, wind direction veered west-northwest and increased to 32-36kts under strong synoptic forcing, while the wave field grew rapidly to 6.7 meters by 05/06Z and continued above 5.5 meters through 05/12Z. Initially at the start of this period of wave growth the air-sea difference underwent a drop from -10^oC to -13^oC then maintained a period average of -13^oC through 05/12Z.

As this intense CAO evolved, buoy 41001 showed little correlation between wind direction and wave growth but strong correlation between wind speed and wave growth.   While there is a period of strong wave growth from 05/00Z to 05/12Z, this increase is only mildly due to localized wind stresses on the ocean surface as a result

of additional momentum mixing down to the surface over buoy 41001. A time sequence of the wave energy spectra (Figure 25) shows the arrival of long period swell generated by synoptic gale force winds off the coastal waters of eastern MD have propagated southeast over buoy 41001 and the local generation of synoptic wind-wave that were primarily responsible for the observed wave field. Figure 30, shows a shift in the peak wave period from 8 to 12.5 seconds and increase in energy spectra over the 6-8 second periods (wind generated waves), the arrival of the long period swell from 05/00Z to 05/12Z.

Buoy 41002, under 24-30kt west-northwest winds, experienced wave height growth of 2-3.5 meters from 04/12Z to 05/00Z (Figures 26-28). With an air-sea temperature drop from -5.5^{o}C to -9°C over this period (Figure 29), wave growth was moderate. From 05/00Z to 05/12Z air-sea temperature differences dropped from -9°C to -15°C, working in tandem with the synoptic forcing to induce and increase the winds to 32 to 36kts from the west-northwest to north-northwest. Resultant rapid wave growth of 3 to 5.7 meters occurred from 05/00Z to 05/06Z.

Similar to buoy 41001, buoy 41002 located 160nmi. south of Cape Hatteras, N.C. at 32.4^{o} north latitude and 75.50^{o} west longitude, showed little correlation of wind directions with wave growth and a strong correlation of wind speed with wave growth. While the wave spectra growth of buoy 41002 (Figure 30) clearly indicates the shift toward longer period swell and an embedded wind-wave at 05/00Z, it is by 05/12Z that the wind-wave field, no longer being heavily forced from the boundary layer mixing of momentum from aloft and the strong synoptic forcing, gradually begins to decay through 06/00Z. While the synoptic forcing is quite strong in this case, the minor effects of a rapid decrease in air-sea temperature difference which causes increased surface wind speeds as a result of momentum from aloft mixing toward the surface is clear.

b.   Coastal Observations

Buoy FPSN7 from 04/00Z to 05/12Z experienced varying wind and wave conditions (Figures 18, 31-32). From 04/00Z to 04/18Z, 15-20kt winds, with a brief peak of 25kts at 04/12Z, backed from west-northwest to west-southwest and then veered back to west-northwest. The wave field during this period slowly decreased from 1.2 to 1 meter, spiked to 1.6 meters at 04/12Z, then decayed back to 1.2 meters by 04/18Z. Air-

sea temperature differences were between 0°C and -2.5^{o}C across the period with a sharp drop from 04/09Z to 04/12Z (Figure 33). From 04/18Z to 05/12Z winds continued to veer northerly as wind speeds increased to a maximum of 43kts at 05/01Z then gradually decreased to 28kts by 05/12Z. The near-shore wave field built from 1.2 meters at 04/18Z to 3.1 meters at 05/01Z then gradually decayed to 1.7 meters at 05/12Z. Air-sea temperature differences experienced the greatest drop of 0°C to -9°C from 04/22Z to 05/06Z with a slow decrease of -9°C to -12°C from 05/06Z to 05/12Z.

Correlation of wind direction with wave growth , for buoy FPSN7 is quite different from the offshore buoys 41001 and 41002. Under varying wind directions, FPNS7's wave field is correlated well with both wind direction and wind speed. Additionally, during both wave growth periods, air-sea differences experienced a rapid drop over just a few hours. The wave field that surrounds buoy FPSN7 is well linked to the secondary mesoscale circulation that brings additional momentum from aloft to the surface and is a direct reflection of air-sea interactions.

Buoy DSLN7, from 04/18Z to 05/04Z, experienced an increase in winds from west at 20kts to northwest at 45kts (Figures 34-35). The surrounding wave field grew rapidly from 1.1 meters at 04/18Z to 3.5 meters at 05/04Z (Figure 17) under a rapid decrease in air-sea temperature difference from -5.7^{o}C at 04/20Z to -13°C at 05/04Z (Figure 36). From 05/04Z to 05/12Z winds continued to veer north-northwest gradually decreasing to 30kts by 05/12Z while the wave field gradually subsided to 2.7 meters. The air-sea temperature difference continued a slow decrease, after 05/04Z, to -15°C over the period.

With less variance in the wind direction than at FPSN7, the wind direction at DSLN7 shows little correlation with rapid wave growth while the wind speed and air-sea temperature differences are strongly linked. In this near-shore, highly fetch-limited location, westerly winds from various directions produce the same wave growth. The close proximity to warmer waters results in rapid decreases in air-sea temperature differences, with wind directions between 240 and 340 degrees and the movement of cold air offshore. This results in rapid wave growth for a variety of wind direction.

B.   CASE II - MARCH 5 – 7, 2001

A CAO occurred over the eastern U.S. early March 2001 surging sub-freezing temperatures across the outer banks and coastal waters of North Carolina. In response to intense air-sea interaction and strong instability in the boundary layer over the coastal waters, wind gradually increased to gale force, developing a steep wave field in protected waters.   The mesoscale induced wind-wave event lasted nearly 12 hours with wind reports of near 50kts and seas in the protected waters of 12ft.

1.   Synoptic Forcing

a.   *Upper Level (500mb) Synoptic Flow*

A strong artic airmass originating over central Canada moved south over Winnipeg then southeast across the U.S. eastern seaboard under a deepening 500mb trough. A 5180m 500mb low over the central Great Lakes at 05/12Z (Figure 37) moved southeast over Hampton Roads, VA and deepened to 5100m by 06/12Z (Figure 38) then continued to move east over the western Atlantic, gradually filling to 5220m by 07/12Z (Figure 39).   An 80kt 500mb jet maximum over southern Wisconsin at 05/12Z moved southeast with an associated upper level low and increased to 120kt as it exited the U.S. over coastal S.C. by 06/12Z then moved east over the western Atlantic and slowly decreased in response to the upper level low filing. Upper level northwest flow over the Gulf Stream began by 06/15Z, as the trough axis passed, and continued through 07/12Z as a weak ridge over the central plains at 05/12Z slowly weakened and moved east.

b.   *Mid Level (850mb) Synoptic Flow*

Weak west-southwest mid-level winds over the mid-Atlantic region at 05/12Z rapidly veered west-northwest to northwest and increased to gale force by 05/18Z as the 850mb trough axis passed to the east. Northwesterly winds maintained strong gale force through 07/06Z then gradually subsided to sub-gale and veered north-northwest by 07/09Z. Cool potential temperatures at 05/12Z dropped nearly 25 degrees as the second cold push from Canada moved southeast under strong northwest flow.

c.   *Surface Flow*

A 996mb low over coastal waters of N.J. at 05/12Z (Figure 40) moved northeast to the southern Gulf of Maine and deepened to 984mb by 06/12Z (Figure 41)

under moderate upper level support. The associated cold front moving off the eastern seaboard by 05/18Z continued to push east into the western Atlantic through 07/12Z, dragging arctic air across the mid-Atlantic coast and western Atlantic waters. This low began to rapidly fill after 06/18Z as upper level support shifted south and east and a triple point low developed. A secondary low developed on the cold front by 06/18Z over the extreme western Atlantic as 500mb support approached from the west. This low continued to deepen to 973mb through 07/12Z (Figure 42) as it moved east-northeast.

West-southwest to northwest wind dominated the mid-Atlantic region through the period. Cold air advection followed FROPA while the strongest cold air advection occurred from 06/09Z through 06/18Z as the 500mb cold pocket moved over the region and into the western Atlantic. The 5400m 1000-500mb thickness lines pushed southeast over northeastern N.C. by 05/21Z then continued across the gulf stream by 06/03Z and remained there through 07/12Z while thickness values continued to drop across the northwall of the Gulf Stream and coastal waters reached a minimum of 5130M at 06/15Z then gradually increased through 07/12Z.

Across the coastal waters, 10 kt westerly winds at 05/12Z increased to 30kts at 05/18Z then gradually veered to the northwest and increased to gale force by 06/09Z. Gale force northwest winds dominated the region through 07/12Z, gradually decreasing to sub-gale after 07/12Z.

d. *Coastal Wave Field*

Along the coast of N.C., near-shore buoy (FPSN7, (DSLN7 was unavailable)) wave heights of 3 meters at 05/12Z decreased to 1.7 meters by 06/02Z as the front moved offshore then rapidly grew through 06/18Z to 3.2 meters when the cold advection increased. Near-shore buoy wave fields gradually decreased after 06/22Z to 2.2 meters by 07/12Z (Figure 43).

Ship reports in the vicinity of the Gulf Stream indicated waves building along coastal N.C. to 3 meters with an 8-second period by 06/00Z and along coastal S.C. to 6 meters with a 4-second period by 06/06Z. The wave field in the northern portions maintained 3 meters through 07/06Z while in the southern portions wave heights decreased to 4 meters by 07/12Z.

In southern N.C. coastal areas, buoy wave periods of 9 seconds at 05/12Z maintained through 06/00Z as wave energy decreased which shows the swell dominated waves associated with variable pre-frontal winds. Buoy wave periods decreased to 6 seconds by 06/12Z as wave energy increased (Figure 44) and winds increased from the north. This decrease in wave period and an increase in wave energy are clear indications of a local wind generated growing wave field.

2. Mesoscale Atmospheric Influences in Observational Data

a. Off-shore Observations

At the offshore buoy 41001, near constant west-northwest 25-30kt. winds from 06/06Z through 06/21Z maintained wave heights of 6 meters (Figures 45-47). Although there is a sharp decrease of strong air-sea temperature differences from -8° C at 06/06Z to -16° C at 06/21Z (Figure 48), which would lead to a severe destabilization of the boundary layer and increase in the vertical mixing of momentum from the atmosphere above to increase in surface wind, there is no increase in surface wind (Figure 47) reported across this time period. Further analysis of the buoy's observational data provide insight into the possible cause of an offsetting mechanism responsible for the surface wind speed time series as seen in Figure 35. Synoptic scale wind forcing near buoy 41001 at 06/06Z (Figure 49) and at 06/12Z (Figure 50) indicated a low pressure trough passing over the buoy and associated weakening of the synoptic pressure gradient over this time period of nearly constant winds. This decrease in the pressure pattern over the area would lead to a decrease in the observed winds, however increased boundary layer mixing from the strong air-sea differences (discussed above) would enhance the surface flow and offset the weakening of the synoptic scale forcing. After 06/21Z the exact opposite occurred over the buoy. The air-sea temperature difference weakened from 06/21Z through 07/12Z, however the synoptic scale wind forcing increased due to the increase in the pressure gradient over the area, as seen in the surface pressure analysis at 07/06Z (Figure 51). This resulted in an increase in the winds over this time frame. It is not until 07/12Z that there was a weakening of both synoptic and boundary layer forcing, resulting in a decrease in surface winds.

At offshore buoy 41002, 20-40kt west-northwest to northwest winds occurred from 06/00Z through 07/12Z, and waves built from 4 meters at 06/07Z to 7.5

18

meters at 06/20Z then decreased to 5.5 meters at 07/12Z (Figures 52-54). The strong air-sea temperature difference underwent a rapid drop from -3°C to -13°C from 06/07Z to 06/18Z (Figure 55) and the wave growth shows no correlation with wind direction variations. However, the wind speed time series and the wave growth time series show strong correlation of wave growth with wind speed increases. Synoptic forcing over buoy 41002 indicates wind speeds from 20-35kts across the period, which is less than the buoy reports. Under similar wind speed and direction, buoy 41001 reports showed clear indication of mesoscale influences on the atmosphere, while buoy 41002 with a less severe air-sea difference (-13°C vice -16°C) did not.

b. *Coastal Observations*

Frying Pan Shoals buoy, FPSN7, data reports from 06/03Z through 07/00Z indicated strong boundary layer mixing influence on the atmosphere as the over ocean wind speeds, where the near surface atmosphere is unstable, are dramatically higher than the nearby coastal regions where the near surface stability is more neutral due to the lack of a warm ocean surface. Under 20-45kt west-northwest winds, the near shore wave field built from 1.7 meters at 06/03Z to 3.15 meters at 06/18Z (Figures 43, 56-57). With a similar correlation pattern as buoy 41002, discussed above, FPSN7 shows no correlation of wave growth with wind direction but shows strong correlation with wind speed. Also, wave growth and increased wind speed occurred under strong air-sea temperature differences that dropped from -6°C to -17°C (Figure 58). Over the same time period wind speeds increased from 20kts to 45kts under a nearly constant atmospheric pressure gradient.

Figures 59-60 show near constant surface pressure differences of 1.6mb over the time period 06/00Z-06/06Z across the area that surrounds buoy FPSN7 while the wind speeds differ greatly. Theoretically, wind speed remains unchanged during constant pressure differences, increase during increasing pressure differences and decrease during decreases in pressure differences. Pressure differences from New River Marine Corps Air Station, N.C. (NCA) across Wilmington, N.C. (ILM) to North Myrtle Beach, S.C. (CRE) are at a near constant of 1.6mb with a spike of 3.3mb at 06/18Z (Figures 61-62). Additionally, pressure differences drop to 1.9mb by 07/06Z (Figure 63) which would produce similar wind speeds as observed around 06/06Z, however observed wind speeds

at this time are 5m/s greater. This increase in pressure difference, which would reflect in an increase in surface wind, also corresponds to the maximum wind speed reports and the maximum air-sea temperature difference across the area. One hypothesis for this spike could be the boundary layer mixing which is reflected as a mesoscale circulation below 850mb over buoy FPSN7 deepened horizontally and built back to along coast regions causing an increase in the pressure difference. With a nearly constant pressure difference pattern and resultant synoptic wind pattern, buoy FPSN7 experienced increased wind speeds over those reported from nearby land observations from Myrtle Beach, S.C and Wilmington, N.C. Figure 64, shows the vertical wind profile from 34nmi west-northwest of Wilmington, N.C. (left edge of plot) to 77nmi southeast of buoy FPSN7 (right edge of plot). The Figure shows a near uniform vertical wind profile over the water where the boundary layer was unstable, causing momentum to be mixed from above and resulting in a homogenous wind profile and a more classic increasing of wind with height over land where instability forced from a warm surface is not as strong as over the water. Due to enhanced instability over the warmer coastal waters during the CAO there was a strong vertical mixing of momentum, which results in a nearly uniform vertical wind profile. It was the vertical mixing of momentum due to strong boundary layer instability, which caused the mesoscale enhancement of the surface winds and the rapid increase in the near shore wave field. This correlation is clearly seen in the analysis of Figures 43, 57-58.

C.   CASE III - MARCH 31 – APRIL 02, 1997

A CAO occurred over the eastern U.S. late March and early April 1997, surging near-freezing temperatures across the outer banks and coastal waters of North Carolina. Over the coastal waters, prolonged gale force winds developed a steep wave field in response to strong synoptic forcing and intense air-sea interaction. The mesoscale induced wind-wave event lasted over 12 hours with wind reports of 40 knots and seas in the protected waters of 12 feet. This case lasted longer and had higher near-shore wave observations than the two previous cases, however the synoptic and near-mesoscale forcing was not necessarily stronger.

1.   **Synoptic Forcing**

   a.   *Upper Level (500mb) Synoptic Flow*

   A strong artic air mass located over southern Canada moved southeast across the Ohio River valley and eastern U.S. under a deepening 500mb trough. At 31/00Z (Figure 65), a 5360m 500mb low located over upper peninsula of Michigan with a positively tilted trough extending southwest to the central Mississippi River Valley moved southeast and deepened to 5280m, reoriented to a negative tilt, exiting the DELMARVA peninsula at 01/00Z (Figure 66). The low continued to deepen to 5210m by 01/15Z as it began to move northeast, and slowly fill to 5230m through 02/00Z located over Georges Bank (Figure 67).   A 70kt jet maximum over Iowa at 31/00Z propagated through the trough and increased to 90kts in response to the deepening low as it exited the eastern U.S. over S.C. at 31/18Z then continued to broaden its coverage across the southern and eastern portions of the trough over the western Atlantic through 02/00Z. Weak ridging over the central and western plains at 31/00Z moved east and built through 02/00Z as it relocated its axis across the Mississippi River Valley, bringing prolonged NW flow over the mid-Atlantic region.

   b.   *Mid Level (850mb) Synoptic Flow*

   Moderate westerly winds over the mid-Atlantic region at 31/00Z gradually became gale force west-northwest by 31/21Z as the trough axis passed over the region. Winds continued to gradually veer to north-northwest through the 02/00Z and increased to strong gale after 01/15Z. Mild temperatures at 31/00Z began falling after 31/06Z and decreased 20 degrees Celsius by 01/06Z as the cold air surged south out of Canada. Temperatures warmed a few degrees through 02/00Z.

   c.   *Surface Flow*

   A 1005mb developing low pressure center along a boundary extending from the western Atlantic to the east side of the Appalachians 31/00Z (Figure 68) moved east-southeast exiting the U.S. along the coast of N.C. by 31/09Z. This system began to rapidly deepen after 31/09Z, tracking northeast across the western Atlantic at 01/00Z (Figure 69) and then to the Georges Bank and deepening to 984mb by 01/06Z. The associated cold front pushed offshore by 01/12Z then continued southeast across Bermuda and the Bahamas through 02/00Z (Figure 70).

21

As the low pressure center vertically stacked with the upper levels, the central pressure slowly filled 2mb through 02/00Z and a triple point low formed south of Nova Scotia by 01/15Z and tracked north-northeast across Sable Island by 02/00Z. Strong cold air advection dominated the coastal waters of Virginia south through S.C. from 31/15Z through 01/06Z then gradually weakened through 02/00Z. The 5400m 1000-500mb thickness line slipped offshore N.C. by 31/18Z moved south and east across northern S.C. and the western Atlantic through 01/12Z before it began to gradually regress northward along the N.C. coast as the polar airmass began to modify over the eastern U.S. and shelf waters. The 5310m-thickness line briefly draped south of the north wall from 01/00Z through 01/09Z during the periods of strongest cold air advection.

Weak southwesterly flow at 31/00Z shifted northwesterly following cold front passage and increased to gale force by 01/00Z. Gale force winds continued to veer north-northwest over the coastal waters of N.C. through 02/00Z while weak northwesterly winds extended west from the Albemarle and Pamlico Sound to the Piedmont.

d.   *Coastal Wave Field*

The coastal wave field, from buoy observations, at 31/06Z was sub 1 meter along the southern portions, and 1 meter along the northern portions of coastal N.C. From 31/06Z through 01/18Z waves rapidly grew to 5.4 meters in the northern portions at DLSN7, maintained above 5 meters through 02/00Z then gradually decreased to 2.5 meters by 03/00Z (Figure 71). Along the southern portions of N.C. at FPSN7, the wave field grew to 2.6 meters by 31/16Z, maintained 2.5 to 2.7 meters through 01/12Z then gradually decreased to near 1 meter through 03/00Z (Figure 72).

The southern N.C. coastal buoy reported wave periods of 5-6 seconds at 31/12Z increasing to 7 seconds by 01/00Z while wave energy increased 10 times (Figure 73). From 01/00Z through 02/00Z wave periods gradually decreased to 5-6 seconds while the wave energy returned to levels similar to 31/12Z observations. This suggests variable wind forcing with little swell production at this near-shore buoy. Along northern portions of coastal N.C. buoy wave periods of 5-6 seconds at 31/12Z gradually increased to 13 seconds through 02/00Z while wave energy increased nearly 300 times (Figure 74),

22

which is indicative of a transition to longer period swells, not generated locally, at this buoy.

2. Mesoscale Atmospheric Influences in Observational Data

a. Off-shore Observations

Offshore buoy 41001 experienced rapidly veering 15-20kt south to west-northwest winds from 31/12Z-31/15Z (Figures 75-76). From 31/15Z to 01/00Z west-northwest winds increased to 32kts (with maximum peak wind of 36kts at 31/21Z) while the seas built from 6 ft to 17ft (Figure 77). Seas continued to slowly build from 17ft at 01/00Z to 25ft at 01/15Z under 35kt westerly winds. Air-sea temperature differences, from 31/12Z to 31/22Z, dropped from -1°C to -9°C (Figure 78), with the steepest drop occurring from 15Z to 22Z from -4.5^{o}C to -9°C.

Under a strong decrease in air-sea temperature difference, buoy 41001 observations showed strong correlation of wind speed and wave growth from 31/15Z to 01/12Z and strong correlation of air-sea temperature difference and wave growth. Over the entire time series there is little correlation of wind direction with wave growth. While the wave growth from 31/15Z to 01/00Z is quite severe, Figure 79 indicates the wave growth over this time frame is locally driven and the wave growth from 01/00Z to 01/12Z is enhanced by the arrival of longer period swell from the northwest.

Buoy 41002, under 22-30kt west-northwest winds, experienced wave growth from 6ft to 12ft from 31/11Z to 31/15Z (Figures 80-82) while air-sea temperature difference dropped from -0.5^{o}C at 31/13Z to -4°C at 31/16Z (Figure 83). From 31/16Z to 01/02Z winds maintained 30-32kts from the west-northwest, while seas continued to slowly build to 15ft (max of 16ft at 01/00Z) and air-sea temperature differences slowly decreased to -5°C at 31/21Z then increased to -4.2^{o}C by 01/02Z. Winds began to rapidly increase from the west-northwest to 35kts from 01/02Z to 01/06Z under rapidly decreasing air-sea temperature differences from -4.2^{o}C to -6.2^{o}C. Seas built quickly over this time frame increasing from 15ft at 01/01Z to 21ft at 01/06Z.

Observations from buoy 41002 show a strong correlation of wind speed and air-sea temperature difference with wave growth. Wind direction and wave growth show little correlation across the time series as the wind maintains a near constant west-northwest direction. Under strong synoptic forcing the wave field surrounding buoy

23

41002 shows growth over the time frame from 31/15Z to 01/00Z despite the weakening of the mesoscale effects caused by the air-sea temperature difference. This growth, while not linked to mesoscale influences, is supported by current wave theory and originated through strong mesoscale forcing at the start of the CAO.

b.   Coastal Observations

Buoy FPSN7, from 31/03Z to 31/09Z, reported near frontal passage veering winds from south-southwest to west-southwest at 10-20kts and seas building from 1.5 to 3 feet (Figures 72, 84-85). Air-sea temperature differences across this time period rose slightly from -0.5°C at 31/03Z to 1.5°C at 31/06Z then dropped to -1.8°C at 31/09Z (Figure 86). Post-frontal winds rapidly veered to the west-northwest and northwest at 30-35kts from 31/09Z to 31/15Z as air-sea temperature differences dropped from -1.8°C at 31/09Z to -6.2°C at 31/12Z further decreasing to -6.8°C at 31/15Z. The wave field that surrounds buoy FPSN7 during this period built rapidly to 5ft by 31/12Z and continued to 6ft by 31/15Z. After 31/15Z, winds backed more westerly to west-northwest maintaining gale force through 04/01Z then veered northwest and dropped to sub-gale after 01/12Z. Air-sea temperature differences dipped slightly to -7°C at 31/17Z, rose to -4.8°C by 01/00Z, then dropped to -11.5°C at 01/12Z. Wave heights of 5-6ft maintained from 31/15Z to 01/12Z then began to decrease after 01/12Z.

Under rapidly changing conditions, wind speed, wind direction, wave height and air-sea temperature differences for buoy FPSN7 do not appear correlated. Closer analysis of the observations shed light into the small time scales of mesoscale effects on wave growth. Early in the time series there is both wave growth and air-sea temperature difference drop in near gale west-southwest flow while the air-sea temperature difference meanders above and below 0°C. It is not until the winds veer northwest from 31/10Z to 31/15Z, directly offshore, is there a correlation of an increase in wave growth with a drop in air-sea temperature difference. In this case, with strong synoptic background flow, direct correlation of wind speed and wave growth is not clear. However, observations show the steady increase in winds under a strongly destabilized boundary layer and the gradual increase in wave height in a fetch limited environment across the time frame from 31/06Z to 01/12Z.

Diamond shoals light buoy DSLN7 experienced near linear wave growth from 2ft to 16ft under varying winds from southwesterly to northerly at 10-45kts as air-sea temperature differences decreased over the period 31/06Z to 01/18Z (Figures 71, 87-89). From 31/06Z to 31/14Z winds veered from west-southwest to northwest and increased from 10kts to 30kts. Seas over this period built from 2ft to 5ft as air-sea temperature differences dropped from 1°C to -8.5°C by 31/14Z. Winds gradually backed to the west by north and maintained 30kts from 31/14Z to 31/21Z as the wave field built slightly to 5.7ft and air-sea temperature differences leveled off at -8.2°C. After 31/21Z winds veered west-northwest to northwest and increased to 45kts by 01/06Z while seas built to 12ft and air-sea temperature difference dropped to -14.5°C. Wind speeds and air-sea temperature differences began to decrease after 01/09Z as the winds continued to veer to the north-northwest by 01/15Z then northerly at 01/18Z. Wave heights leveled off at 11-12ft for a brief period from 01/06Z to 01/15Z then increased to 16ft at 01/18Z.

Synoptic conditions surrounding buoy DSLN7 from 31/00Z through 02/00Z were highly variable and provide a different insight into the mesoscale forcing of near-shore ocean wave. While not obvious at first analysis, there is good correlation of wind speed with air-sea temperature difference and wave growth. Across the time frame from 31/14Z to 31/21Z a near constant air-sea temperature difference corresponds with a near constant surface wind speed and only slight wave growth, due primarily to wind speed duration and fetch. The periods of strongest air-sea temperature increase, 31/09Z-31/14Z and 31/21Z-01/05Z, yields similar trends of wave growth and wind speed. Of interesting note, the maximum wave height occurs after peak wind speed and maximum air-sea temperature difference. Figures 72 and 74 provide insight to the peak wave height, as there is a significant shift in the peak energy in the spectra at 02/00Z in Figure 74, corresponding with the wind direction tangent to the coastline in the time series of Figure 87. This shift in the wind direction to the right of 340° allows swell generated along the coastal waters of southeast VA to propagate south across DSLN7. Further emphasis of this theory can be seen through empirical wave predictions where under the fetch limited conditions of northwest flow, wind speeds on the order of 80-100kts would be required to produce a similar wave field.

THIS PAGE INTENTIONALLY LEFT BLANK

IV. WAVE MODEL ANALYSIS

Through the analysis of offshore buoy data, discussed in Chapter III, it is clear that during east coast CAO rapid wave growth occurs in fetch limited environments during periods characterized by rapid increases of wind and strong decreases in the air-sea temperature difference. These periods of rapid wave growth occurred in a very short period, sometimes less than four hours. In an attempt to simulate and capture the timing and peak of the wave growth, Wave watch III model simulations were conducted over the exact 48 hour period and nested grids as COAMPS simulations, with the 10 meter wind output from the 81km and 9km COAMPS grid, as well as the same land mask features used for the atmospheric simulations. Comparisons of the 81km and 9km wave field outputs were analyzed and are discussed for the near-shore areas below. Additionally, to simulate accurate near shore forcing, and eliminate errors in the atmospheric forcing, if present, uniform wind fields were generated from buoy observations and replaced the simulated 10m atmospheric wind forcing in the wave model. This uniform wind field was used with Wave watch III to simulate near-shore wave growth in the vicinity of the respective buoy, discussed separately for each case, under near perfect atmospheric forcing. In all three cases, Wave watch III was initiated in a cold-start mode, with no preexisting wave field present. Due to the conditions in which the wave model was initiated, model output for the first 12-14 hours is considered unreliable as the interaction of surface winds on the ocean surface was unrealistic.

A.   CASE I - FEBRUARY 4 - 6, 2002

1.   81 and 9km Grid Wave Simulations

Wave watch III wave simulations, with output every two hours, for the period 04/00Z-06/06Z were conducted for both the 81km and 9km COAMPS atmospheric forcing over the 9km gridded area. Over the entire time period, wave growth for both model grids were in good agreement with the environmental forcing provided from COAMPS. Under moderate westerly wind conditions, the wave field displayed the

largest errors as compared to the observed data, along coastal regions during the initial model output times from 04/00Z-04/16Z (Figures 90-94) where the errors in the wind speed were less than 10kts and directional errors were less than 20 degrees. The wave field heights over this time period eroded offshore with simulated wave heights of less than two meters for all four buoys. While the wave field prediction for the near-shore buoys had errors of less than 1 meter from 04/00Z-04/18Z, the wave field simulation for the offshore buoys had errors approaching 2 meters, nearly a 50% error in the significant wave height. While the errors in the initial output times of the wave model can be attributed to multiple sources, the errors from 04/00Z-04/16Z were predominately a result of the speed and directional differences in the forcing provided by the atmospheric model, the cold-start of the wave model, and the lack of a preexisting wave field.

From 04/18Z to 05/12Z, simulated wave heights grew across the domain with the max occurring at all four buoys near 05/12Z (Figures 95-99). The two model simulations of the significant wave height began to separate and show differences in coastal wave growth starting at 04/18Z growing to 1.5 meters by 05/00Z then slowly decreasing to near zero by 05/06Z. Differences in the wave model simulations can be easily explained through analysis of the atmospheric 10m wind fields. At 04/18Z the COAMPS 81km and 9km wind fields (Figure 100) along the coastal region show significant differences in the forcing provided to Wave watch III. At 04/18Z, wind speed errors of 5-10kts and directional errors of 30 degrees translated directly into the errors seen in Figures 95-99 of the wave field. For the time period from 04/16Z-05/00Z, the 81km wind fields indicated a more westerly wind than did the 9km wind field. This variation in the wind direction effectively increased the 81km wave simulation fetch for the wind forcing on the ocean waves by nearly 30 percent. Fetch and surface stress are the two important components to wave growth. With the 81km wind field effectively providing a more fetch favorable (increased) wind trajectory for wave growth it was not surprising to observe the 81km wave field begin to grow coastal prior to the 9km wave field. After 05/00Z, the 81km and 9km wind fields begin to show indiscernible differences. It is also during this time period that the differences between the wave field simulations begin to decrease, and by 05/06Z the 81km and 9km wave simulations are nearly superimposed on each other and continue to grow along coastal regions through 05/12Z. From 05/12Z-06/00Z significant

28

wave height simulations began to decrease along the coastal regions as the atmospheric forcing across both grids begins to weaken.

2. Observed DSLN7 Buoy Wave Simulations

From 04/00Z-06/06Z observed hourly wind data for DSLN7 was obtained from NDBC and utilized as the atmospheric forcing in Wave watch III. Wave simulations with this atmospheric forcing were quite good, nearly eliminating all of the error in significant wave height field surrounding DSLN7 (Figure 101). Through the comparison and analysis of the 81km and 9km 10m wind fields from COAMPS and the observed buoy wind direction and speed profiles from DSLN7 (Figures 34-35) it is clear that the observed data has greater directional and speed variability and the onset and duration of stronger winds is much earlier and longer, respectively, in the observed data. The rapid increase in wind speed observed by the buoy began by 04/18Z while the increase in the modeled wind fields did not occur until 05/00Z. The product, or result, of the delay in the onset of increased winds is seen as the delay in the time of the maximum significant wave height analyzed in the 81km and 9km wave simulations above, and is clearly seen in Figure 101. These errors in simulated wind speeds from the environmental model have significant impacts in the correct modeling of the resultant wave field. The difficulty in accurately modeling wave fields is compounded in the near-shore environment where the effective fetch can be dramatically altered with a shift in the wind direction of 10 degrees or more. However, in this case minor variations in wind directions during the height of the CAO did not greatly effect the fetch as the wind direction was nearly perpendicular to the coastline. The wind direction shifts have the most effect on the fetch in offshore oblique wind angles.

B. CASE II - MARCH 5-7, 2001

1. 81 and 9km Grid Wave Simulations

Wave watch III wave simulations, with output every two hours, for the period 05/12Z-07/18Z were conducted for both the 81km and 9km COAMPS atmospheric forcing over the 9km gridded area. Throughout the model simulation, wave fields generated by Wave watch III were in good agreement with COAMPS provided forcing.

Across the entire simulation period, differences between the COAMPS 81km simulation and the 9km simulations were less than 10 degrees of wind directional error and 5kts or less error in wind speed along the coastal areas of N.C. south of Cape Hatteras. As a result wave field simulations from the 81km and 9km grids are nearly identical in these regions with differences between the two simulations of less than 0.3 meters throughout the entire period.

From 05/12Z through 05/18Z, sub-gale winds were from the southwest to west in the frontal zone flow, and then the winds veered to west-northwest by 05/18Z. The 81km and 9km wave height simulations along coastal regions responded appropriately to these variable wind conditions by eroding to near 1 meter by 06/00Z while the offshore wave heights built to over 3 meters by 05/18Z while remaining in the southwesterly flow. From 05/18Z to 06/16Z simulated coastal wave height grew to between 2-3 meters by 06/12Z then maintain through 06/16Z as the west-northwest winds increased to gale force by 06/12Z (Figures 102-105). As winds increase to strong gale from the northwest by 06/21Z, simulated wave fields begin to grow along the coastal regions reaching a maximum of near 3 meters in the vicinity of FPSN7 by 07/04Z (Figure 106). Wave heights gradually decrease to near 2 meters along coastal regions after this time as the northwest winds slowly weaken to sub-gale through 07/12Z (Figure 107).

2.   **Observed FPSN7 Buoy Wave Simulations**

From 05/12Z-07/18Z observed hourly wind data for FPSN7 was obtained from NDBC and utilized as the atmospheric forcing in Wave watch III. As in the previous case, the buoy forced wave simulation was very accurate, yielding errors when compared to observed significant wave height of less than 0.5 meters from 06/03Z through 07/18Z in the area surrounding FPSN7 (Figure 108). From 05/12Z through 06/00Z simulated wave height gradually decreased to near one meter under variable wind conditions (Figures 56-57), with a wave height time series profile similar to that seen in the 81km and 9km simulations. From 06/00Z to 07/18Z, the buoy simulated significant wave height field grows and decays in very good agreement with the observed significant wave height time series while there is an obvious lag in the 81km and 9km growth rates and timing of the two observed max events that occurred at 06/09Z and 06/18Z. The 81km and 9km simulation time series for FPSN7 indicated a max wave height event at 06/14Z

and 07/03Z, a 5 to 9 hour time lag. Observed wind speeds at Frying Pan Shoals increased to gale force by 06/09Z, a brief period of sub-gale at 06/12Z and then another increase to strong gale by 06/15Z (Figures 56-57). These correlate well with the observed significant wave height time series. As discussed above, the COAMPS provided wind fields for both the 81km and 9km grids depict an obvious error in the onset of stronger northwest winds with the two maximum simulated wind events occurring at 06/12Z and 06/21Z. While there is little directional error between the observed and simulated wind fields, the delay in the onset of strong winds depicted in the COAMPS wind field is the dominate source of error that translated directly to the delay in wave growth, causing errors in significant wave height to grow to over 1 meter.

C.   CASE III - MARCH 31-APRIL 2, 1997

1.   81 and 9km Grid Wave Simulations

Wave watch III wave simulations, with output every two hours, for the period 31/00Z-2/06Z were conducted for both the 81km and 9km COAMPS atmospheric forcing over the 9km gridded area. Over the entire time period, wave simulations were in good agreement with the provided environmental forcing. Under veering wind conditions associated with the passage of the cold front discussed in Chapter III, section c, a comparison of the 81km and 9km simulated wave fields indicated the largest errors between the two simulations occur from 31/00Z to 31/18Z. In post-frontal northwesterly flow from 31/18Z-02/00Z, simulated wave fields grow in the offshore waters to a maximum height of 6 meters.

In the vicinity of DSLN7, both simulated coastal wave fields, grow from 1 meter at 31/18Z (Figure 109) to near 3 meters at 01/14Z (Figure 110) under northwesterly flow that gradually increases to gale force by 01/03Z. The wave fields begin to gradually erode after 01/14Z to near two meters by 01/18Z (Figure 111) as the environmental forcing of both the 81km and 9km wind field weaken to sub-gale force and maintain northwest direction. After 01/18Z and through the end of the simulation period, the 9km wave simulated significant wave heights begin to rapidly increase along the coastal regions of N.C. under near storm force northwesterly winds. Errors between the 81km

and 9km wave heights grow to one meter as the magnitude of the environmental forcing of the two simulations diverges. With nearly no difference in wind direction between the two COAMPS provided forcing, the 9km wind speeds increase to gale force by 01/21Z then near storm force by 02/00Z. The 81km wind speeds are significantly weaker, increasing to gale force northwest of DSLN7 and sub-gale in the remaining coastal regions by 01/21Z, increasing to gale force throughout the area by 02/00Z. Wind speed differences between the two environmental simulations approach 25kts along near coastal regions over the time period of 01/18Z to 02/00Z. In Case I, near-shore wave growth under variable wind directions yielded different wave growth patterns. In this case differences in wind directions were not present, while wind speed errors approached nearly 50 percent of the speed. This wind speed error between the simulated 10m wind output from the two grids is directly responsible for the variability in the growth rates of the simulated near-shore wave fields.

2.   Observed DSLN7 Buoy Wave Simulations

From 31/00Z-02/06Z observed hourly wind data from DSLN7 was obtained from NDBC and utilized as the atmospheric forcing in Wave watch III. Wave field simulation provided by Wave watch III under these conditions were quite good, reducing the significant wave height error to less than one-half meter during locally generated wave fields from 31/00Z to 01/15Z (Figure 112) while errors among all three simulations grow to over one meter in the observed forced wave field and nearly three meters in the 81km and 9km forced wave fields from 01/15Z to 02/06Z.

From 31/00Z to 01/15Z, Figure 112 clearly shows a significant difference between the 81km, 9km and bouy forced wave simulations. The twelve hour lag in the start of the wave growth seen in the 81km and 9km simulations is a direct result of the environmental model lagging behind in the onset of strong winds. In the 81km and 9km COAMPS simulated wind fields surrounding DSLN7, wind speeds begin to approach 30kts by 31/15Z (Figure 113) and maintain 30kts or less through 01/00Z then increase to gale force. Observed data from DLSN7 (Figures 87-88) indicated wind speed of 30kts or greater beginning at 31/09Z, increasing to gale force by 31/18Z, then near storm force by 01/00Z. Directional errors between the three simulations are small, less than 15 degrees, however it is the large speed errors and failure of the environmental model to properly

initialize the onset of strong winds that is the cause for the lag in the wave growth seen in the 81km and 9km wave fields.

From 01/15Z to 02/00Z, errors in the three wave simulations (seen in Figure 112) are evident when compared to the observed significant wave height at DSLN7. Differences in wind speed between observed buoy data and COAMPS simulated wind fields are 5kts or less across this time period. However, wind directional errors between the COAMPS simulated wave fields and the observed buoy data, not seen in the previous 39 hours, begin to arise and approach 25 degrees. Compounding this directional error is the nature of the coastline where the slight variation of wind direction from 325 degrees (simulated wind directions) to 350 degrees (observed wind directions) effectively increased the fetch ten-fold. Over this period, simulated wind fields maintain a northwesterly flow, continuing to limit the fetch of the wind for wave growth. By 01/15Z, observed winds veer from north-northwest to north, becoming tangent to the coastline or slightly onshore, allowing for an increase in the effective fetch, which results in the further growth of the wave through 02/00Z. The wave growth during this period was not completely generated by local wind forcing. The spectral wave energy plot for DSLN7, Figure 74, discussed in Chapter III, section C, indicated that wave growth after 01/12Z through 02/00Z is the result of longer period swell arriving from the north where it was generated in a more fetch unlimited environment. While the buoy simulated wave field indicates wave growth across DSLN7 over this period, the error between this simulation and the observed buoy significant wave height grew to nearly 1.5 meters.

Across the three cases discussed in this research, errors between the buoy simulated wave field and the observed wave field have consistently been less than 1 meter, and typically been 0.5 meters or less. It is in this case that we observed the near coastal wind field to be in a more fetch unlimited environment, allowing for longer period waves to be superimposed on the locally generated wave field as seen in Figure 74. The growth in error between the buoy simulated wave field and the observed significant wave height time series can not be specifically attributed to one source, although the lack of spectral energy in the longer period frequency bins at the initialization of Wave watch III would explain the lack of growth in the simulated wave fields that are produced through longer period processes (fetch unlimited environments).

The failure of Wave watch III to capture this growth in the buoy simulated wave field is not characteristic of the ocean wave model and is predominately caused by the conditions with which we initialized the model.

V. DISCUSSION

Further analysis of the atmospheric observations and wave model simulations have led us to develop a model <u>for the interaction of mesoscale</u> atmospheric processes and rapid wave growth, observed during conditions associated with a gulf stream north wall event. The discussion in this chapter will explain in detail and tie key concepts in the observed and modeled data discussed in the previous two chapters.

A.   WIND DIRECTION AND AIR-SEA TEMPERATURE CONDITIONS

In the three case studies, wind direction was predominately west to northwest during rapid wave growth. While variations existed between near-shore and offshore buoys, rapid wave growth occurred under similar post-cold frontal CAO conditions.

Wind trajectory is critical for the development and onset of a gulf stream north wall event. The angle at which the wind exits the coastline and transits over the relatively warmer coastal waters affects the heat and moisture characteristics of the air parcels. In perpendicular offshore flow, the trajectory of cold dry air parcels have limited exposure and receive less modification from the warm and moist conditions that exist over the western Atlantic coastal waters and gulf stream as compared to a more along shore flow trajectory that would warm and moisten through surface mixing. The perpendicular flow provides for the greatest contrast between the cold, dry air parcels that are moving offshore and the air parcels located over the ocean waters. The air-sea temperature difference (Figure 36) and wind direction profile (Figure 34) of DSLN7 from 2002 clearly illustrates this effect. From 04/22Z to 05/01Z the wind quickly backs from an offshore northwest direction to an oblique, cross-shore, direction. The resultant air-sea temperature difference time series results in a downward negative trend during this period except for a brief period from 04/23Z to 05/00Z where the air-sea temperature difference tends toward an upward positive direction. Similar correlation in the two profiles can be seen in the FPSN7 buoy data from 2002 as well. While the variations in wind direction during the north wall events tend toward the backing of wind and the

relative decrease in the negative air-sea temperature difference, the same effect can be seen when the winds veer more northerly and take on the same relative along shore wind trajectory. The contrast seen in these segments of the profiles are not as clear as the southwesterly flow directions due to the relatively colder coastal waters located to the north along coastal Virginia. It must also be stated that these processes are taking place in localized regions while the larger air mass may also be undergoing synoptic scale modification, and for this reason we are unable to quantify in this research the mesoscale effects observed on wind speed and direction from the localized air-sea temperature differences.

Not directly part of this research, but a factor that directly affects the air-sea temperature difference, is the horizontal surface temperature profile of the coastal waters. As previously discussed, the gulf stream, which is the strongest warm western boundary current in the world was present during the three cases analyzed in this study. It is premature to clearly state what absolute effects the width, intensity and location of the gulf stream have on the air-sea temperature difference profiles, but the fact that a deep warm current was located in and around all four buoys has no doubt enhanced the negative trends observed in the air-sea temperature difference time series. Coupled with the warm current, the shelf waters also play a critical role in the air-sea temperature differences, but the extent is unknown. For near-shore buoys, colder shelf waters have a diminished affect on air parcel temperature modification due to a decrease in heat transfer flux from the ocean, but similarly the smaller the air-sea temperature difference that would occur. In contrast, a warm wide gulf stream current and warm shelf waters would increase the negative air-sea temperature differences, while also increasing positive heat fluxes to air parcels. Clearly these work against each other, but it is interesting to note that in the selection of cases for this research, the strongest north wall events occurred from January to March, when the coastal shelf waters are cool and the climatologically stable Gulf Stream is still present along the coastal regions. To clearly understand the true effects from the structure of the Gulf Stream and the coastal shelf waters, simulations with constant atmospheric forcing with various structures in the gulf stream and shelf water locations would need to be conducted.

The detailed analysis of the buoy time series explains the link between preferred wind directions and a maximum air-sea temperature difference. In the three cases analyzed, both DSLN7 and FPSN7 experienced the largest drops in air-sea temperature differences during wind directions that were between 290 and 310, a perpendicular cross-shore flow. While it would be beneficial to correlate these same preferred wind directions to maximum observed wind speeds, analysis of the time series did not yield such ability.

B.   AIR-SEA TEMPERATURE AND WIND SPEED CONDITIONS

The increases in wind speed during CAO are a result of strong synoptic forcing as well as the localized additive mesoscale forcing resulting from strong destabilization of the boundary layer. The trajectory of the offshore wind is crucial to the modification of the air parcels (ie., air-sea temperature difference) which is linked to increases in wind speed in localized regions where the air-sea temperature difference in maximized. The temperature contrast between the air and sea is maximized under the northwesterly flow for the near shore buoys, which can easily be translated into near surface stability. Under similar synoptic forcing (ie. wind speed), for larger negative values of air-sea temperature difference, the atmosphere will have greater instability. For the three cases discussed in this research, strongly negative air-sea temperature differences resulted in stability in the lower half of the boundary layer to be absolutely unstable (Figure 7). Absolutely unstable conditions during CAO lead to strong vertical mixing of momentum from above, which then forces the larger wind speeds located at elevation to be forced down toward the surface. In absolutely unstable conditions, Figure 64 shows a near uniform wind speed located over the warm coastal waters (right side) while over the land regions (left side) there is an increasing of winds with height. Absolutely unstable conditions cannot exist for any extended period, as the atmosphere will continually mix the instability in the vertical to achieve neutral state. It is important to also notice that during periods of strong air-sea temperature differences there is no observed increase in surface wind speeds. Detailed analysis of the air-sea temperature difference time series from the buoys show that during slow and moderate negative trends air-sea temperature difference time

series, the atmosphere most probable mixed out the instability developed in surface temperature field. In fact, during some instances surface winds occasionally decreased during these periods (Figures 81 and 83, buoy 41001 April 1997 01/03Z-01/12Z). However, it was only during the strongest destabilization periods where air-sea temperature differences dropped at least 1°C per hour that the maximum wind increases were always observed.

C.   WAVE GROWTH

DSLN7 and FPSN7 are located in a near-shore fetch limited environment. In these locations and under offshore wind forcing, wave growth is directly related to the momentum that the surface winds imparts on the ocean surface. From the above discussion, air-sea temperature differences are clearly linked to wind direction and wind speed. Both the wind direction and speed play a critical role in the development, rapid growth, and sustaining of high waves.

Wind direction from the northwest that optimizes air-sea temperature differences and increases in wind speed, also minimizes the dynamic fetch that wave fields experience. For instance, DSLN7 with a west-northwest wind has a fetch of 12.5nmi for the waves and the wave field to grow and propagate to the buoy location. It is also this same direction that the increased effects from mesoscale processes (vertical mixing of momentum) which increased wind speeds occur as a result of the minimizing the modification of air parcel characteristics and the resultant negative air-sea temperature differences. However, for a west wind, DSLN7 has a fetch of 26nmi and for a west-southwest wind a fetch of 43nmi. Under both of these wind conditions, air-sea temperature differences would be minimized and the mesoscale effects in wind speed increase would be reduced. Similar fetch calculations from FPSN7 or any other near-shore buoy would yield similar variability as a result of the irregular coastline.

Under offshore flow, wind speed is clearly the driving force of the near-shore wave growth. The momentum imparted on the ocean surface from the surface wind is the primary mechanism for wave growth. Unlike the conditions of on-shore flow where long period wave fields (swell) may propagate into coastal waters, near-shore wave fields

developed under offshore flow are completely wind driven. Throughout the three cases, the near-shore wind speed time series for FPSN7 and DSLN7 are in phase with the respective significant wave height growth profiles. With that said, and because of the direct relation of wind speed and air-sea temperature difference discussed above, similar relationships of wave growth and air-sea temperature differences can be made. In the buoy time series, maximum wave growth occurs under the strongest negative air-sea temperature decay rates of 1°C per hour.

D.   EFFECTS OF ERRORS IN THE MODELS

The accurate mesoscale modeling of the atmosphere in offshore, strongly unstable conditions is critical to capture the proper growth and peak of the coastal wave field. Wave watch III's primary forcing mechanism for wave growth is the 10m-wind output from the atmospheric model. Inaccuracies in atmospheric forecasting of the winds are directly transposed to errors observed in the wave model output. This is clearly seen from Chapter IV, where wave model simulations failed to properly capture wave growth for DSLN7 (2002 and 1997 case) or FPSN7 (2001 case). It was the small speed and direction errors in the high-resolution model output of the winds that were the primary cause of the errors in the wave model output. For the majority of the time steps in the wave model, errors in the simulated atmospheric wind were 10kts or less in speed and 15 degrees in direction, but at a few time steps errors were 15kts and 40 degrees. It was these minor variations in the surface winds, along with the relationships discussed above that can quickly lead to significant wave height errors, sometimes as much as 200%.   As discussed and illustrated in Chapter IV, under the true atmospheric forcing at the buoys DSLN7 and FPSN7, Wave watch III simulations provided a more accurate and timely significant wave height forecast. These uniformly forced simulations where compared to the simulations conducted with the original forecasted atmospheric data and the result provided great insight as to the location and source of the errors driving the erroneous output in the wave model simulations. When Wave watch III was provided the actual observed winds, it remarkably reduced the significant wave height error to typically less than a half of a meter while the error in the timing of the peak in the wave field was

dramatically reduced to near zero. This "near perfect" wave model simulation clears shows that errors in the atmospheric model are the direct cause of the majority of the near-shore wave field error. While some error still existed under the "near perfect" simulations as a result of the highly non-linear wave processes that occur under strong atmospheric forcing, the present Wave watch III model displays an accurate depiction of near-shore wave growth.

One additional error source that exists in nearly all models and can provide large inaccuracies in the wave model output is the definition of the land-sea boundary. While the land-sea interface was as accurately depicted as possible in the atmospheric and wave model simulations conducted in this thesis (less than 2nmi error), a large error in near-shore significant wave height predictions can exist in coarser resolution models when the land-ocean boundary (land mask) is not properly depicted. The land mask resolution is directly related to the model resolution through grid point spacing. Both atmospheric and ocean operational global models, which typically have a coarser grid resolution than the regional mesoscale models have difficulty resolving the land mask properly. When this occurs, inaccurate wind speeds ingested into the wave model can occur through unresolved mesoscale processes occurring as a result of air-sea temperature differences. Inaccurate wind speeds coupled with inaccurate fetch lengths can lead to significant errors in near-shore wave fields. While it is not the goal of this research to address these errors, forecasters and interpreters of such data should be aware these errors exist.

VI. CONCLUSION

The results of this study provide insight into the coupled forcing between the atmosphere and ocean under highly unstable boundary layer conditions during periods of rapid wave growth.

Specifically this research showed:

1. That large decreases in air-sea temperature difference are linked to increases in surface wind speed and a rapid increase in significant wave height.

2. That rapid wind-wave growth events in a near-shore environment have a preferred wind direction that is nearly perpendicular to the coastline.

3. That small errors in the atmospheric model can lead to large errors in the growth rate and peak of the near-shore wave field.

In the three case studies studied the coarse and fine resolution atmospheric model did not capture all the variability in the observed wind direction and speed at the buoys. In the cases studied and other cases with complex coastlines, the failure of the atmospheric model to capture small-scale variability is a source of wave growth error in the nearshore region. In all three cases, the timing of the event in the simulation lagged the actual event. This lag occurred due to both a lag in the wind forcing in the atmospheric model as well as model resolution. The start of the wave growth in the 81km grid wave simulations compared to the 9km grid wave simulations for all three cases showed a systematic lag. This indicates that the location of grid points is crucial to accurately capture the surface forcing on the ocean waves. With lower resolution model coastal regions, a grid point over in the coarse resolution atmospheric model the inland areas resulted in slower wind speeds on the wave model grid as compared to the over water wind speeds. This one inland grid point reduced the atmospheric model surface wind speeds provided to Wave watch III right along the coast. This effect was reduced for the

higher resolution models for these cases but did not eliminate this lag. Higher resolution models improve near-shore wind depiction and allow for a finer resolution land-mask which if improperly depicted is the largest error source for near-shore wave growth. This study strongly indicates that highly accurate resolution wind fields are required to properly model the wave field.

A. RECOMMENDED RESEARCH

As stated earlier in this work, the Gulf Stream region was specifically examined in this research. The source of warm water that the Gulf Stream supplies is a large factor in the development of the unstable boundary layer during the CAO and should be examined more thoroughly. Effects from the current speed, width, temperature, cold and warm rings, filaments, and primary location all play a role in these rapid wave growth events. To clearly understand the role of the Gulf Stream and these additional effects in these types of events, an analysis of a large sample of case studies is recommended.

A constant struggle for marine meteorologists is the availability of data, or the lack thereof. With just four NDBC buoys and a handful of ship observations available for analysis in the forecasting of the events discussed in this work, it is no wonder that they are inaccurately modeled and forecast. It is strongly recommended that the quality and utility of remote sensed wind and wave data be examined in these cases.

Currently the U.S. Navy's environmental production centers provide high-resolution environmental models to the operational forces. The developers and managers of these models are strongly encouraged to re-think the method in which these models are administered. It is recommended that accurate placement of the mesoscale grids for local wave modeling be taken into account in order to eliminate systematic errors in the output, further enhancing the tactical forecasting support.

APPENDIX A. FIGURES

The following pages of figures are grouped together in this appendix in order to facilitate the reading of this thesis.   The following key can be used in all figures:

COAMPS1	-	COAMPS 81km Grid
COAMPS3	-	COAMPS 9km Grid
COAMPS4	-	WWIII 9km Grid
MM5	-	WWIII 9km Grid
COAMPS5	-	WWIII 81km Grid
MM5c	-	WWIII 81km Grid
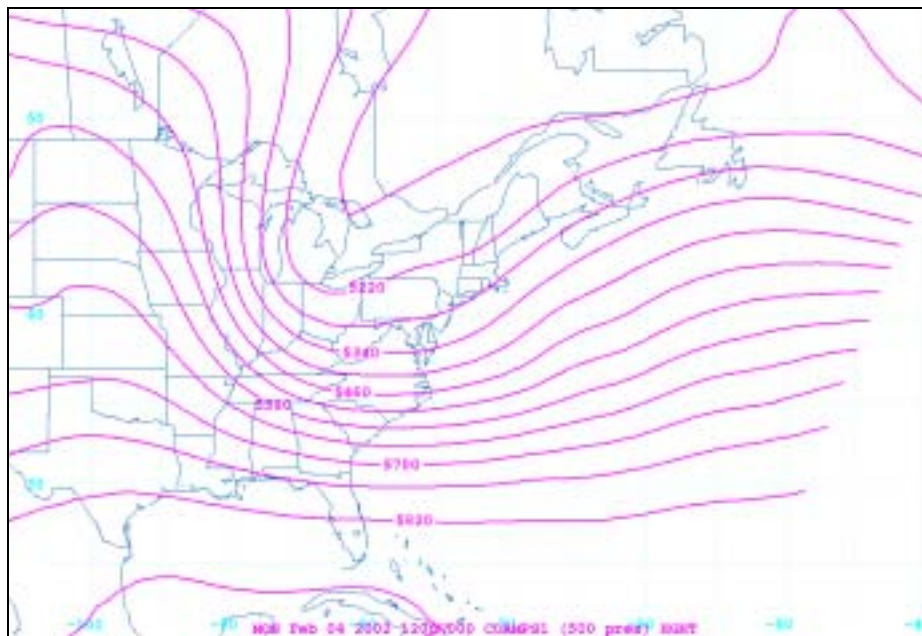
Figure 1. COAMPS 500mb Height Contours (1200Z 04FEB02)
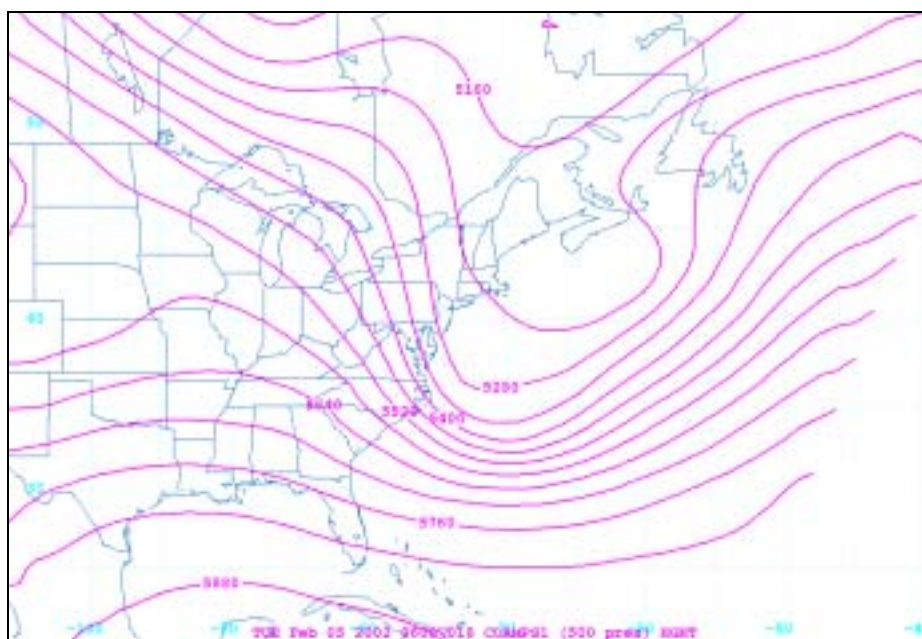
Figure 2. COAMPS 500mb Height Contours (0600Z 05FEB02)
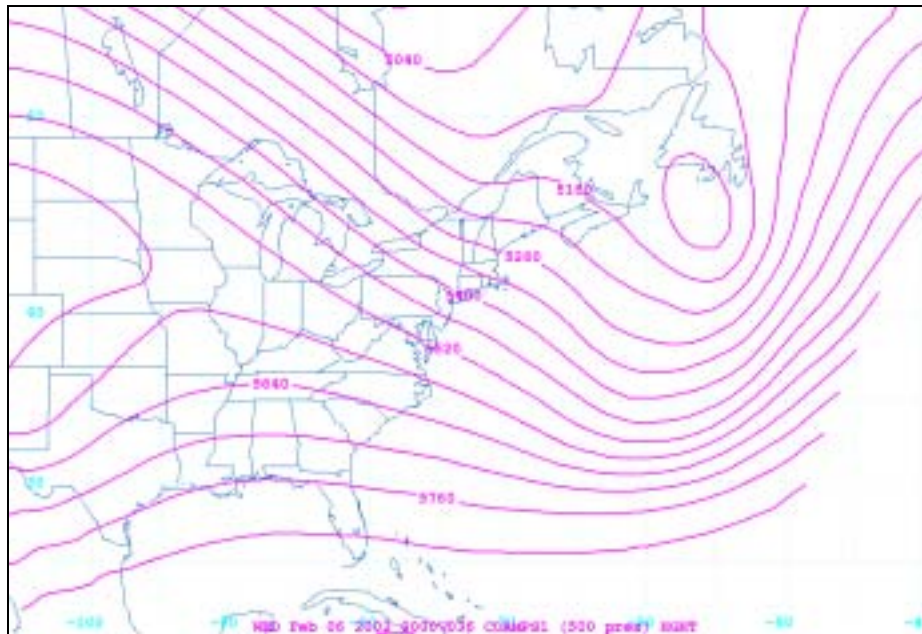
Figure 3. COAMPS 500mb Height Contours (0000Z 06FEB02)
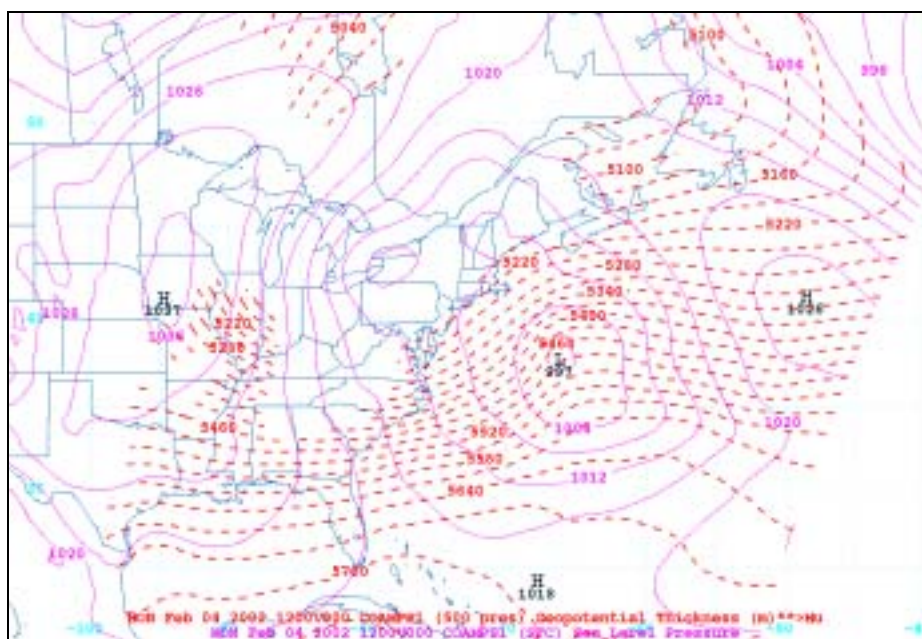
Figure 4. COAMPS Sea Level Pressure and 1000-500mb Geopotential Thickness
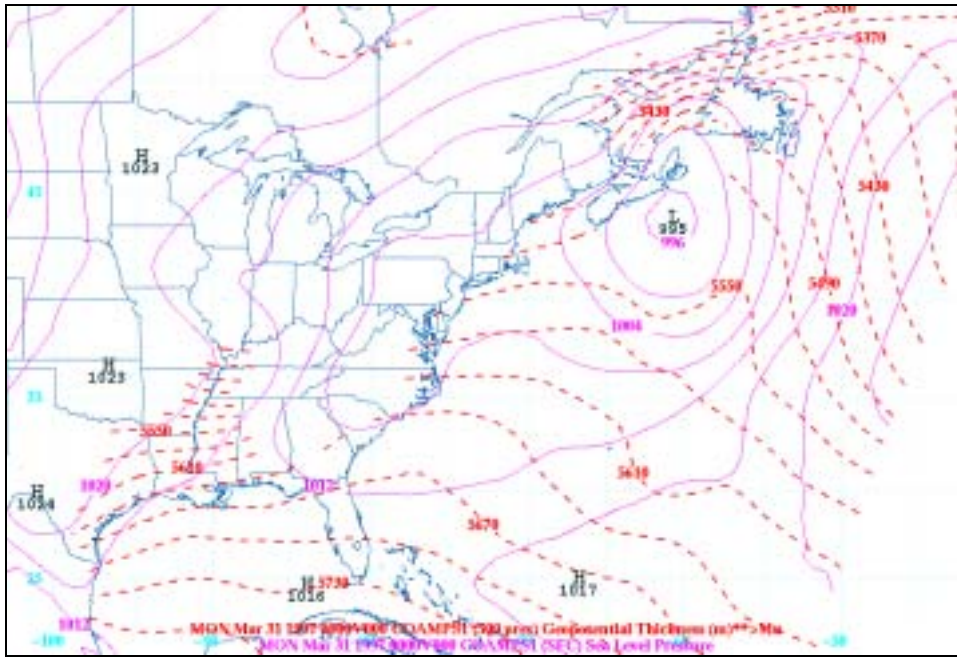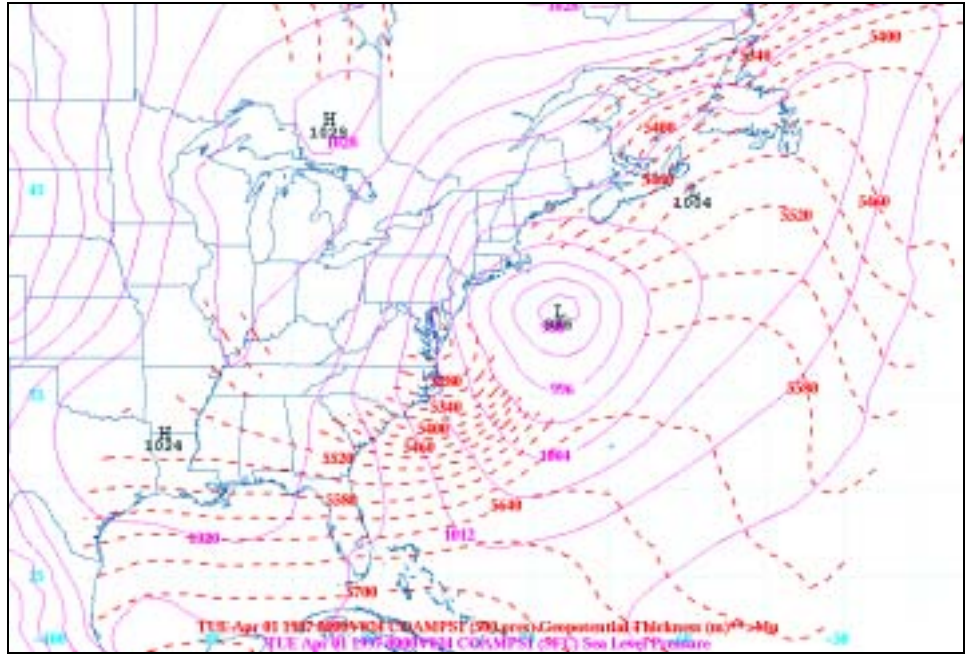Contours (1200Z 04FEB02)
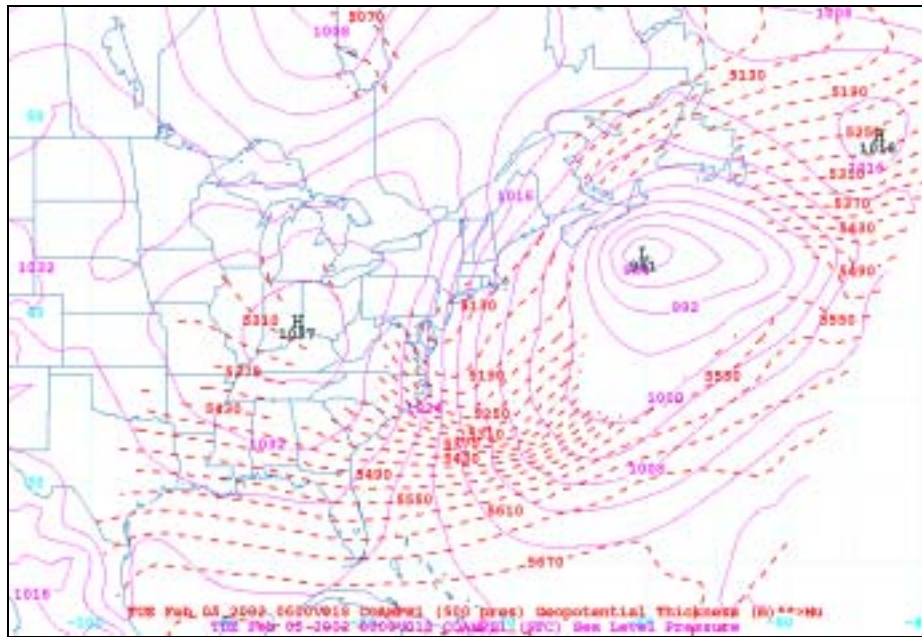
Figure 5. COAMPS Sea Level Pressure and 1000-500mb Geopotential Thickness Contours (0600Z 05FEB02)
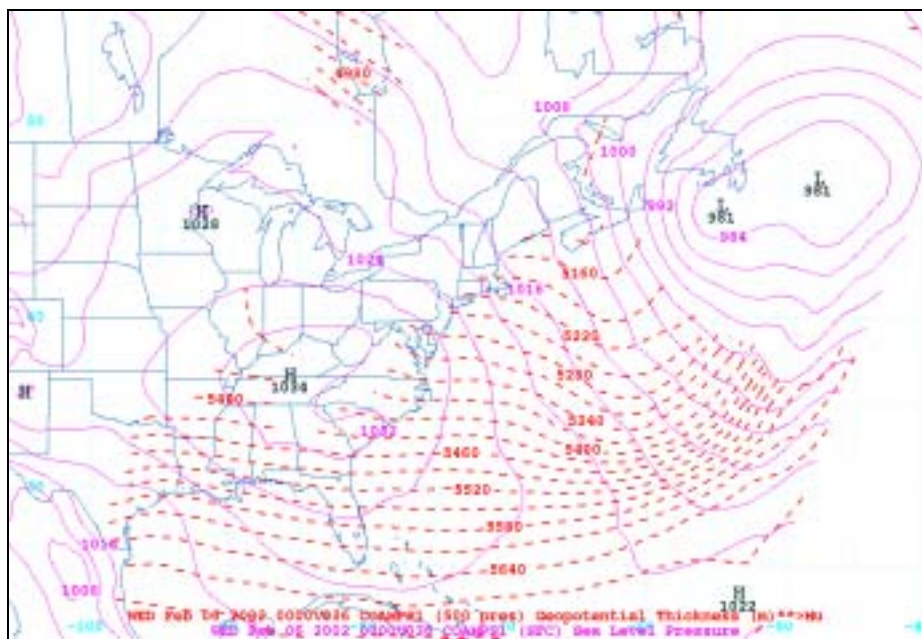
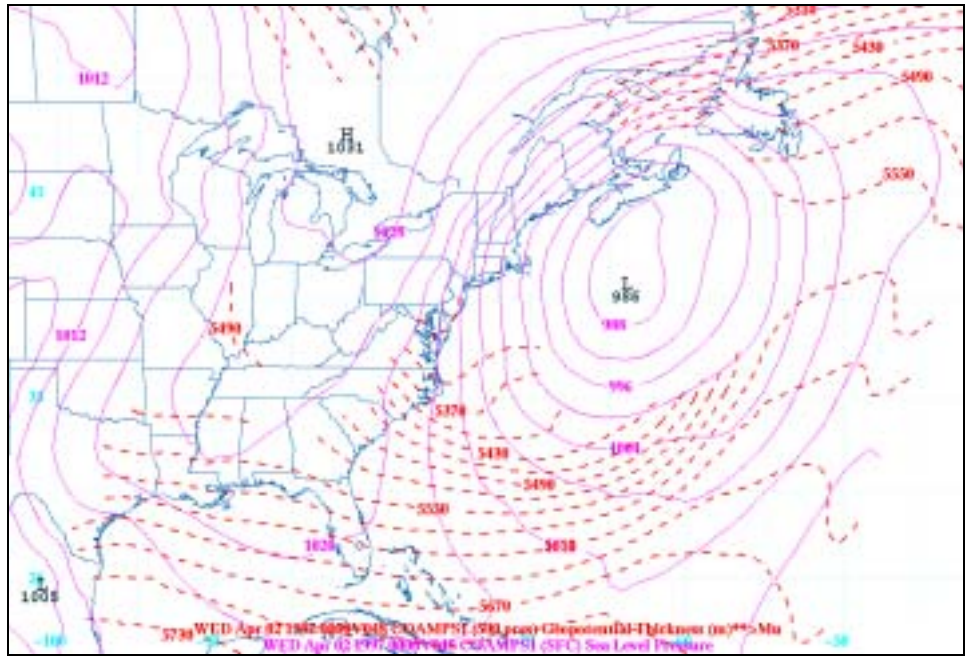Figure 6. COAMPS Sea Level Pressure and 1000-500mb Geopotential Thickness Contours (0000Z 06FEB02)
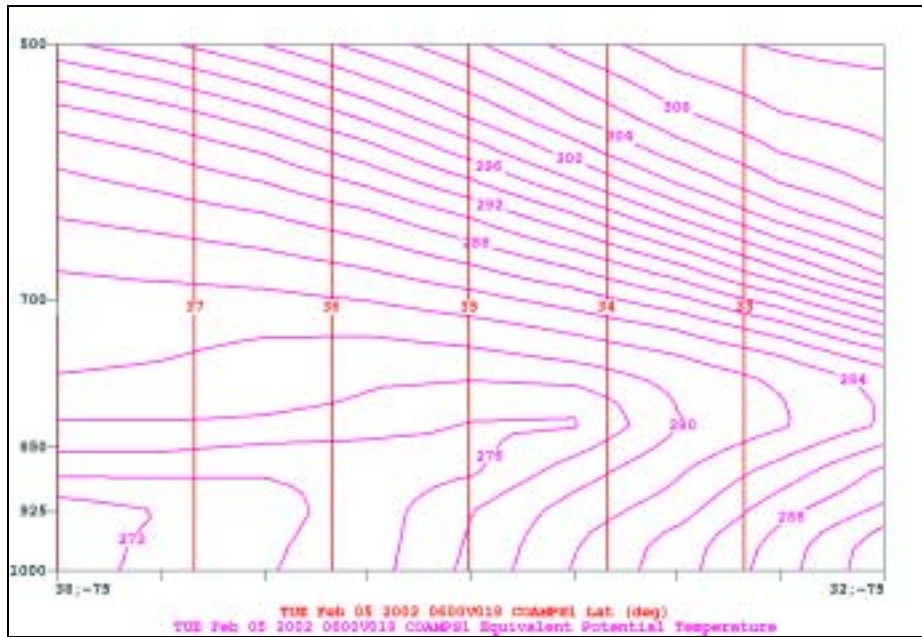
Figure 7. COAMPS Theta-E Vertical Contours and Latitude Across the Gulf Stream
(0600Z 05FEB02)
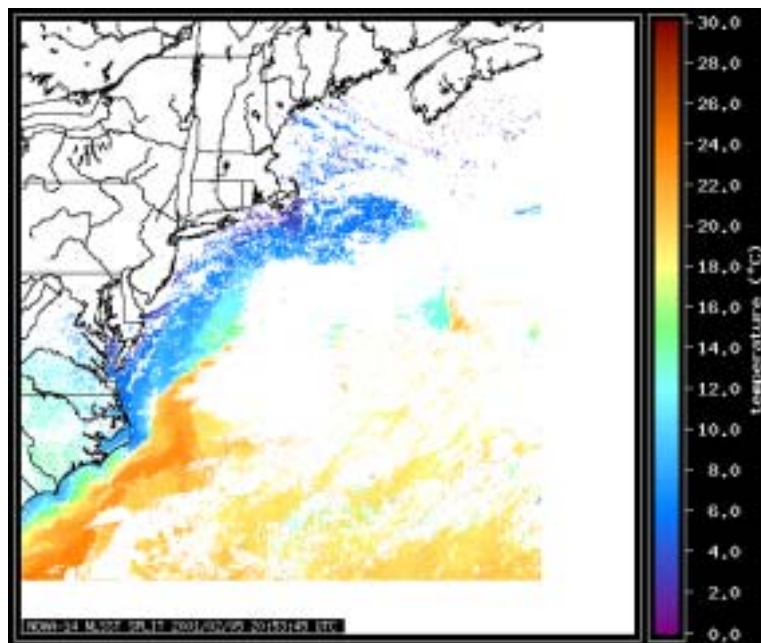
Figure 8. Typical NOAA-14 MCSST Image of the Gulf Stream During the Winter
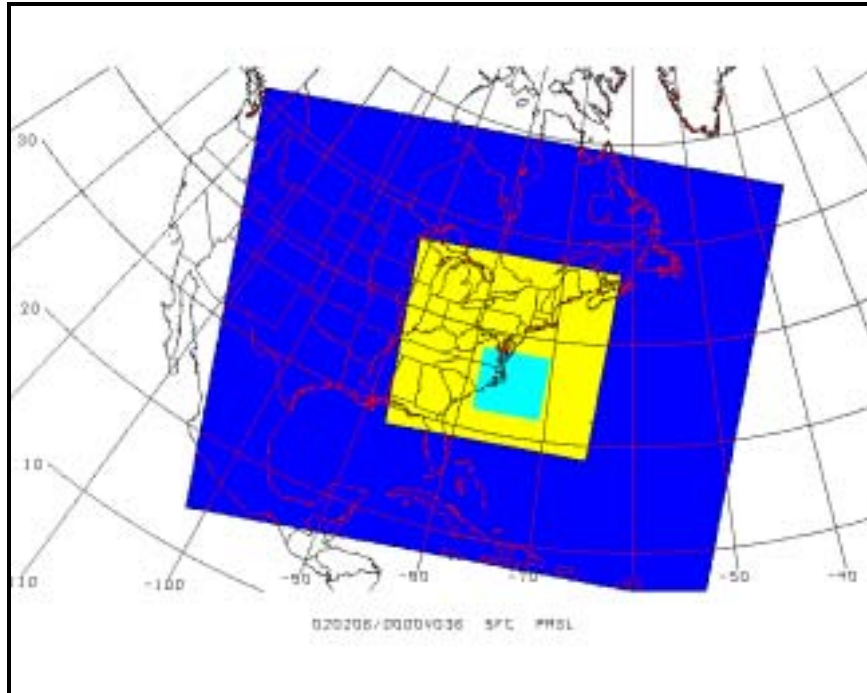
Figure 9. COAMPS 81, 27 and 9 km Nested Grids Used for the Experiment
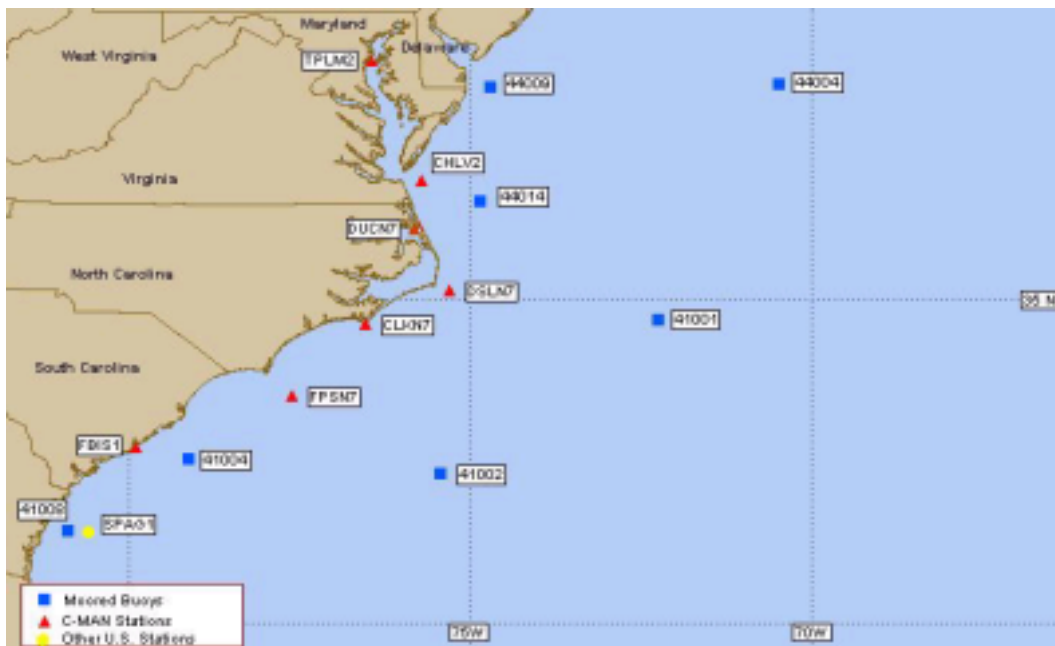
Figure 10. NDBC Buoy Locations Along the Mid-Atlantic Coast
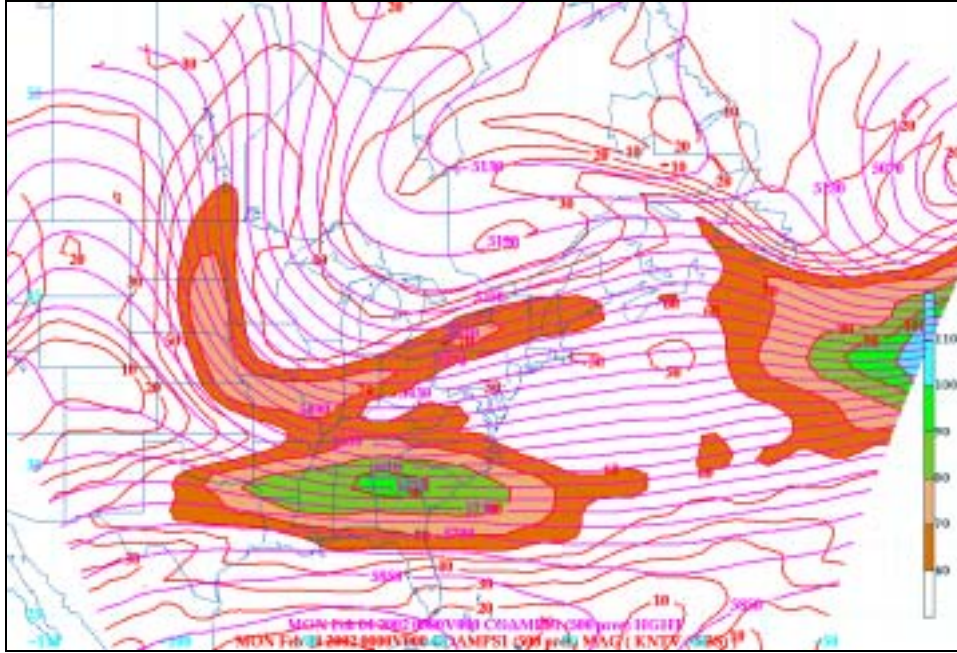
Figure 11. COAMPS 500mb Height Contours and Isotachs (0000Z 04FEB02)
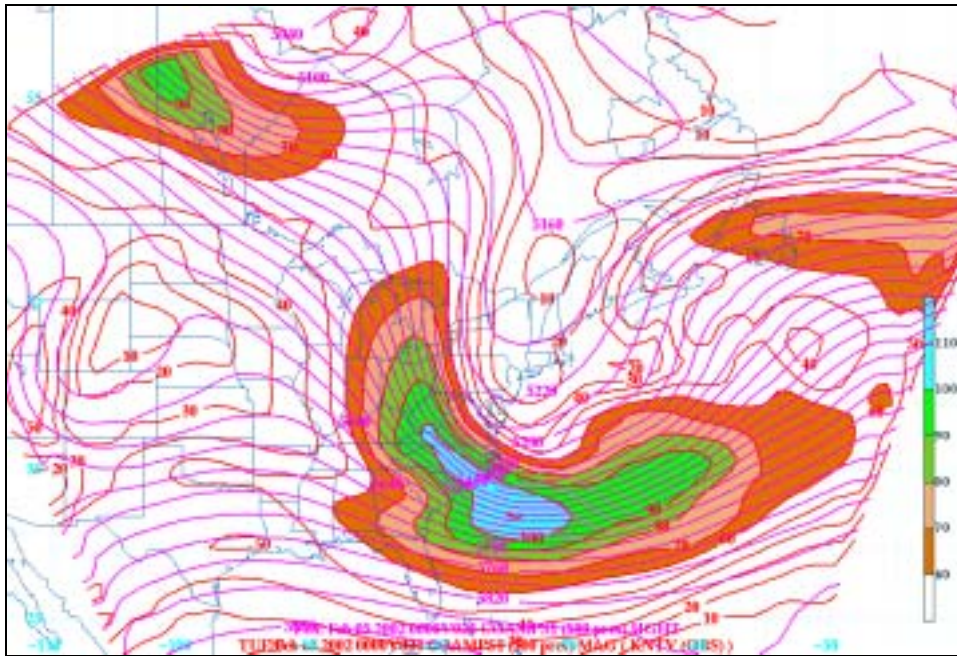
Figure 12. COAMPS 500mb Height Contours and Isotachs (0000Z 05FEB02)
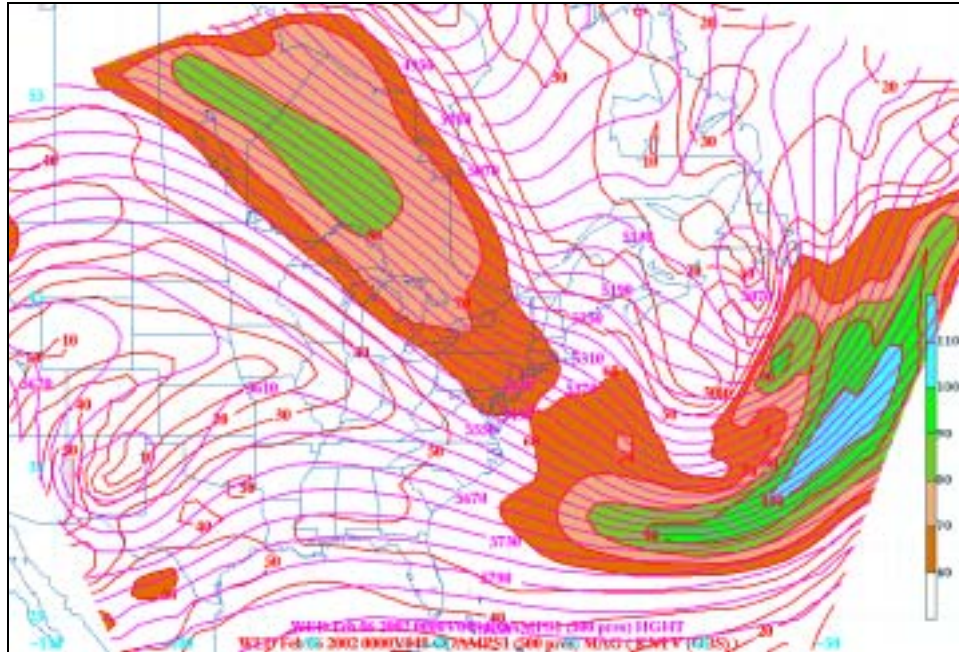
Figure 13. COAMPS 500mb Height Contours and Isotachs (0000Z 06FEB02)
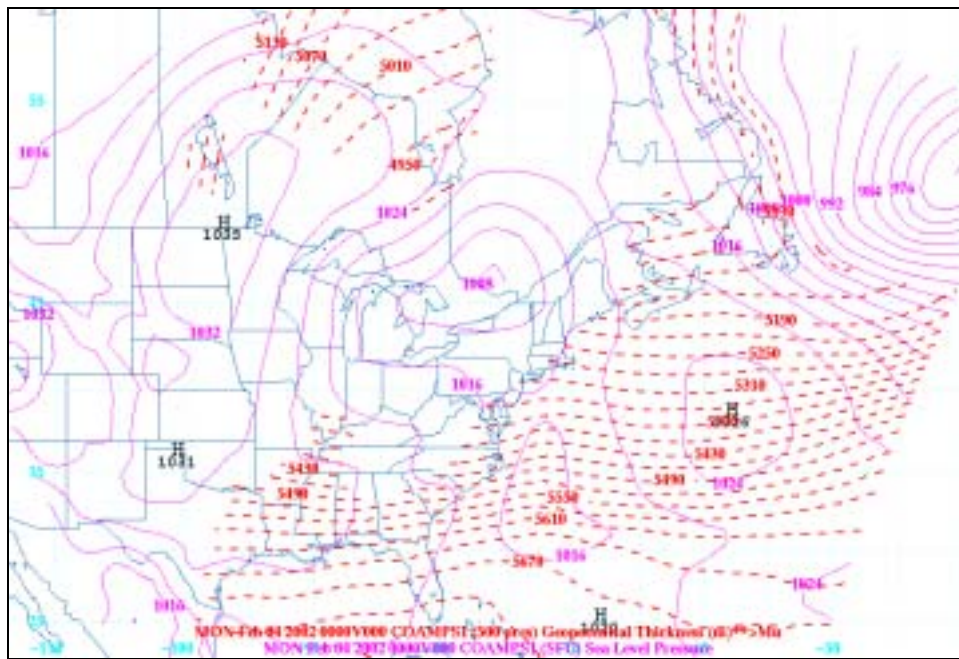
Figure 14. COAMPS Sea Level Pressure and 1000-500mb Geopotential Thickness
Contours (0000Z 04FEB02)
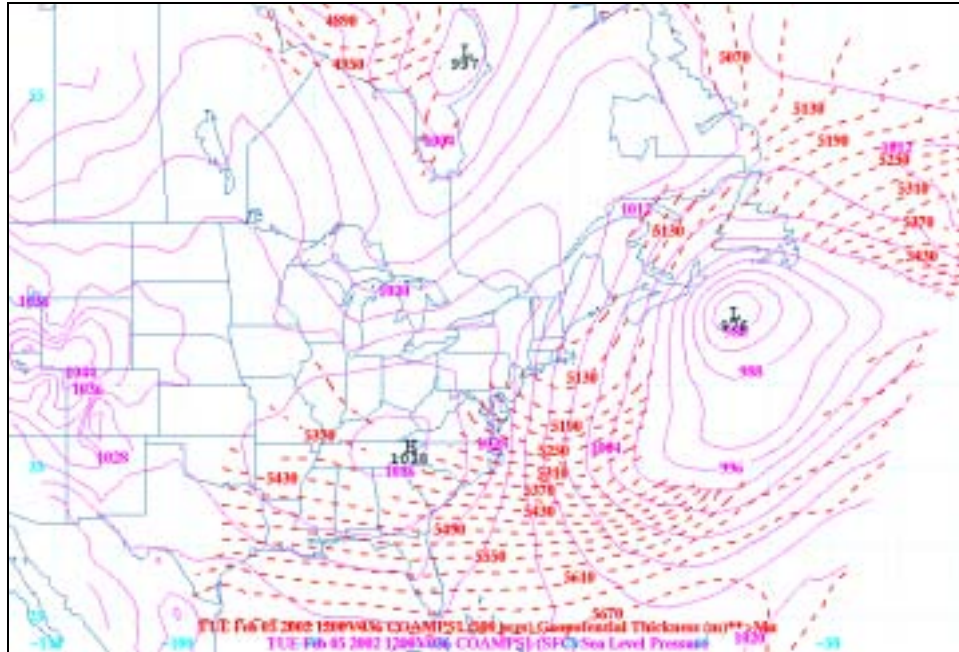
Figure 15. COAMPS Sea Level Pressure and 1000-500mb Geopotential Thickness Contours (1200Z 05FEB02)
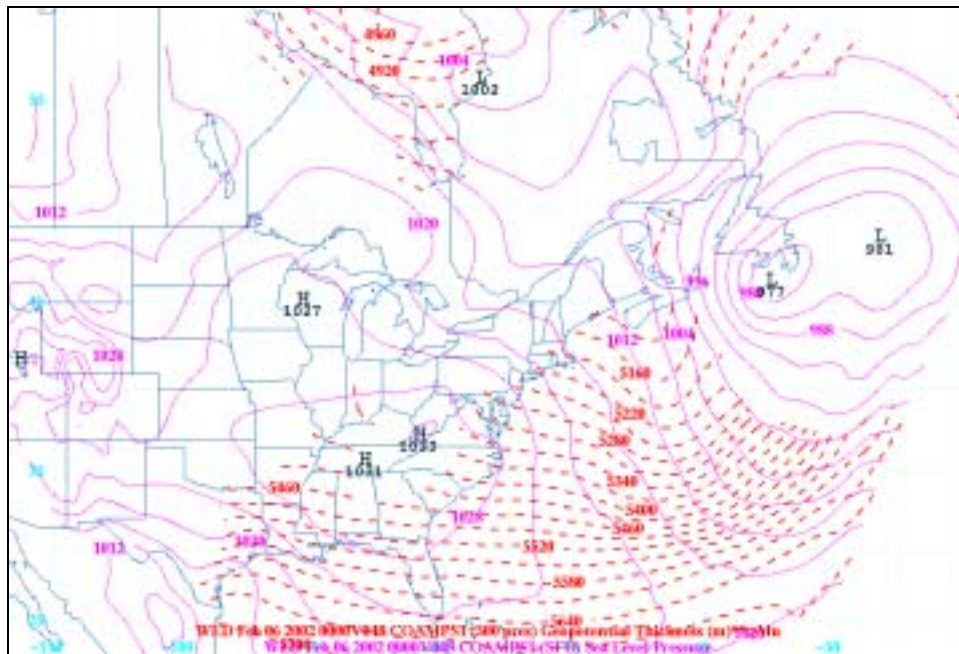
Figure 16. COAMPS Sea Level Pressure and 1000-500mb Geopotential Thickness Contours (0000Z 06FEB02)
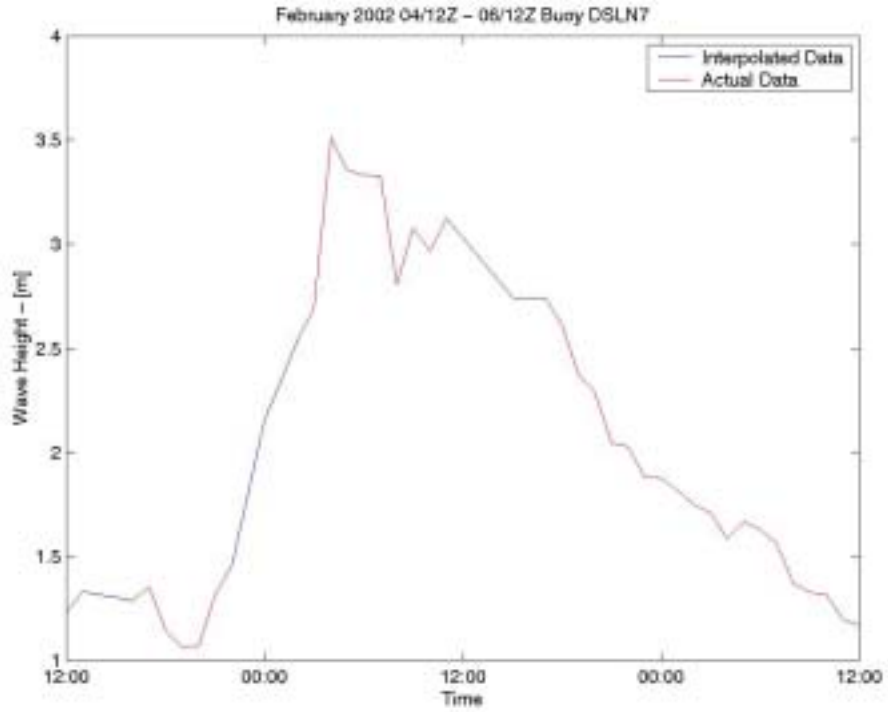
Figure 17. Buoy DSLN7 Significant Wave Height (February 2002 04/12Z-06/12Z)
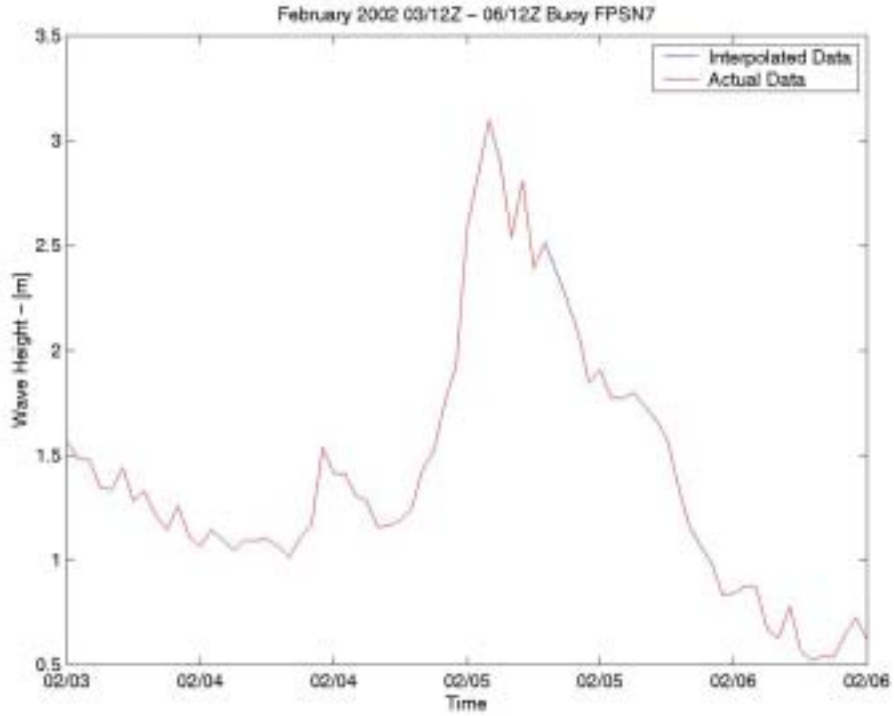
Figure 18. Buoy FPSN7 Significant Wave Height (February 2002 03/12Z-06/12Z)

52
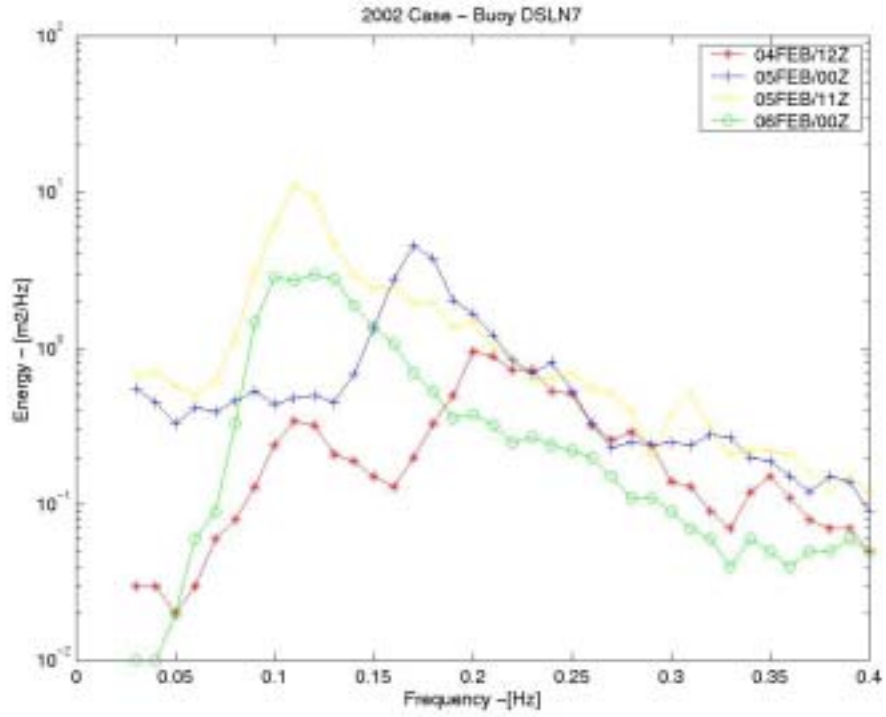
Figure 19. Buoy DSLN7 Wave Energy Spectra (February 2002)
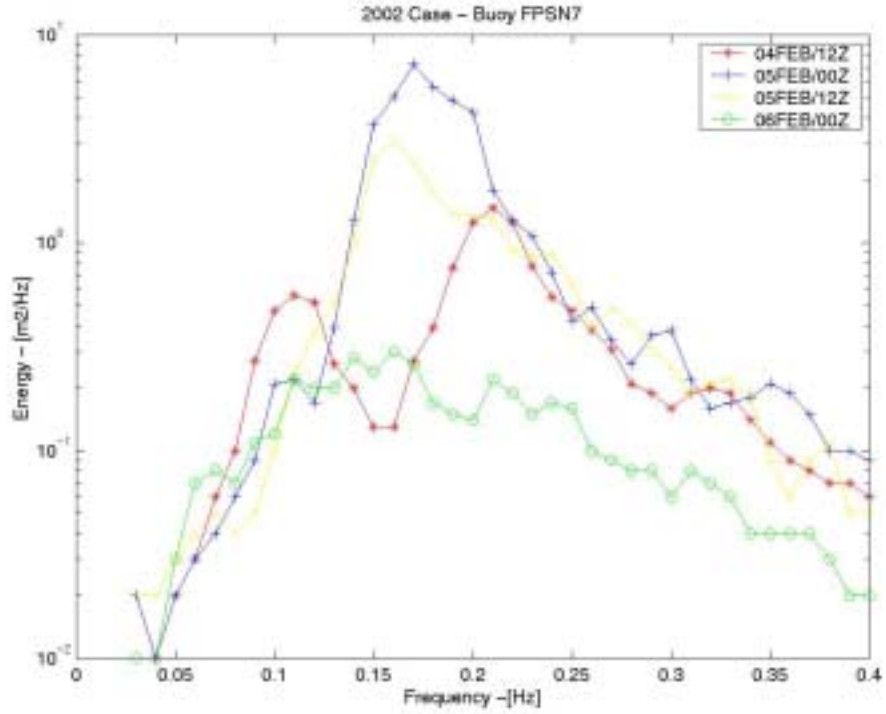
Figure 20. Buoy FPSN7 Wave Energy Spectra (February 2002)

53
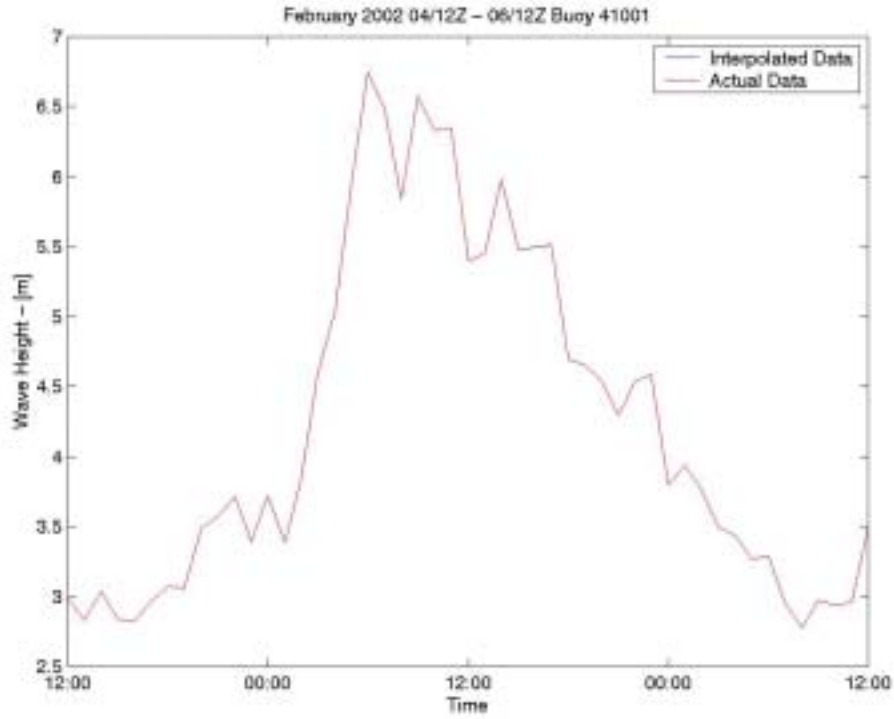
Figure 21. Buoy 41001 Significant Wave Height (February 2002 04/12Z-06/12Z)
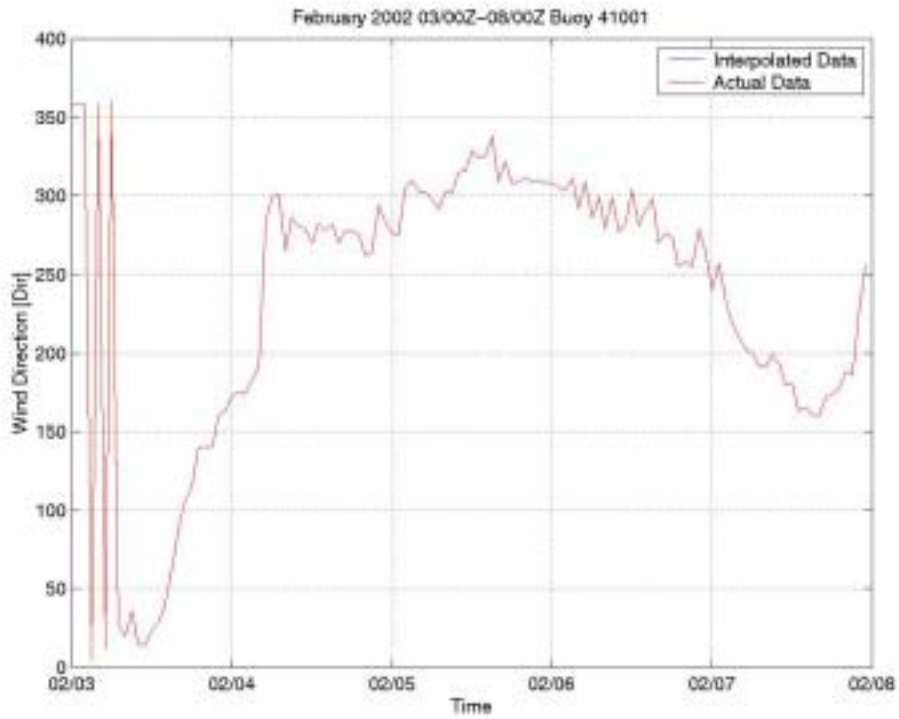
Figure 22. Buoy 41001 Wind Direction (February 2002 03/00Z-08/00Z)
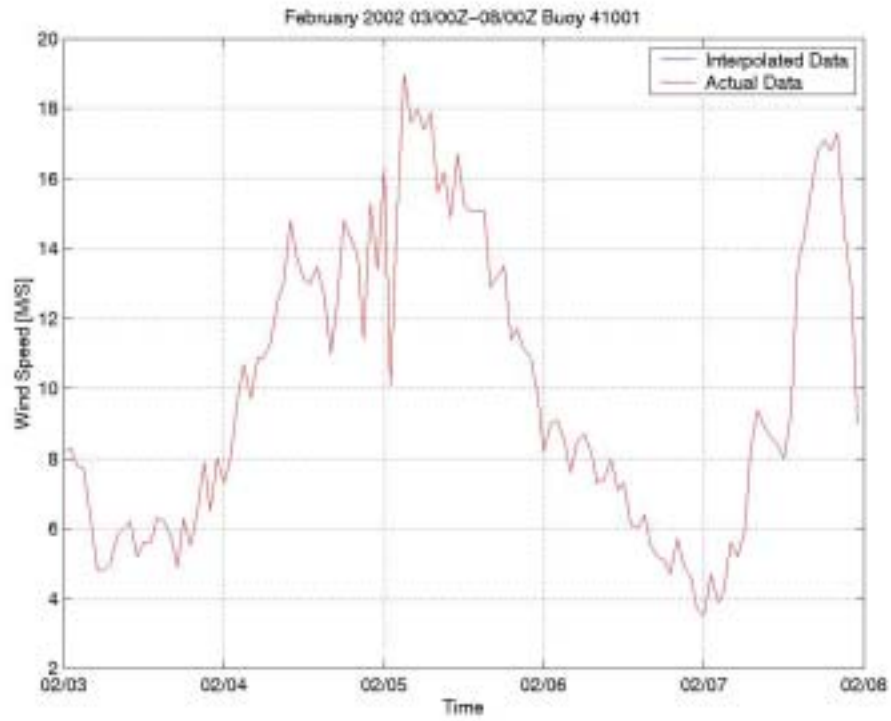
Figure 23. Buoy 41001 Wind Speed (February 2002 03/00Z-08/00Z)
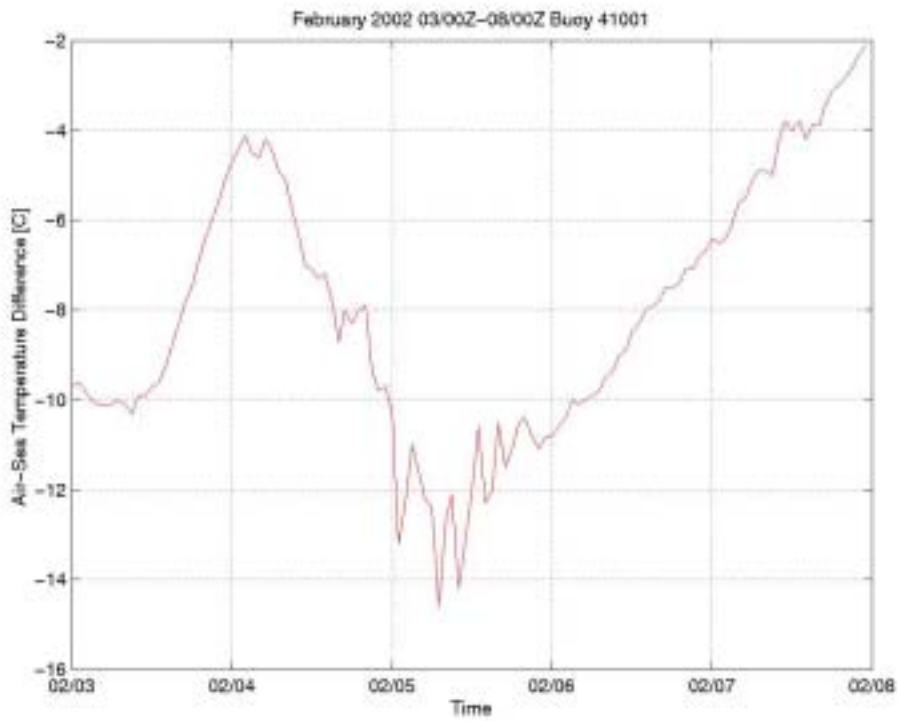
Figure 24. Buoy 41001 Air-Sea Temperature Difference
(February 2002 03/00Z-08/00Z)
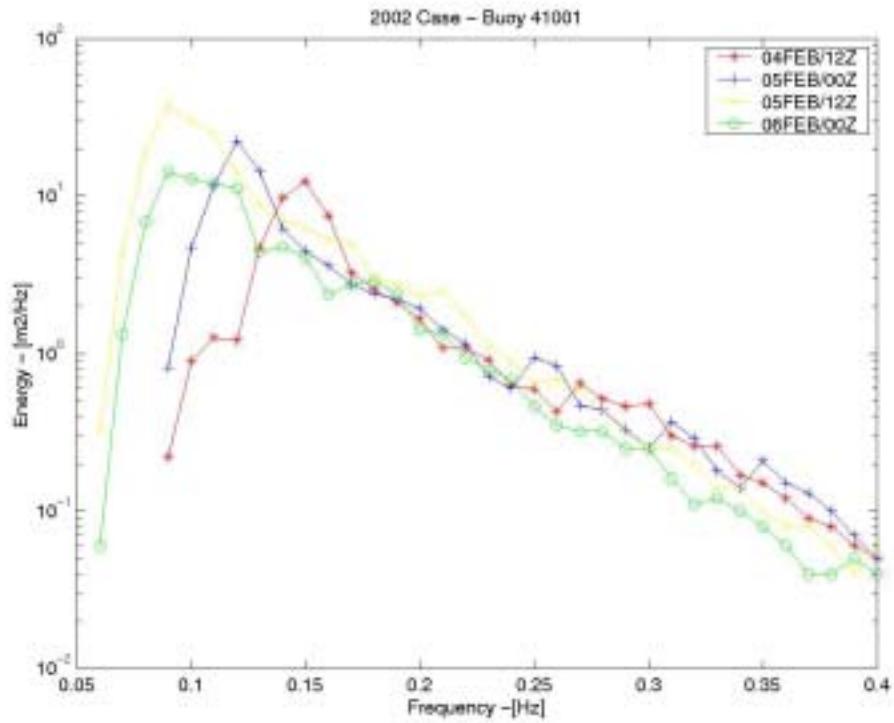
Figure 25. Buoy 41001 Wave Energy Spectra (February 2002)
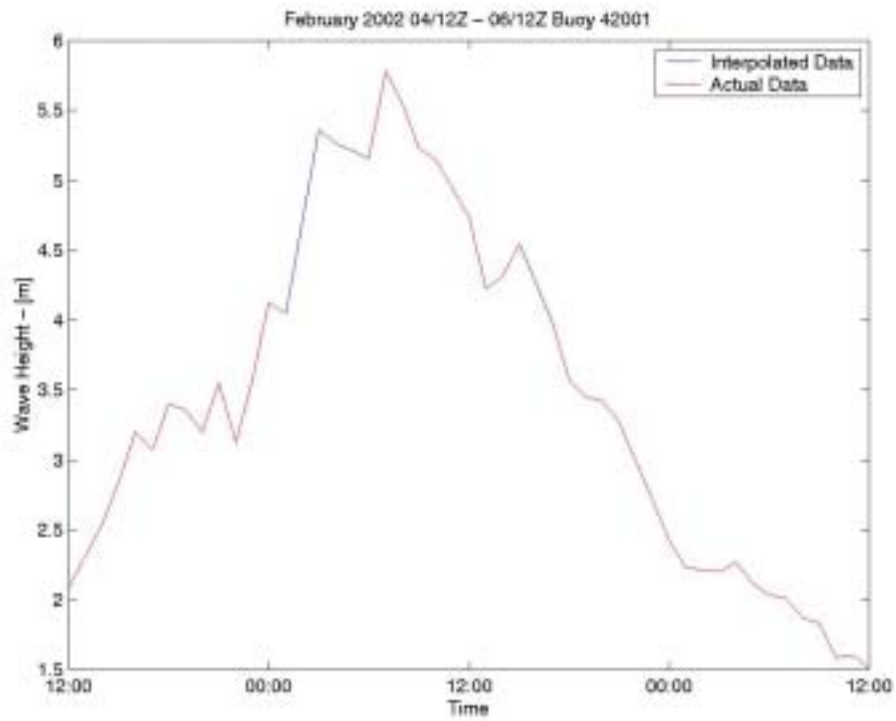
Figure 26. Buoy 41002 Significant Wave Height (February 2002 04/12Z-06/12Z)
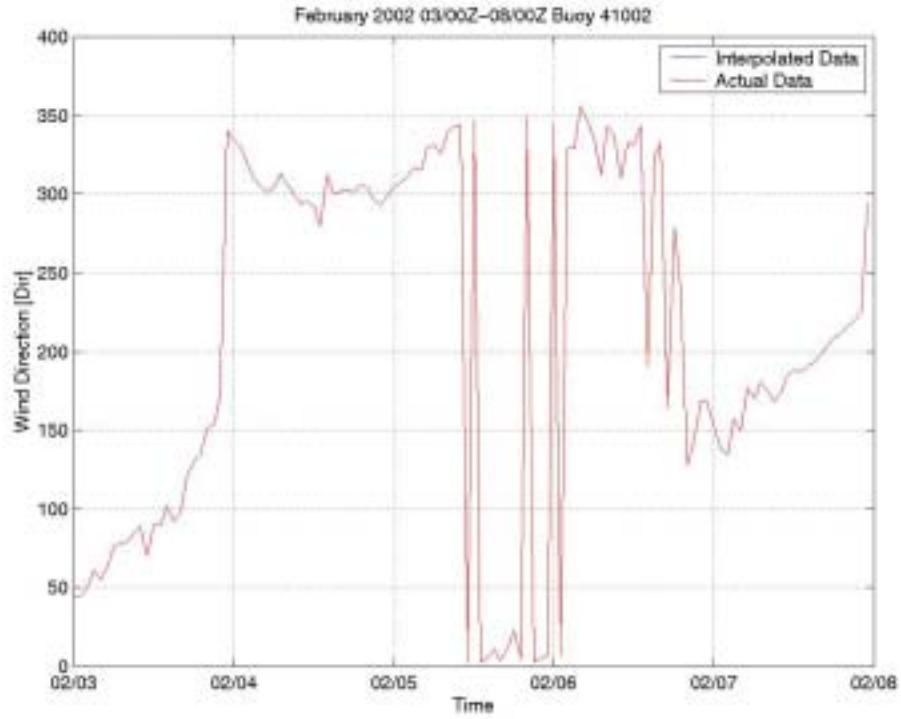
Figure 27. Buoy 41002 Wind Direction (February 2002 03/00Z-08/00Z)
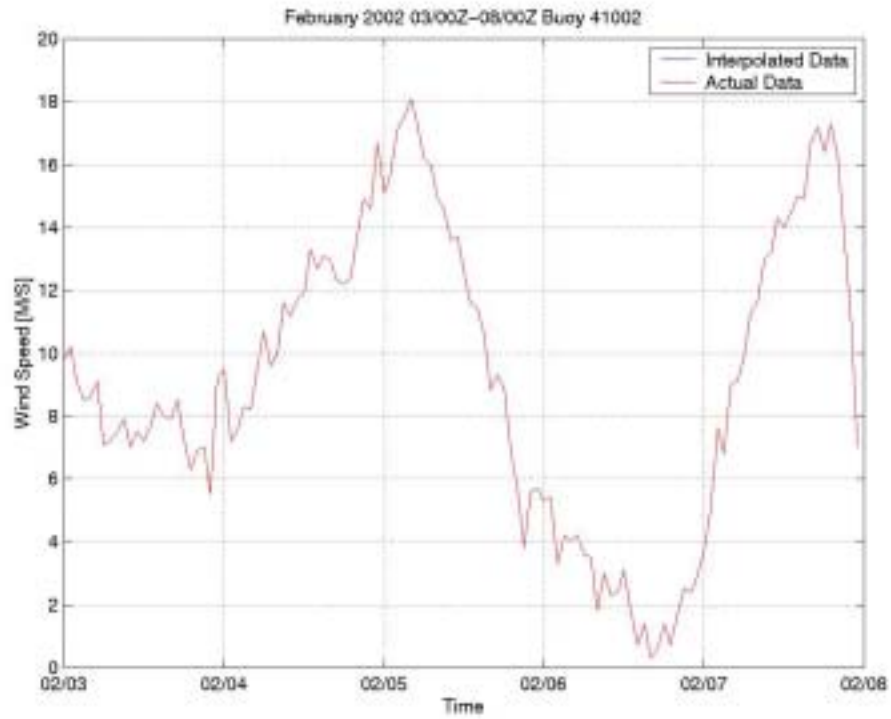
Figure 28. Buoy 41002 Wind Speed (February 2002 03/00Z-08/00Z)

57
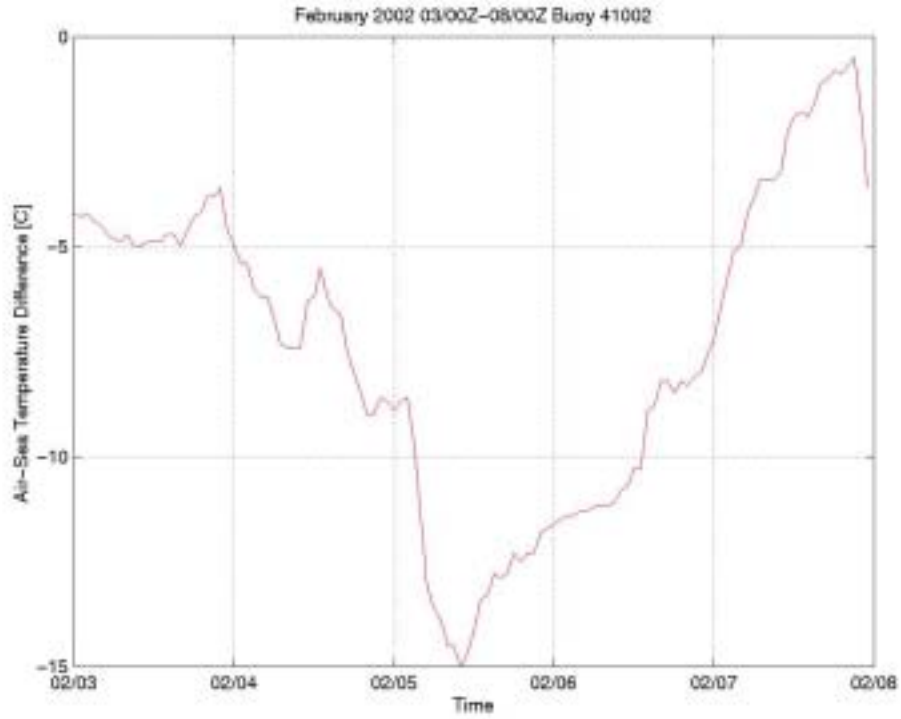
Figure 29. Buoy 41002 Air-Sea Temperature Difference
(February 2002 03/00Z-08/00Z)
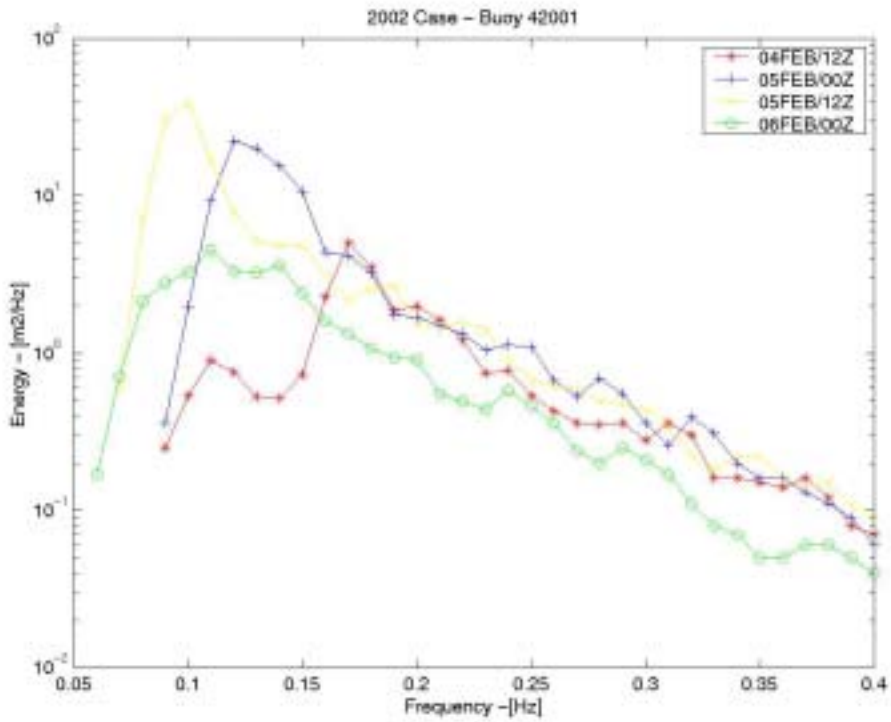
Figure 30. Buoy 41002 Wave Energy Spectra (February 2002)
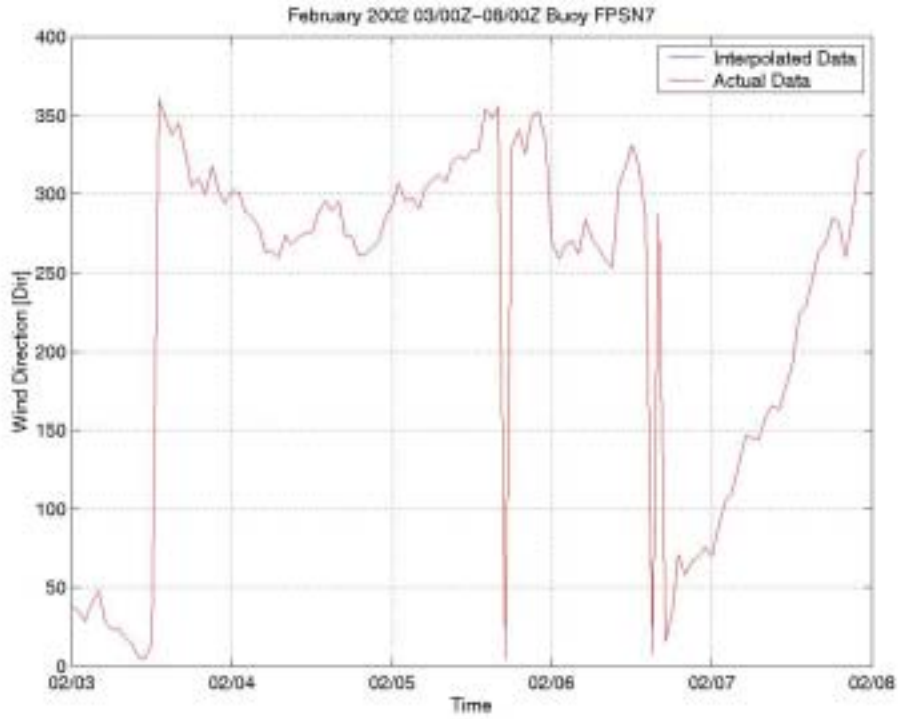
Figure 31. Buoy FPSN7 Wind Direction (February 2002 03/00Z-08/00Z)
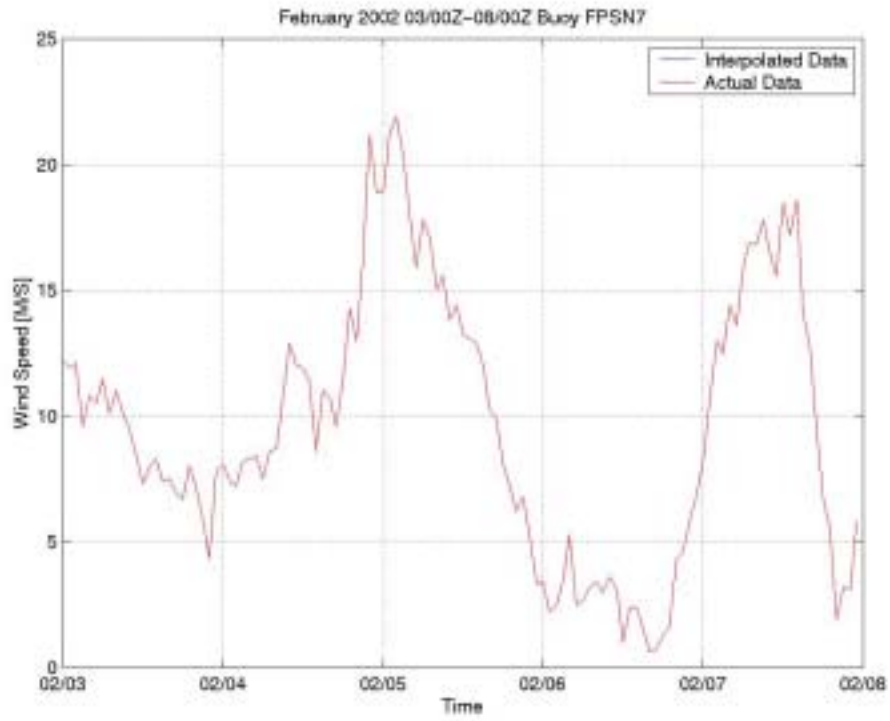
Figure 32. Buoy FPSN7 Wind Speed (February 2002 03/00Z-08/00Z)

59
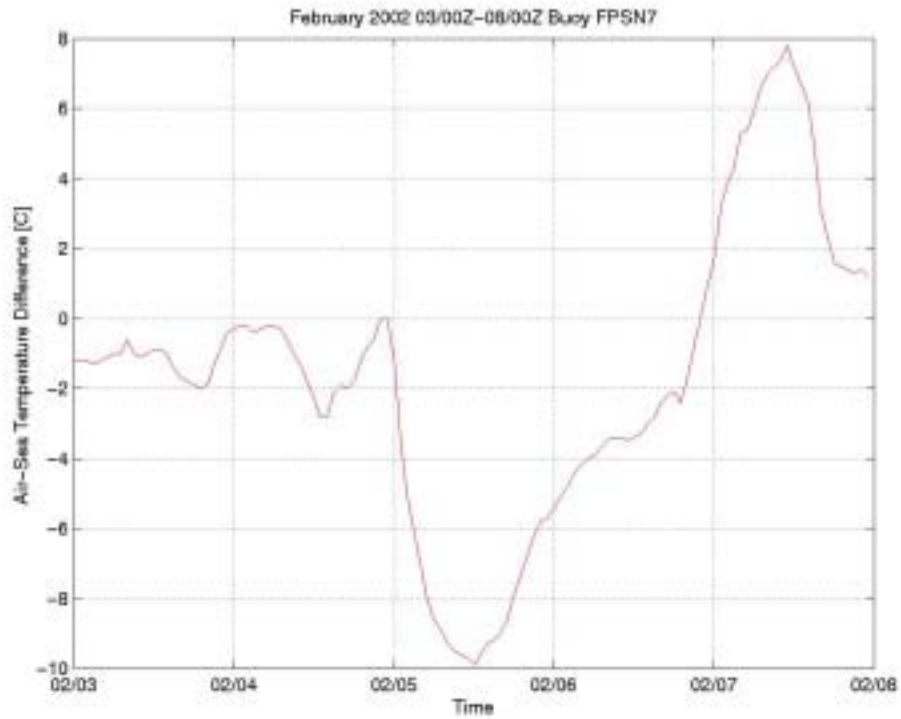
Figure 33. Buoy FPSN7 Air-Sea Temperature Difference
(February 2002 03/00Z-08/00Z)
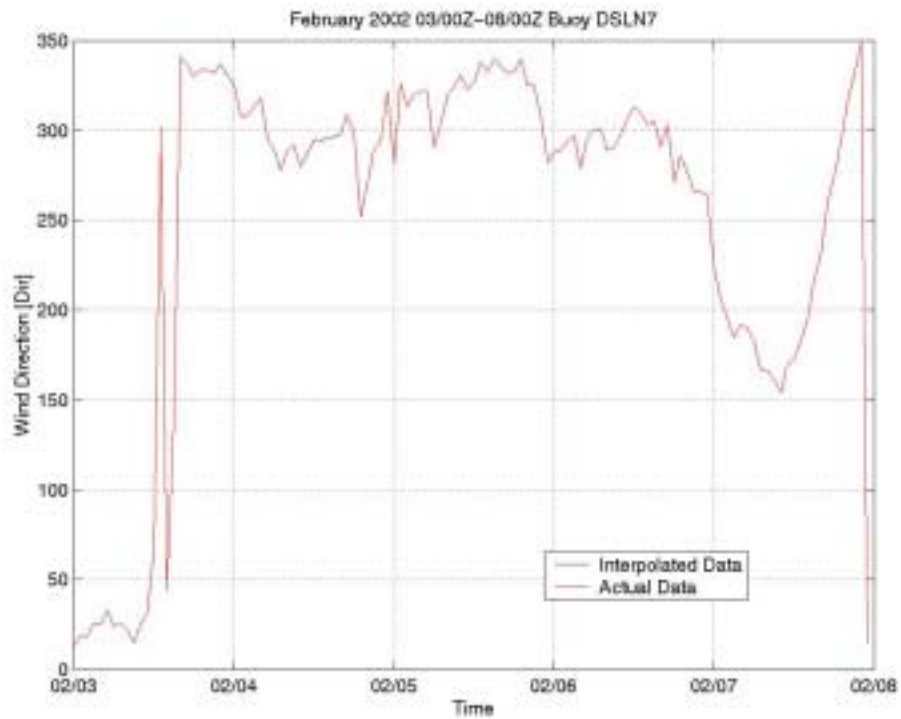
Figure 34. Buoy DLSN7 Wind Direction (February 2002 03/00Z-08/00Z)
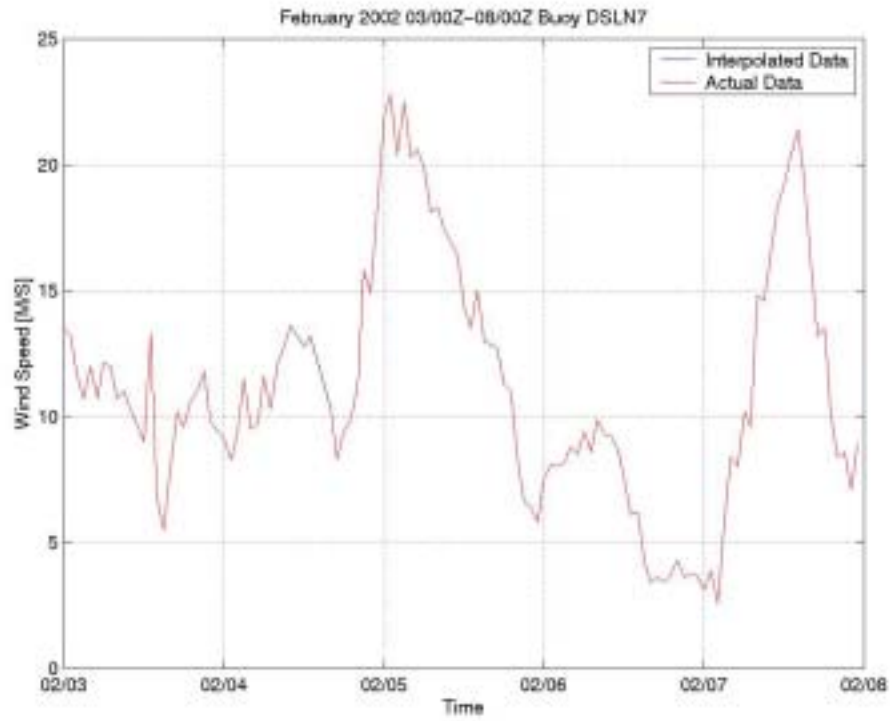
Figure 35. Buoy DSLN7 Wind Speed (February 2002 03/00Z-08/00Z)
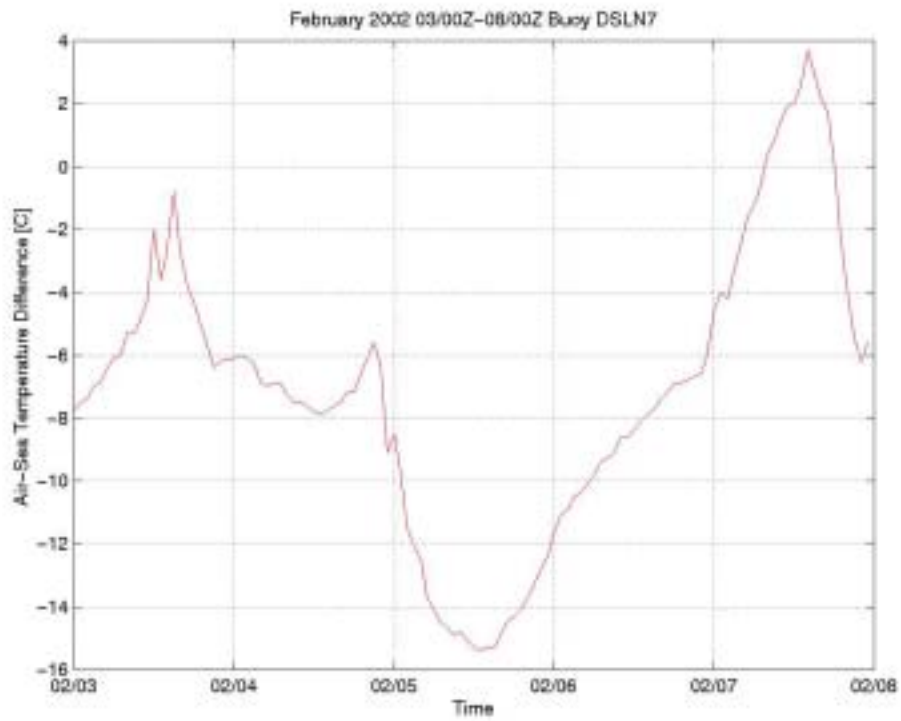
Figure 36. Buoy DSLN7 Air-Sea Temperature Difference
(February 2002 03/00Z-08/00Z)

61
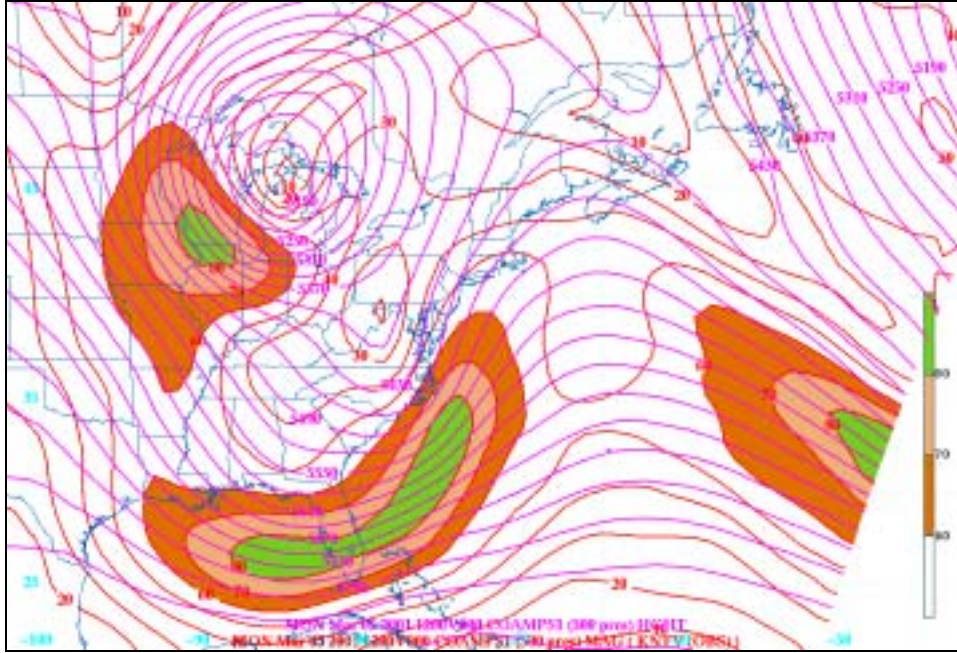
Figure 37. COAMPS 500mb Height Contours and Isotachs (1200Z 05MAR01)
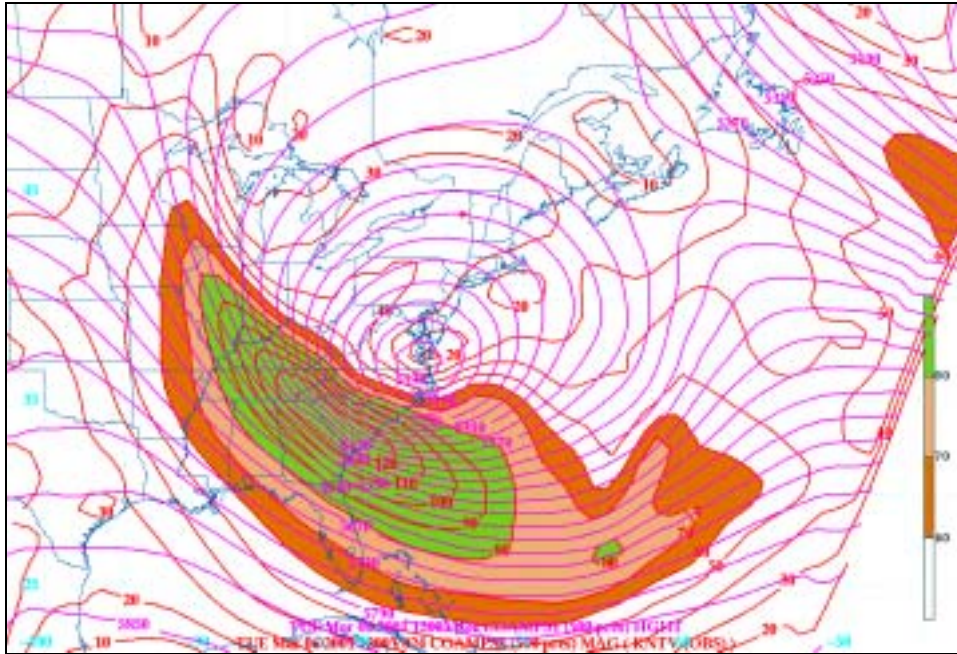
Figure 38. COAMPS 500mb Height Contours and Isotachs (1200Z 06MAR01)
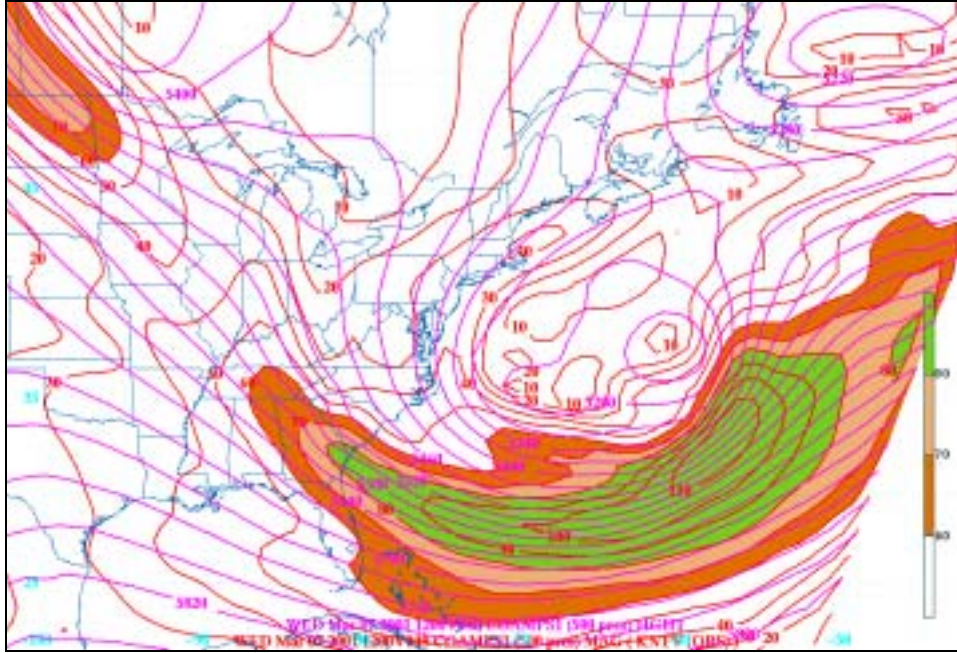
Figure 39. COAMPS 500mb Height Contours and Isotachs (1200Z 07MAR01)
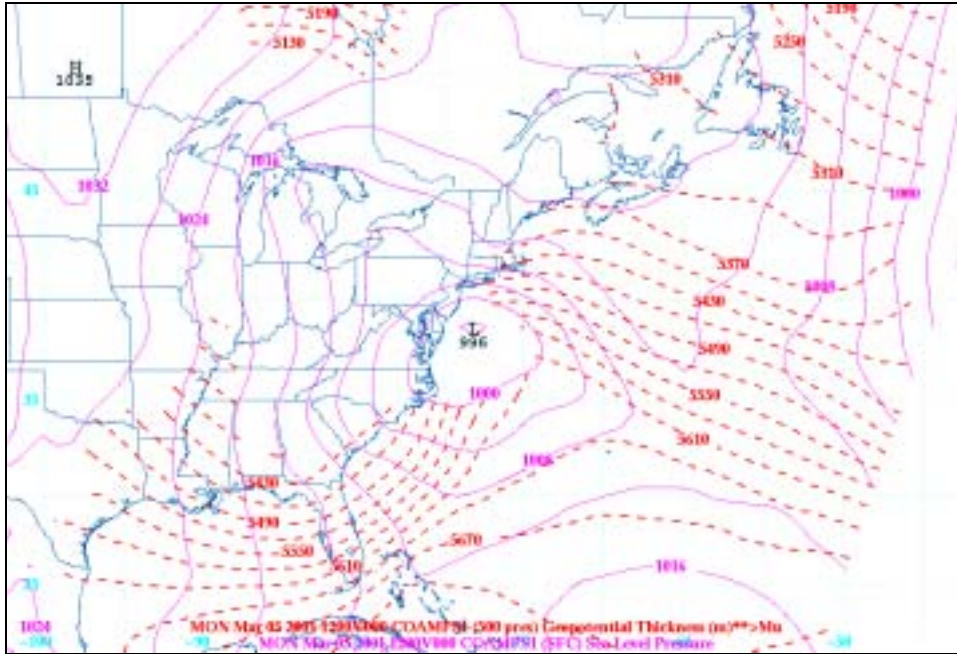
Figure 40. COAMPS Sea Level Pressure and 1000-500mb Geopotential Thickness
Contours (1200Z 05MAR01)
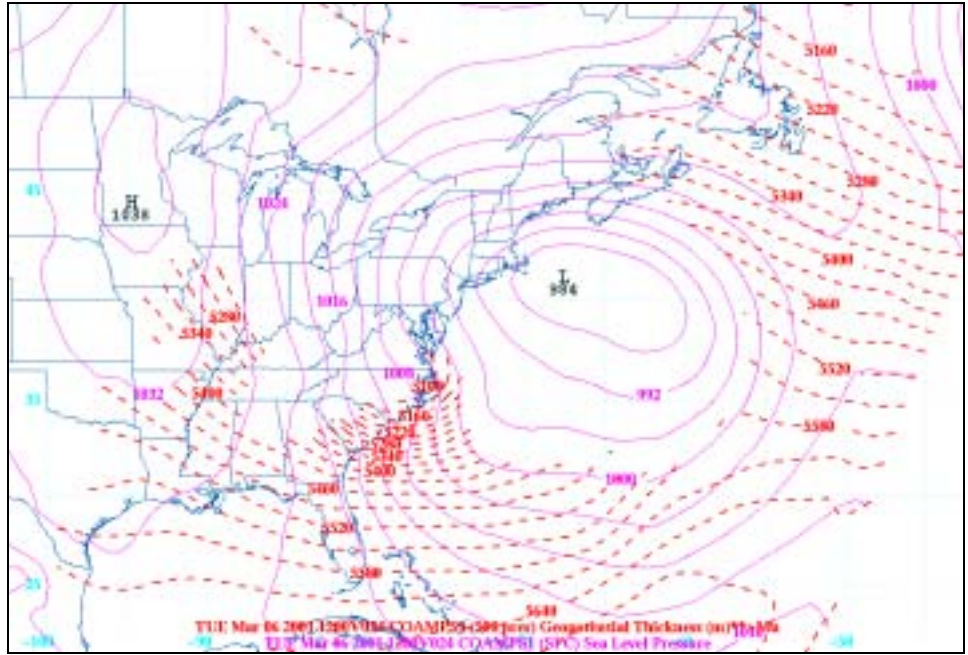
Figure 41. COAMPS Sea Level Pressure and 1000-500mb Geopotential Thickness
Contours (1200Z 06MAR01)
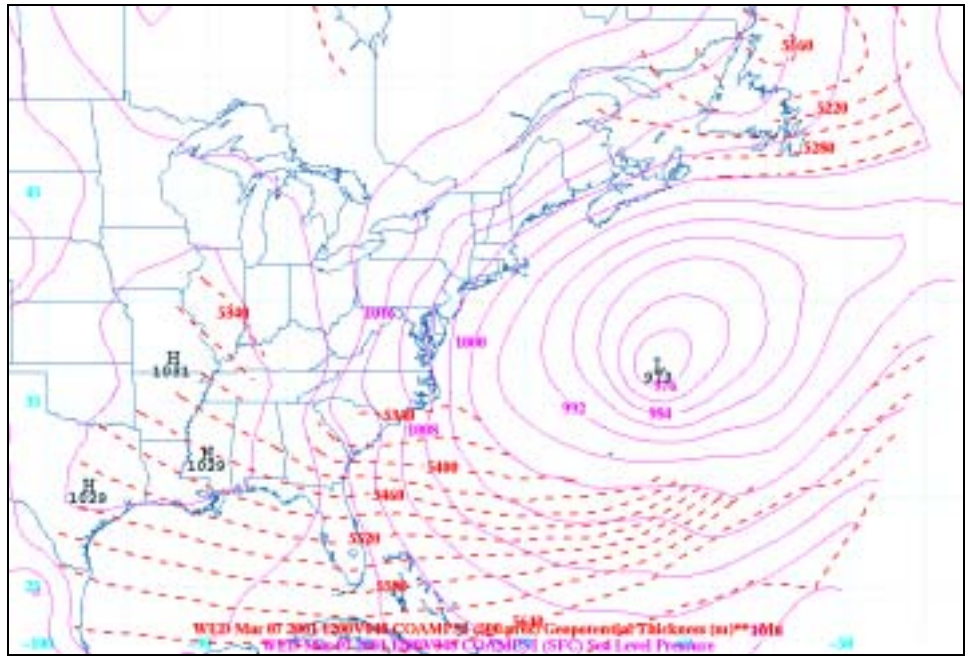
Figure 42. COAMPS Sea Level Pressure and 1000-500mb Geopotential Thickness
Contours (1200Z 07MAR01)

64
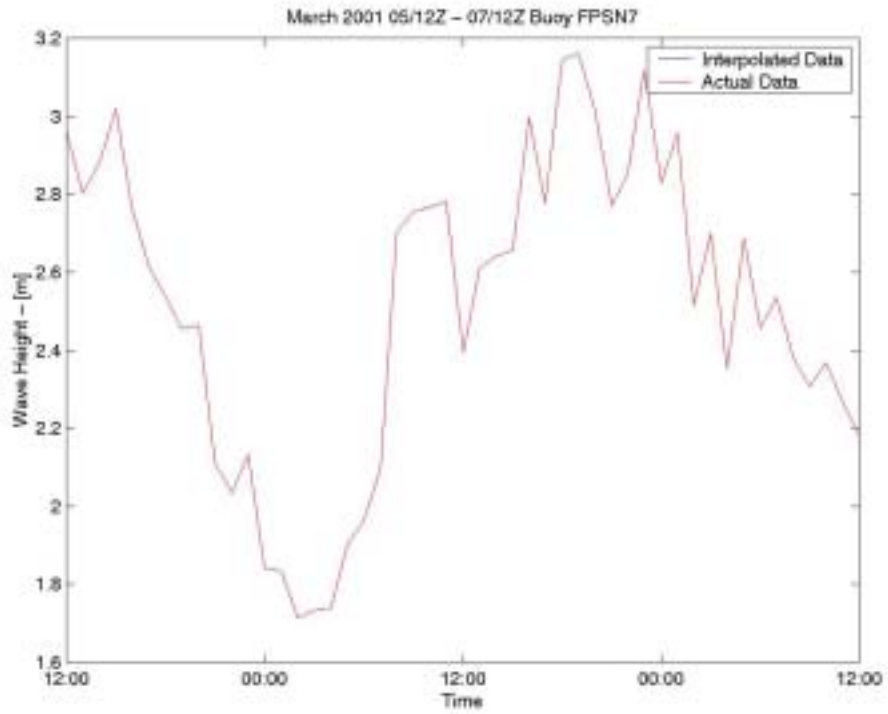
Figure 43. Buoy FPSN7 Significant Wave Height (March 2001 05/12Z-07/12Z)
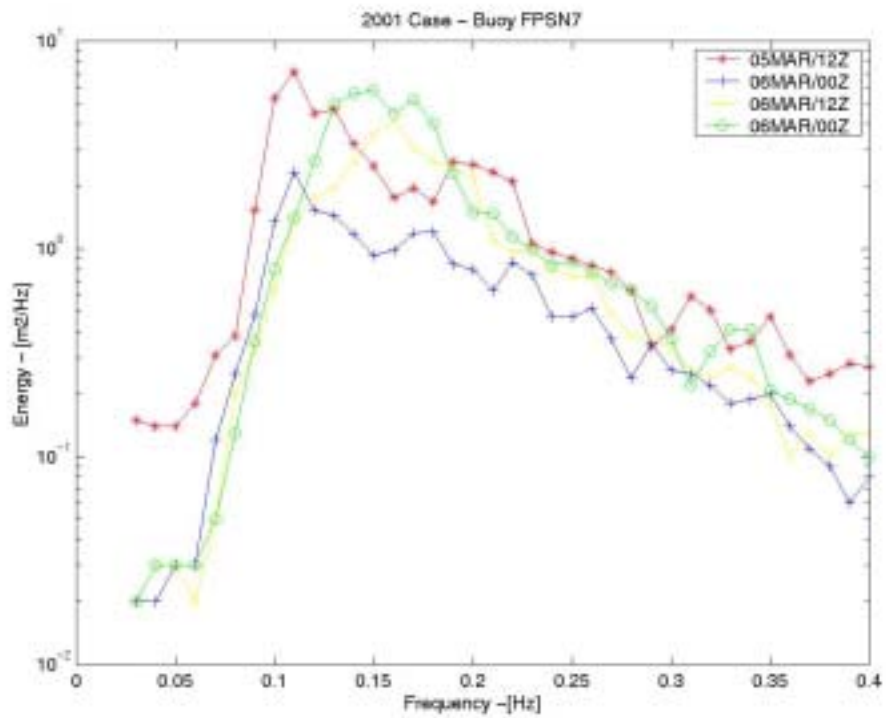
Figure 44. Buoy FPSN7 Wave Energy Spectra (March 2001)
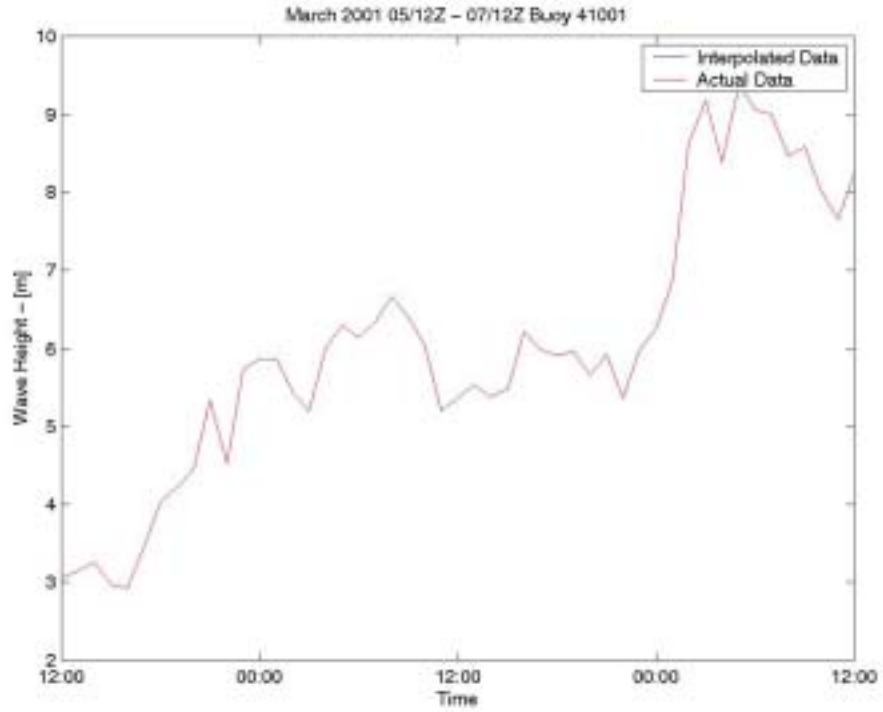
Figure 45. Buoy 41001 Significant Wave Height (March 2001 05/12Z-07/12Z)
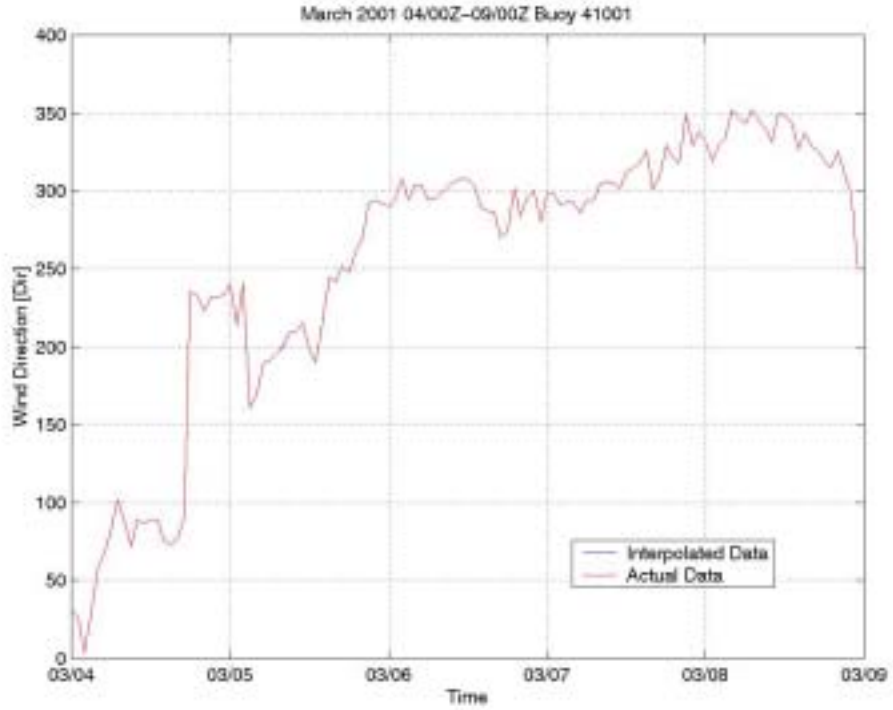
Figure 46. Buoy 41002 Wind Direction (March 2001 04/00Z-09/00Z)
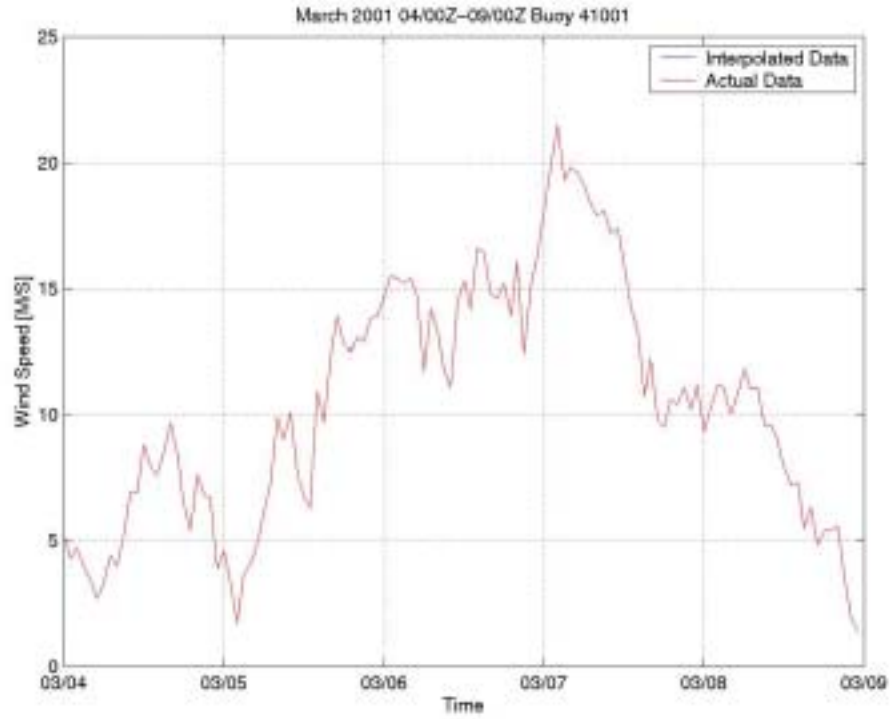
Figure 47. Buoy 41001 Wind Speed (March 2001 04/00Z-09/00Z)

Figure 48. Buoy 41001 Air-Sea Temperature Difference
(March 2001 04/00Z-09/00Z)
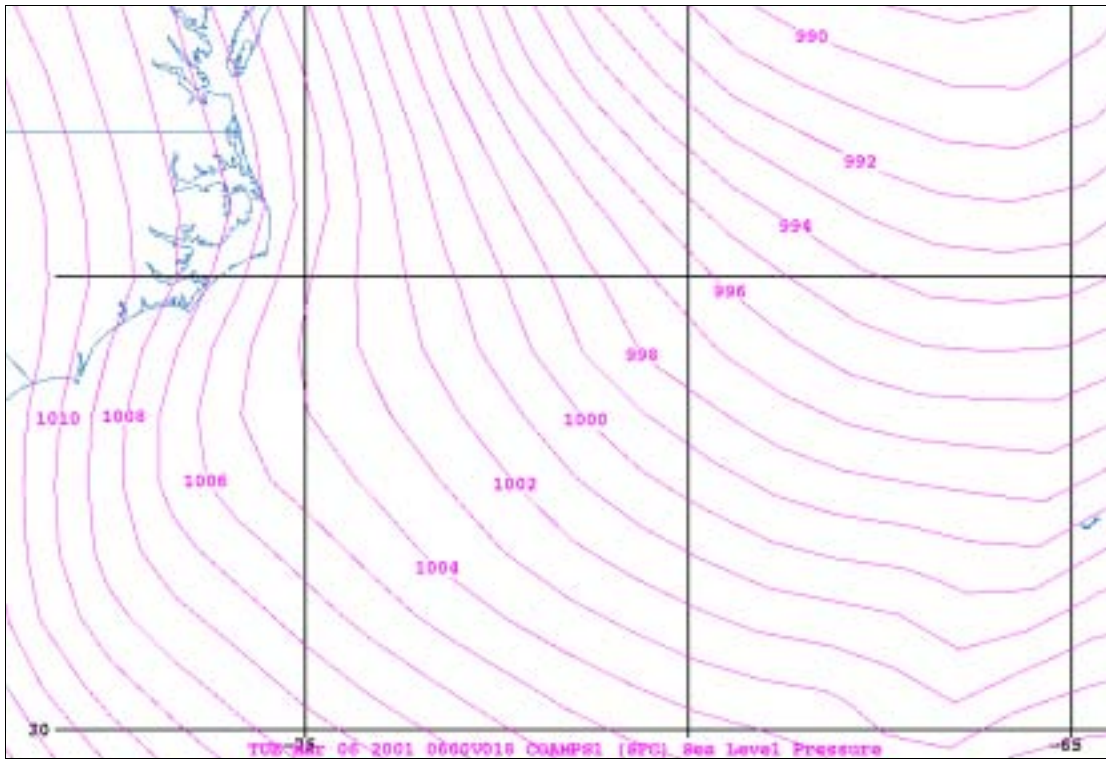
Figure 49. COAMPS(81km grid) Sea Level Pressure (March 2001 06/06Z)
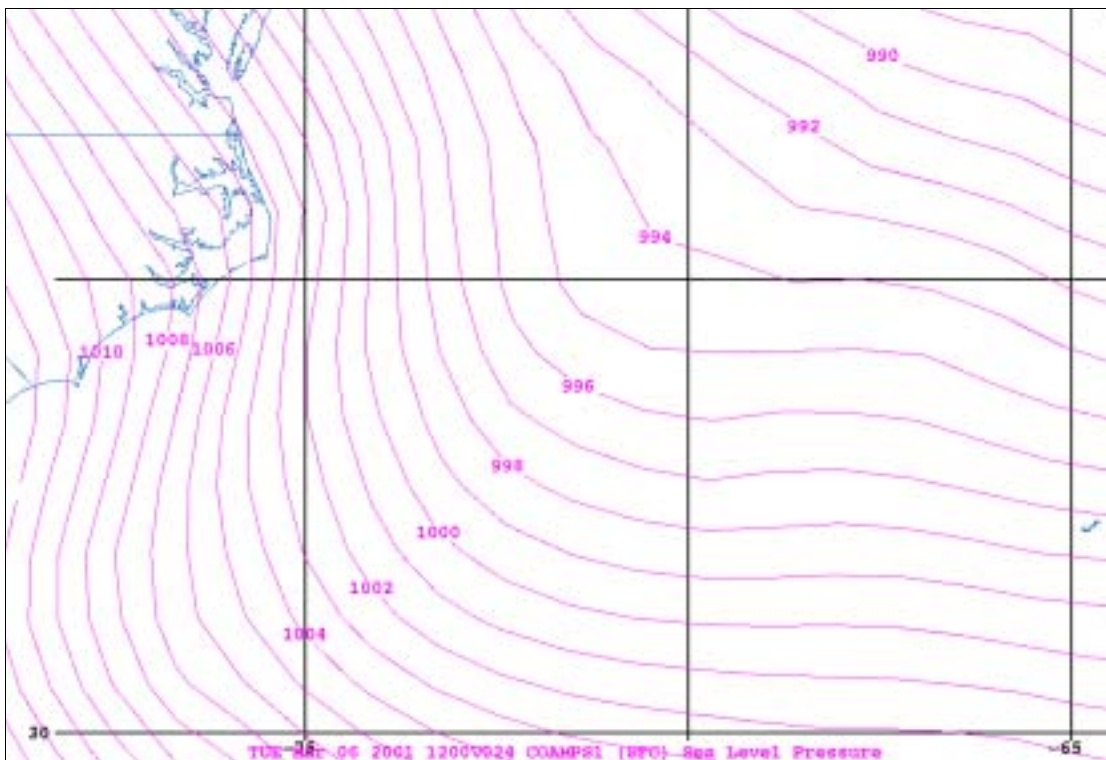
Figure 50. COAMPS(81km grid) Sea Level Pressure (March 2001 06/12Z)

68
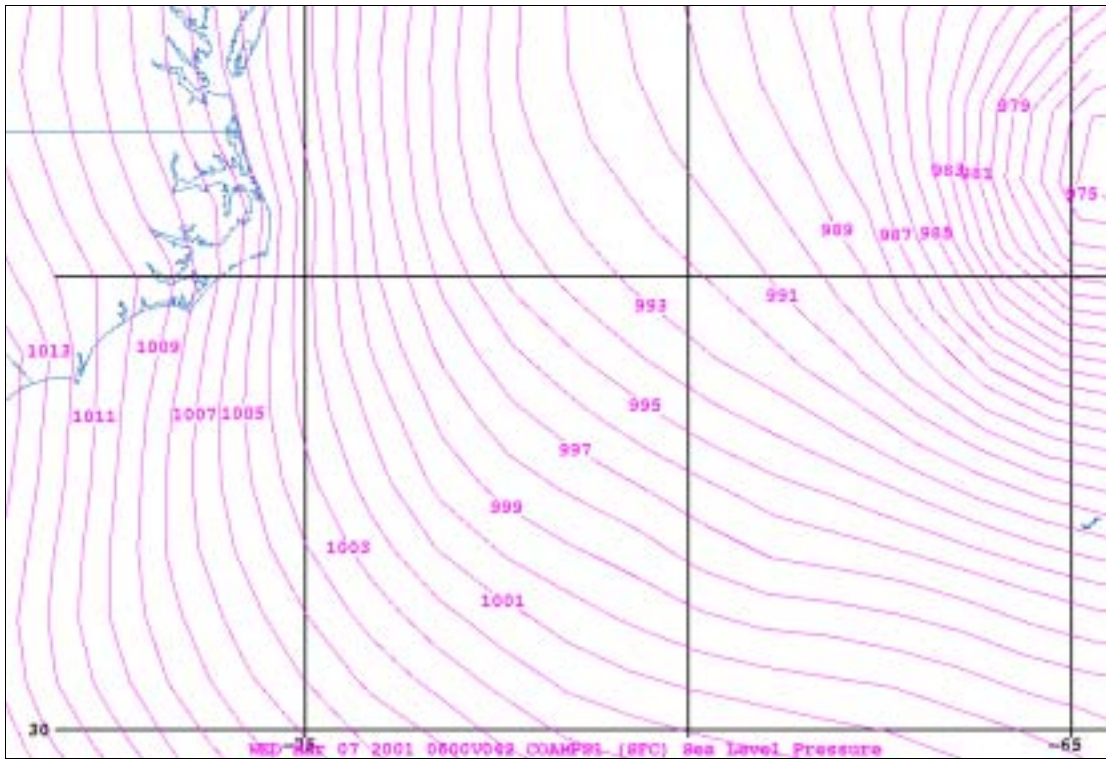
Figure 51. COAMPS(81km grid) Sea Level Pressure (March 2001 07/06Z)
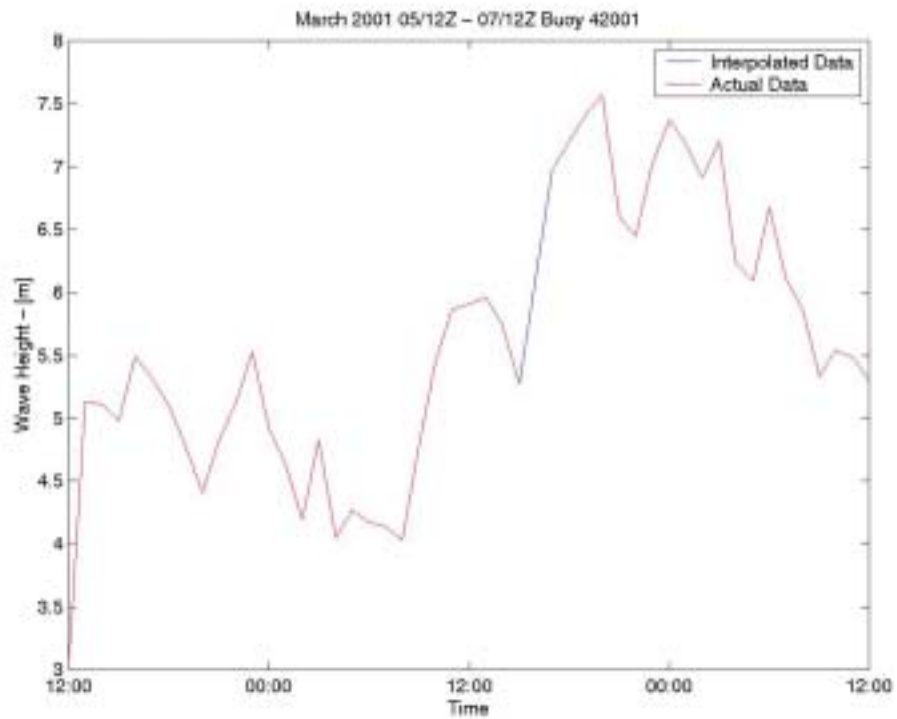
Figure 52. Buoy 41002 Significant Wave Height (March 2001 05/12Z-07/12Z)
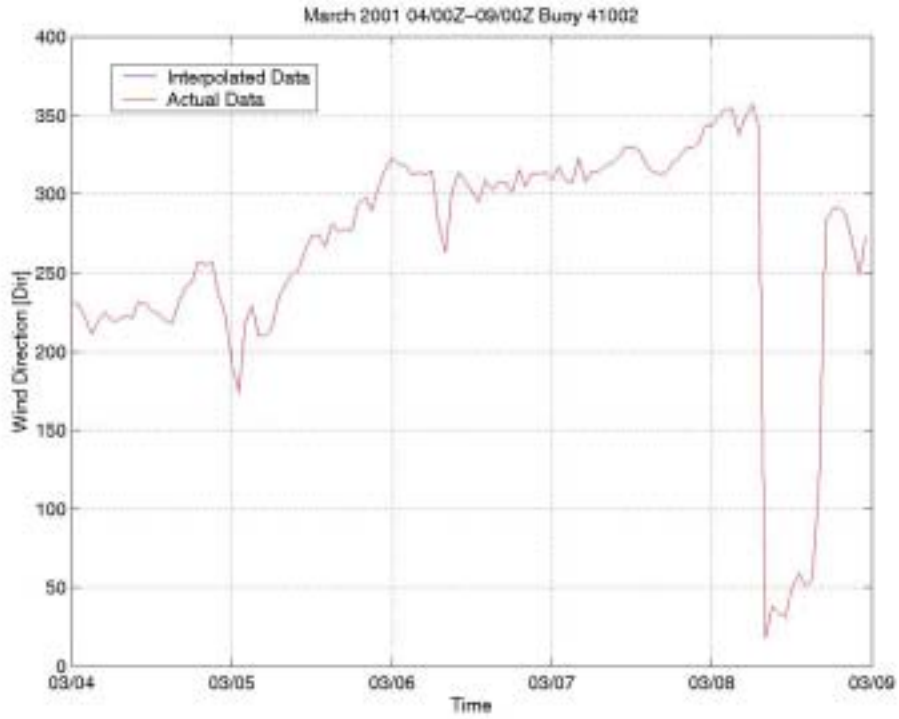
Figure 53. Buoy 41002 Wind Direction (March 2001 04/00Z-09/00Z)
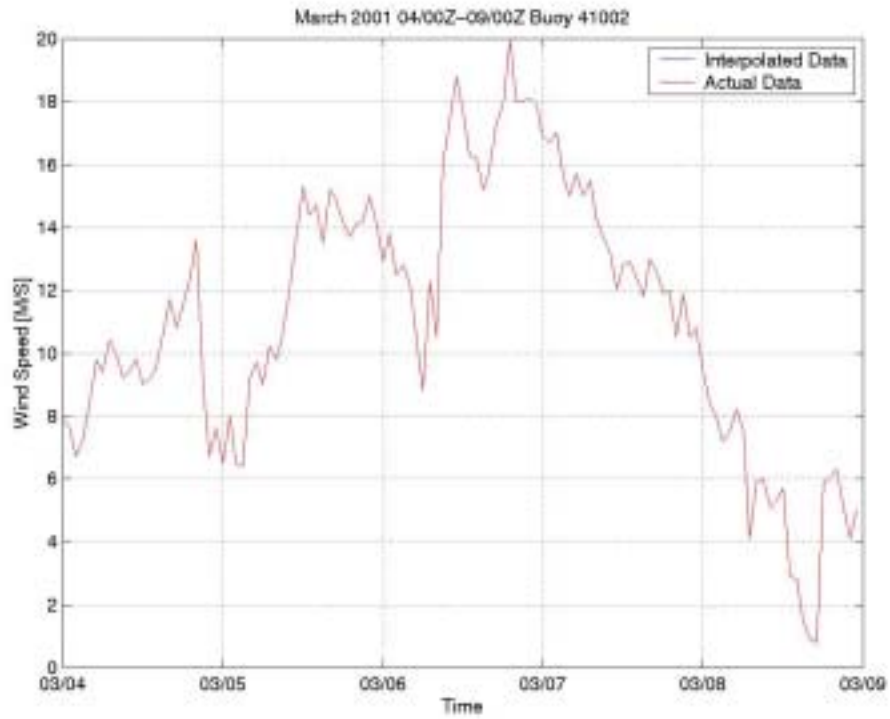
Figure 54. Buoy 41002 Wind Speed (March 2001 04/00Z-09/00Z)

70
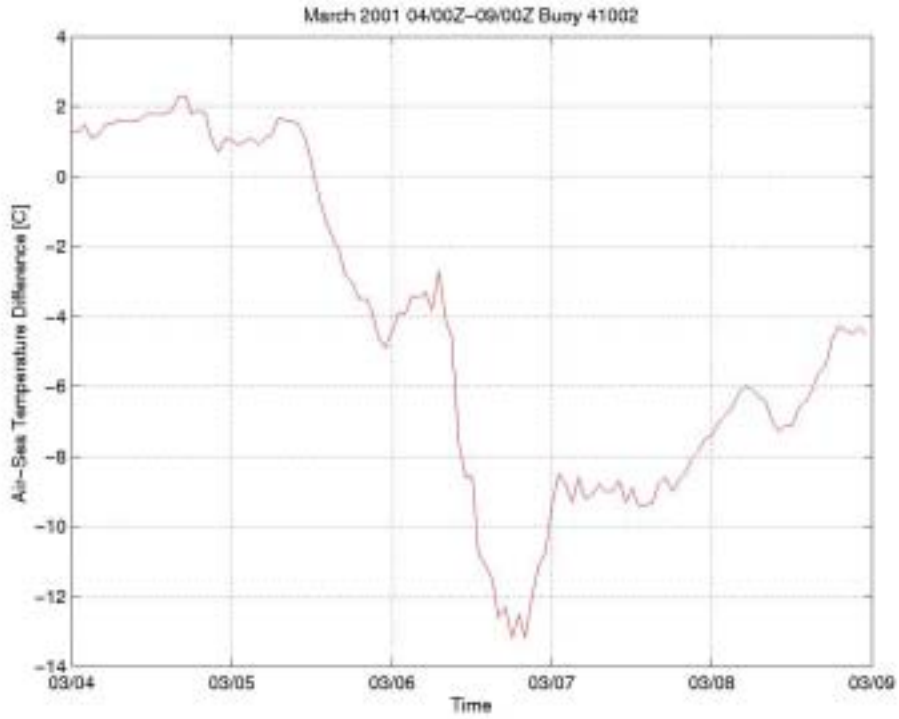
Figure 55. Buoy 41002 Air-Sea Temperature Difference
(March 2001 04/00Z-09/00Z)
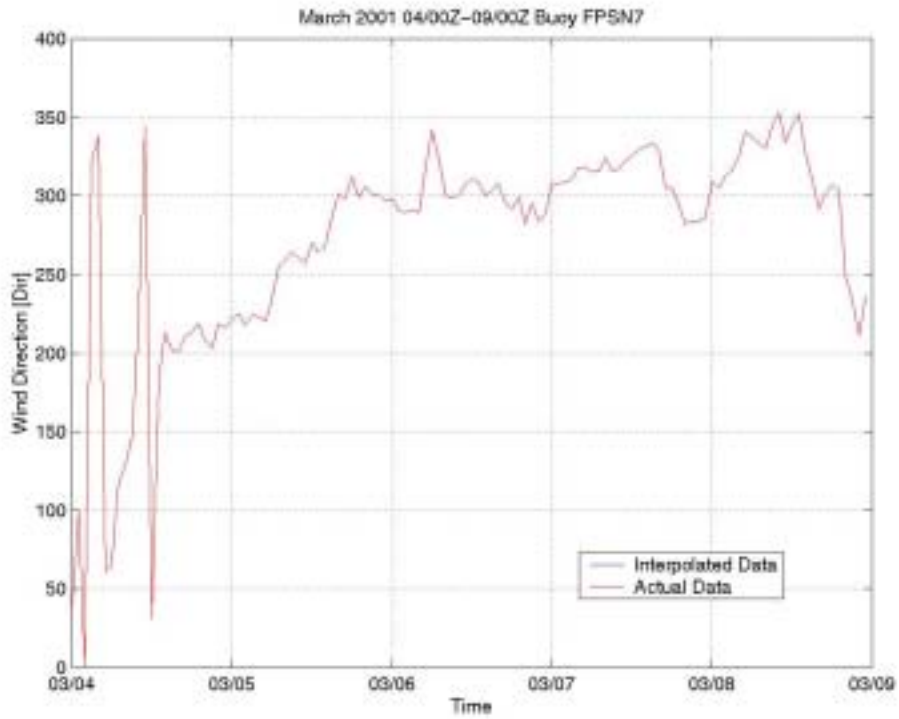
Figure 56. Buoy FPSN7 Wind Direction (March 2001 04/00Z-09/00Z)

71
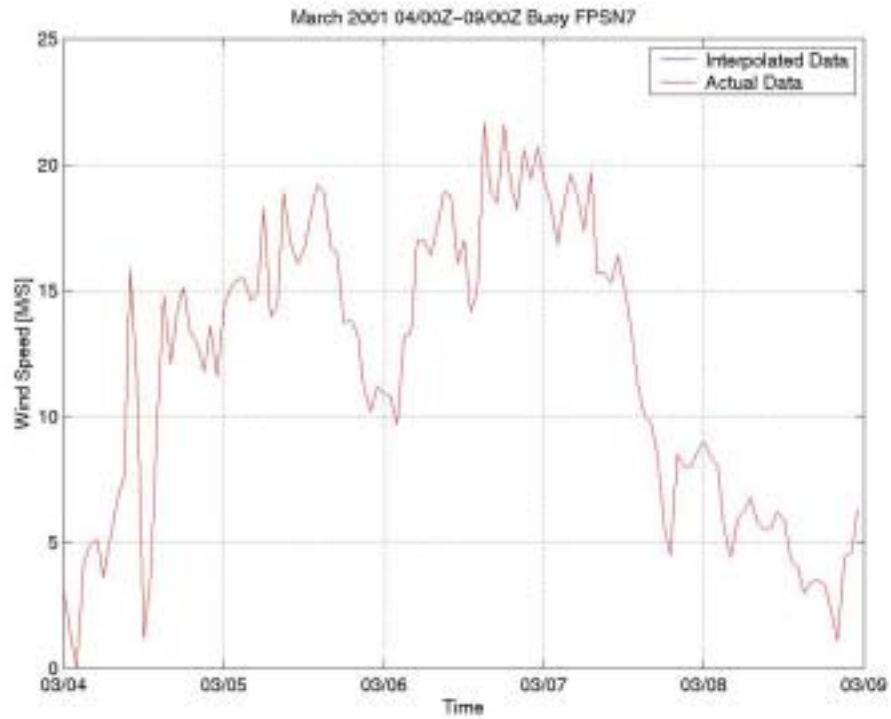
Figure 57. Buoy FPSN7 Wind Speed (March 2001 04/00Z-09/00Z)
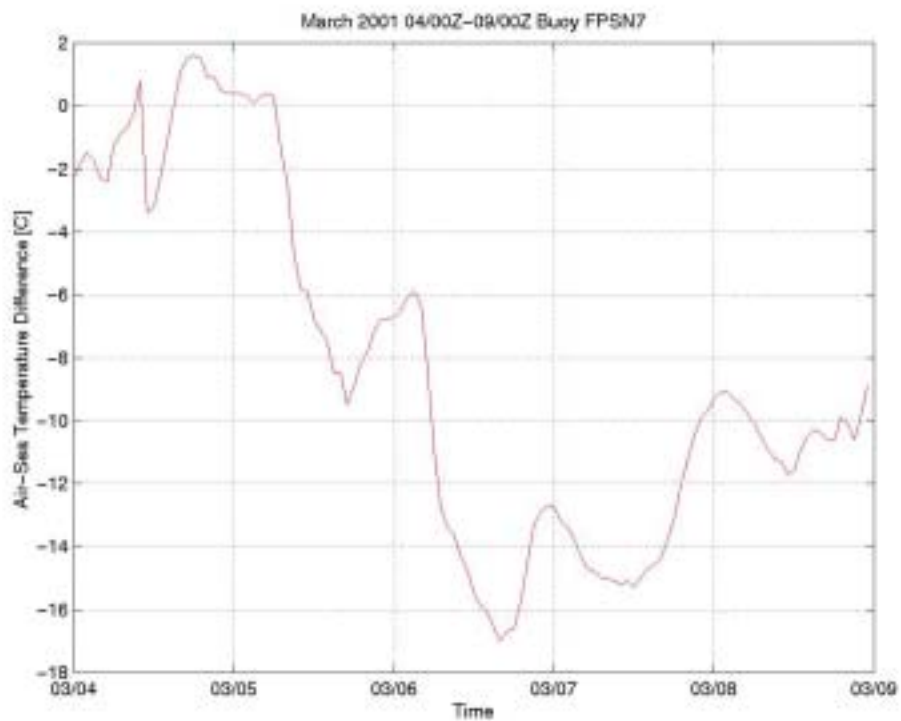
Figure 58. Buoy FPSN7 Air-Sea Temperature Difference
(March 2001 04/00Z-09/00Z)

72
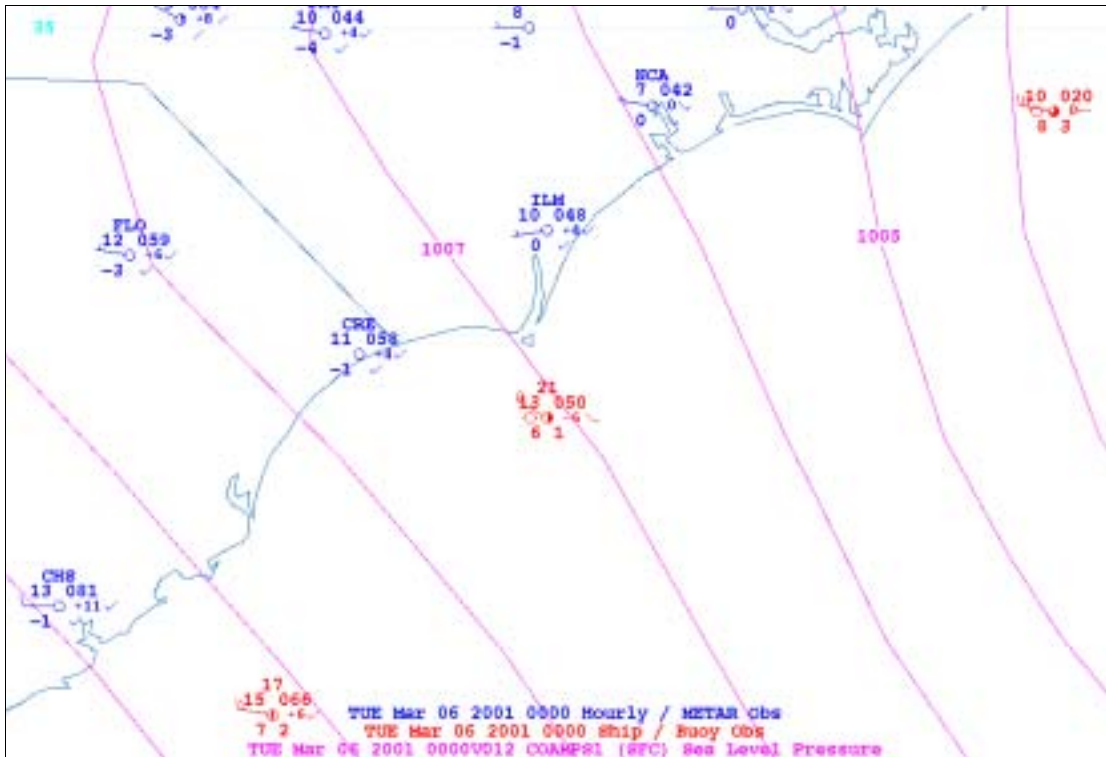
Figure 59. COAMPS(81km grid) Sea Level Pressure (March 2001 06/00Z)
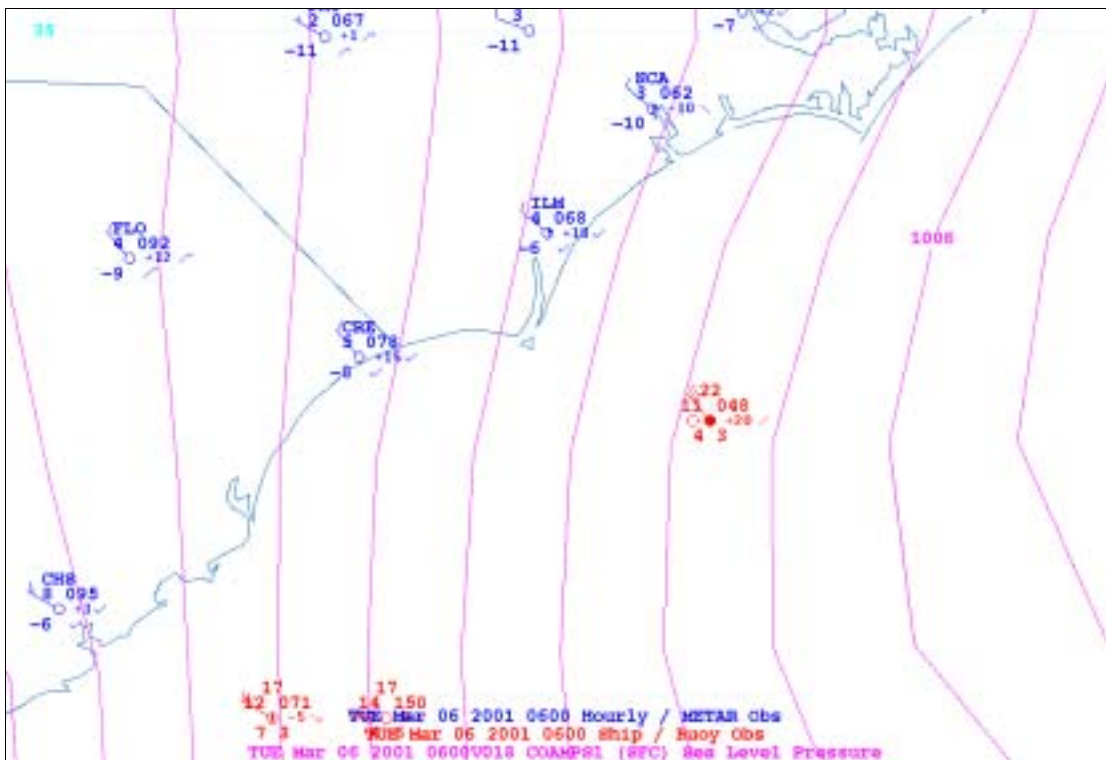
Figure 60. COAMPS(81km grid) Sea Level Pressure (March 2001 06/06Z)
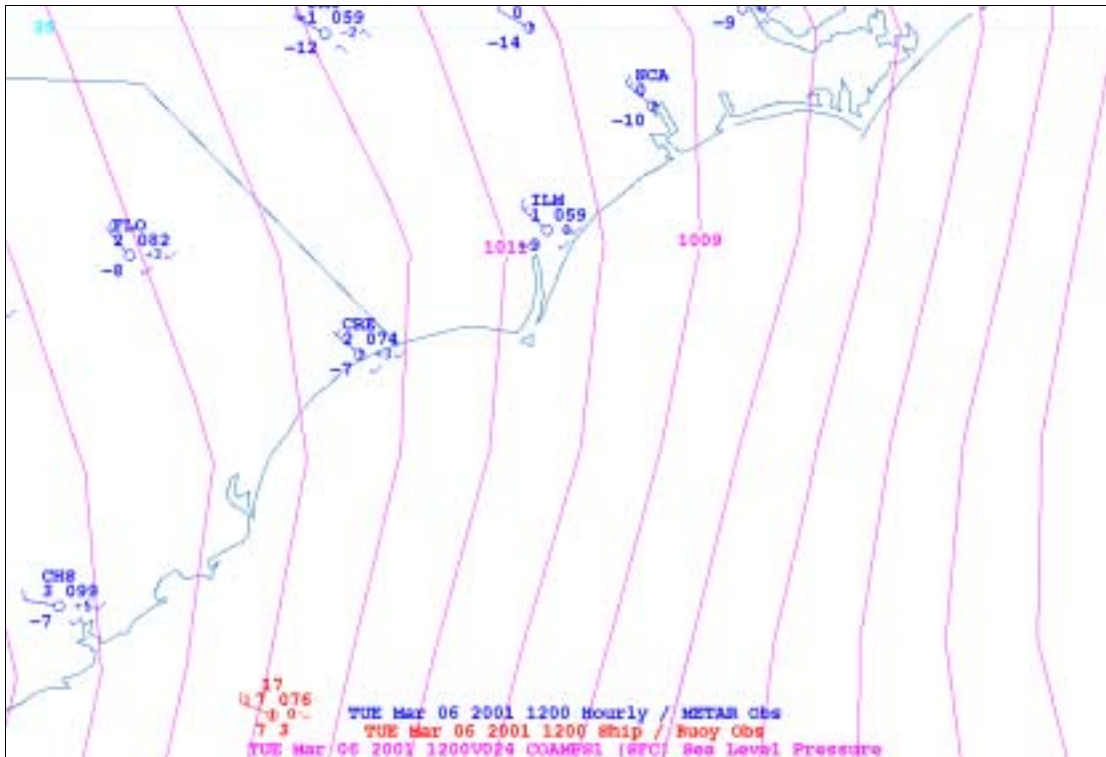
Figure 61. COAMPS(81km grid) Sea Level Pressure (March 2001 06/12Z)
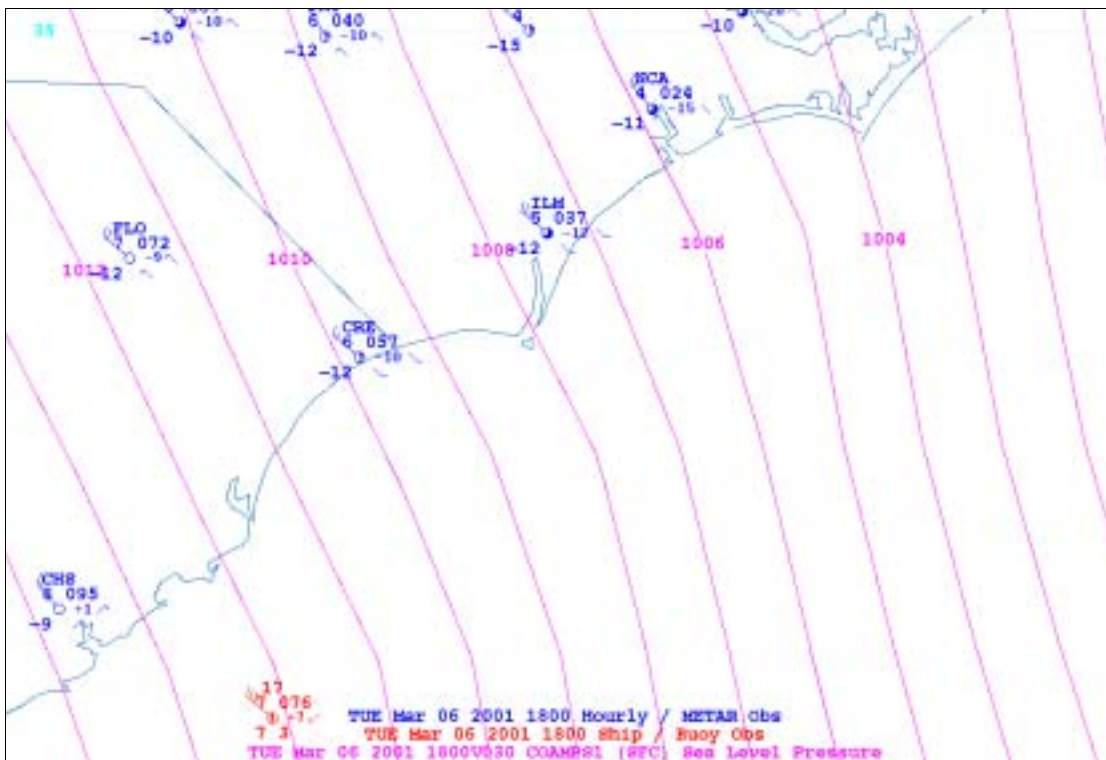
Figure 62. COAMPS(81km grid) Sea Level Pressure (March 2001 06/18Z)

74
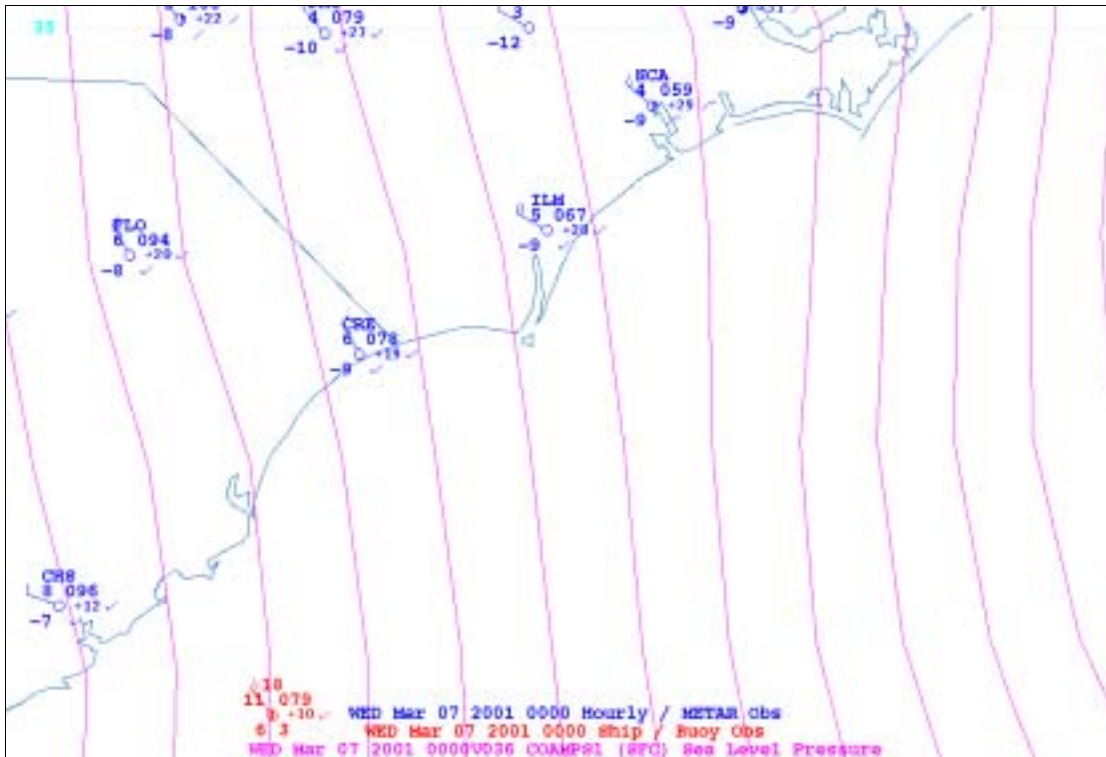
Figure 63. COAMPS(81km grid) Sea Level Pressure (March 2001 07/00Z)
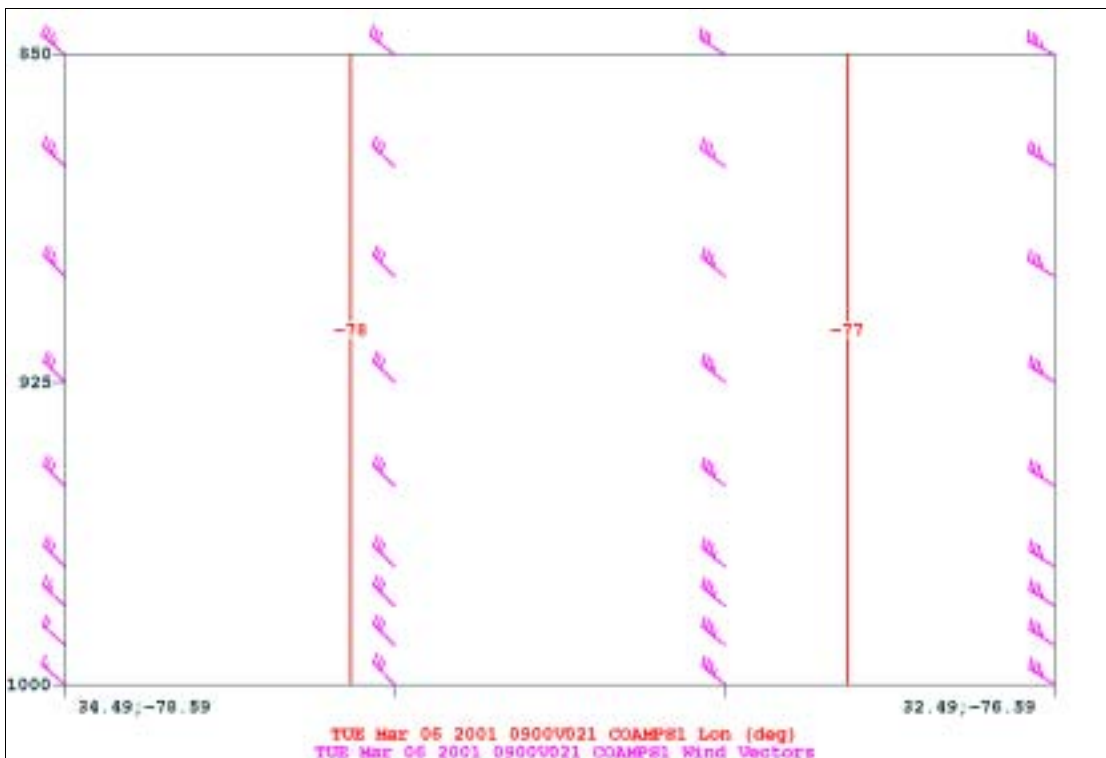
Figure 64. COAMPS(81km grid) Vertical Cross Section of Wind (March 2001 06/09Z)
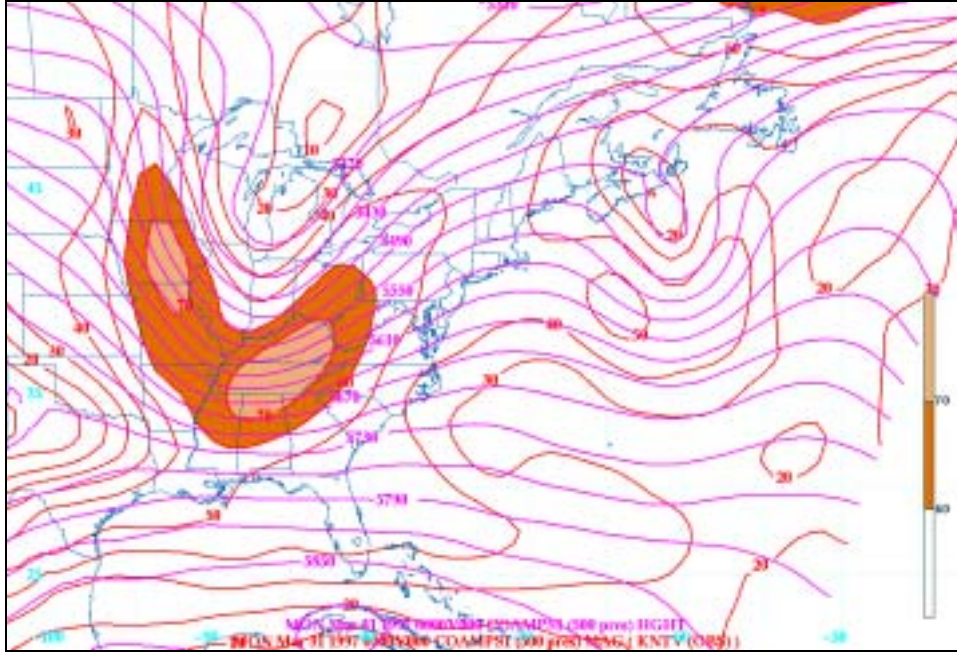
Figure 65. COAMPS 500mb Height Contours and Isotachs (0000Z 31MAR97)
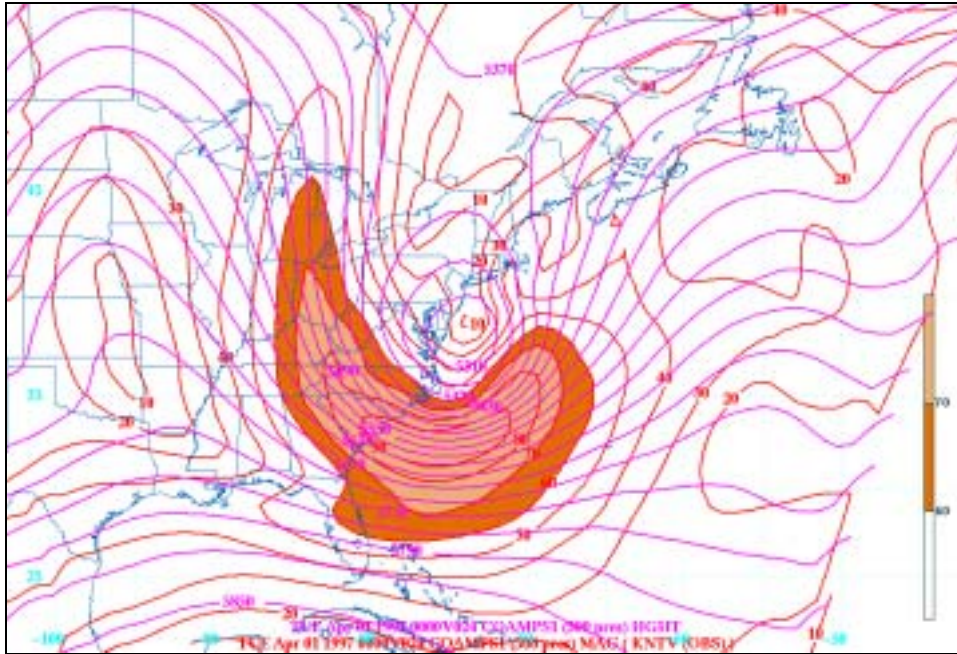
Figure 66. COAMPS 500mb Height Contours and Isotachs (0000Z 01APR97)
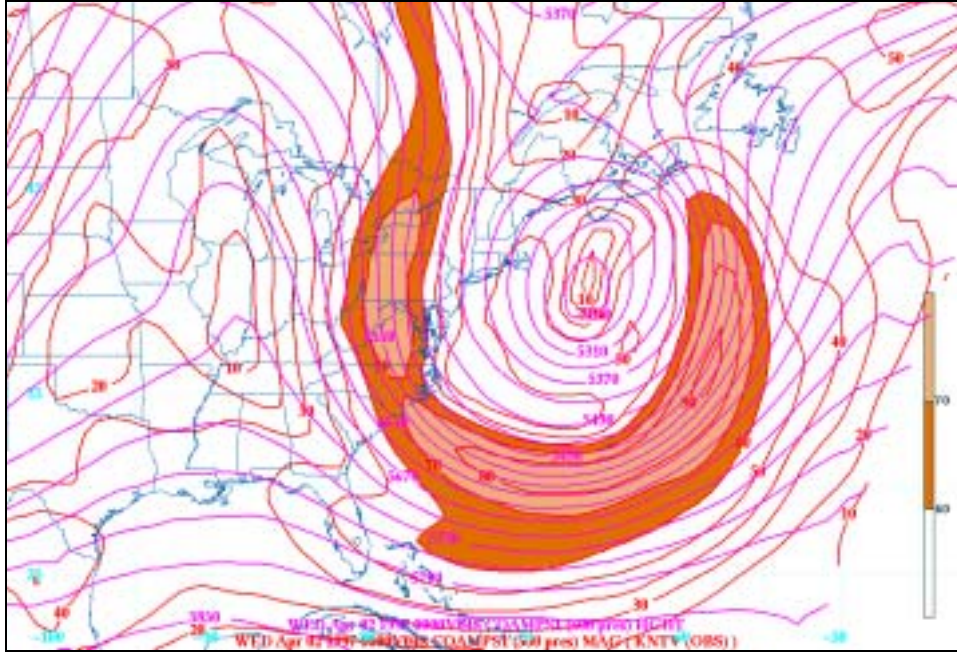
Figure 67. COAMPS 500mb Height Contours and Isotachs (0000Z 02APR97)

Figure 68. COAMPS Sea Level Pressure and 1000-500mb Geopotential Thickness Contours (0000Z 31MAR97)

Figure 69. COAMPS Sea Level Pressure and 1000-500mb Geopotential Thickness Contours (0000Z 01APR97)

Figure 70. COAMPS Sea Level Pressure and 1000-500mb Geopotential Thickness Contours (0000Z 02APR97)
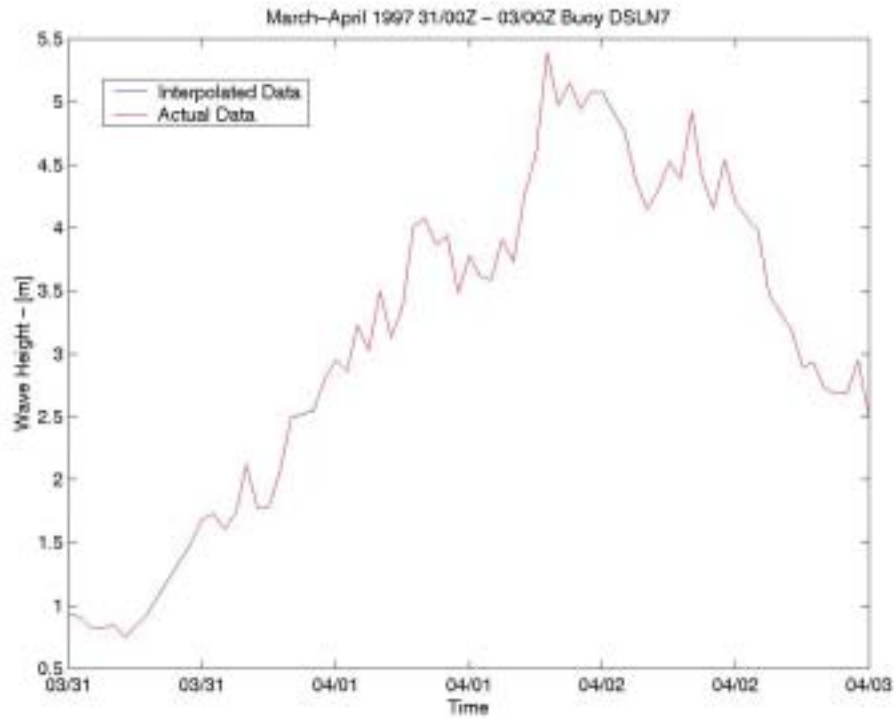
Figure 71. Buoy DSLN7 Significant Wave Height (March-April 1997 31/00Z-03/00Z)
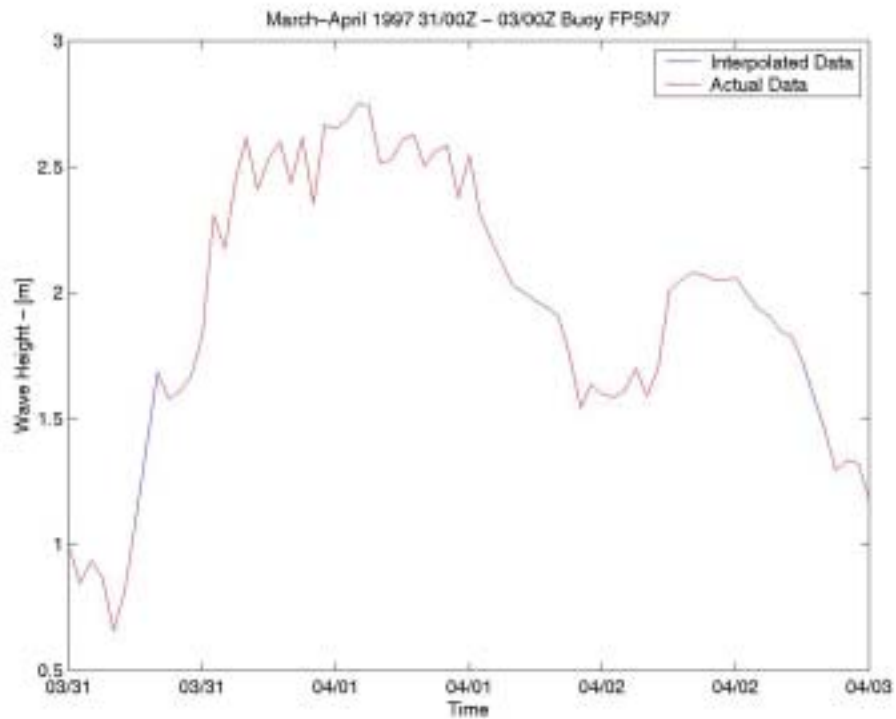
Figure 72. Buoy FPSN7 Significant Wave Height (March-April 1997 31/00Z-03/00Z)
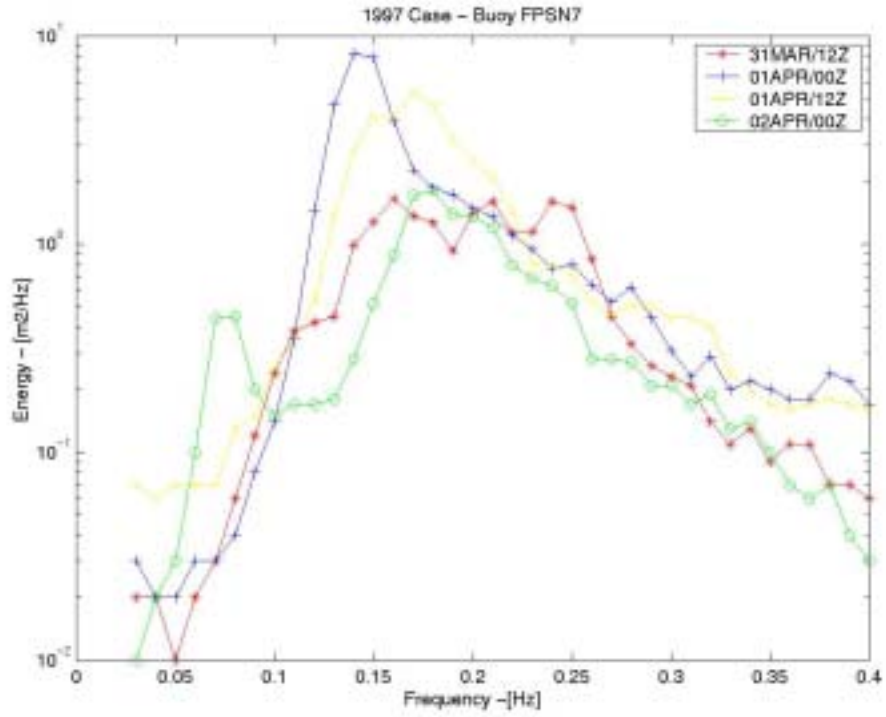
Figure 73. Buoy FPSN7 Wave Energy Spectra (March-April 1997)
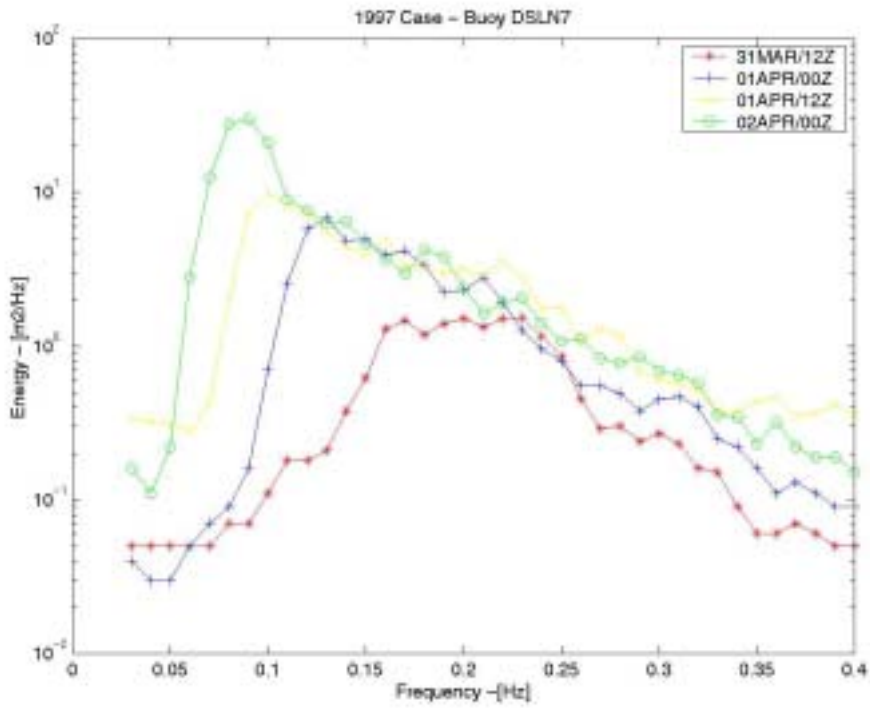
Figure 74. Buoy DSLN7 Wave Energy Spectra (March-April 1997)

Figure 75. Buoy 41001 Wind Direction (March-April 1997 31/00Z-03/00Z)
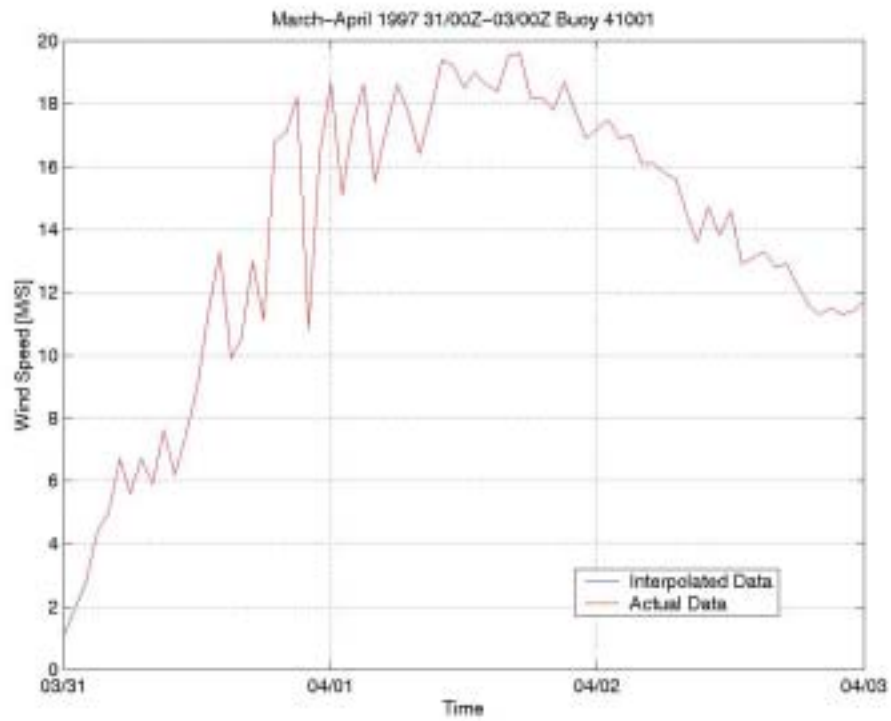
Figure 76. Buoy 41001 Wind Speed (March-April 1997 31/00Z-03/00Z)
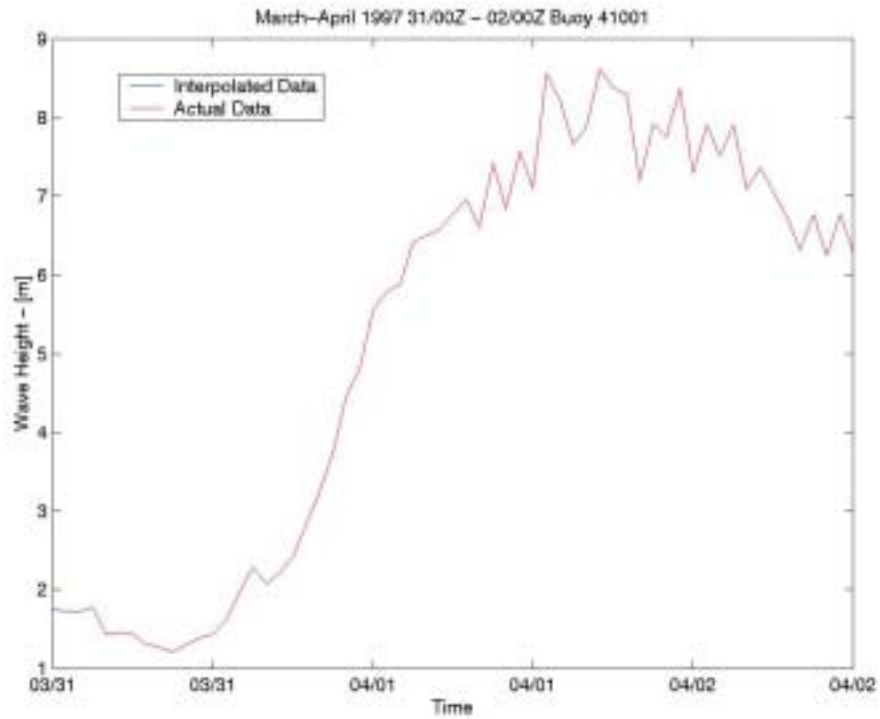
Figure 77. Buoy 41001 Significant Wave Height (March-April 1997 31/00Z-03/00Z)
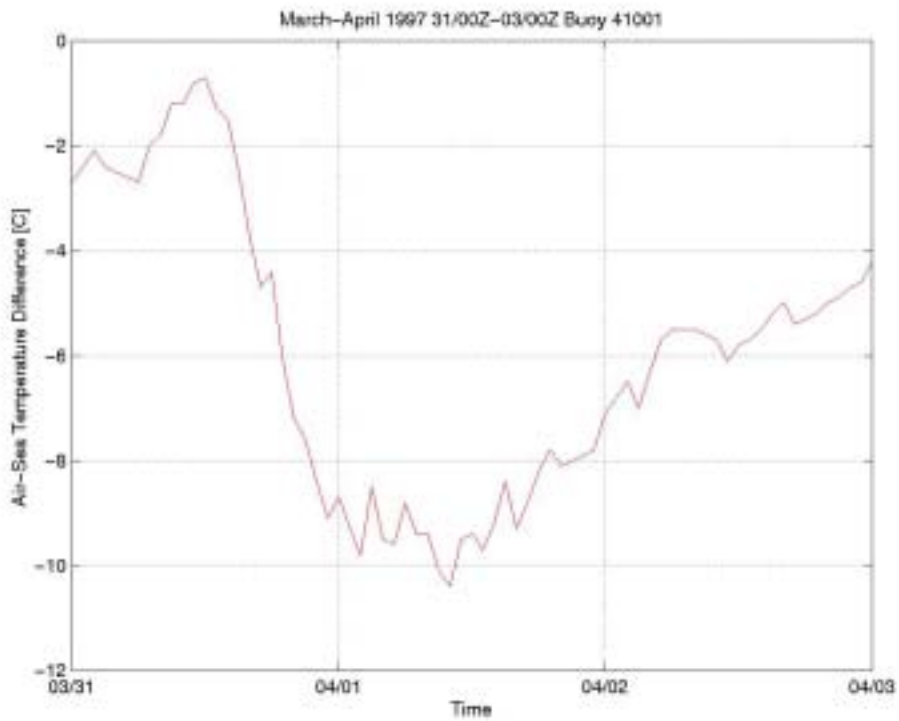
Figure 78. Buoy 41001 Air-Sea Temperature Difference
(March-April 1997 31/00Z-03/00Z)
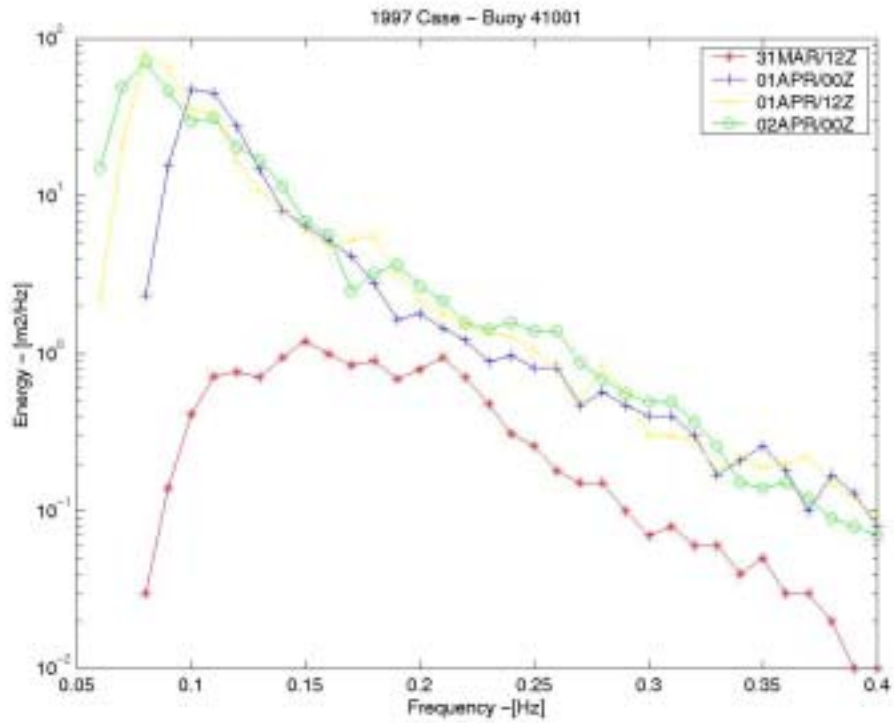
Figure 79. Buoy 41001 Wave Energy Spectra (March-April 1997)
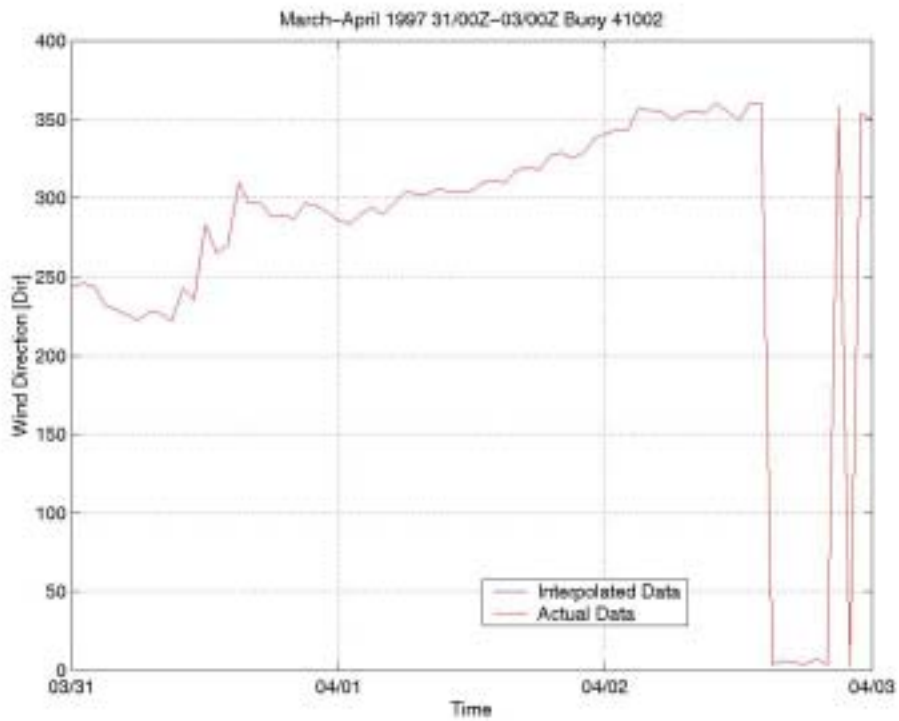
Figure 80. Buoy 41002 Wind Direction (March-April 1997 31/00Z-03/00Z)

83
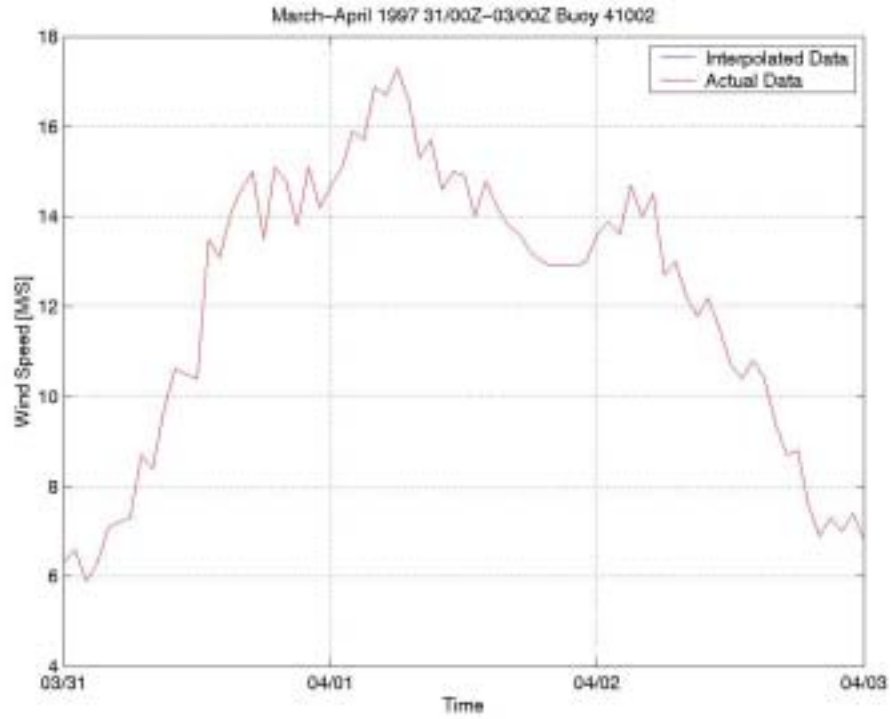
Figure 81. Buoy 41002 Wind Speed (March-April 1997 31/00Z-03/00Z)
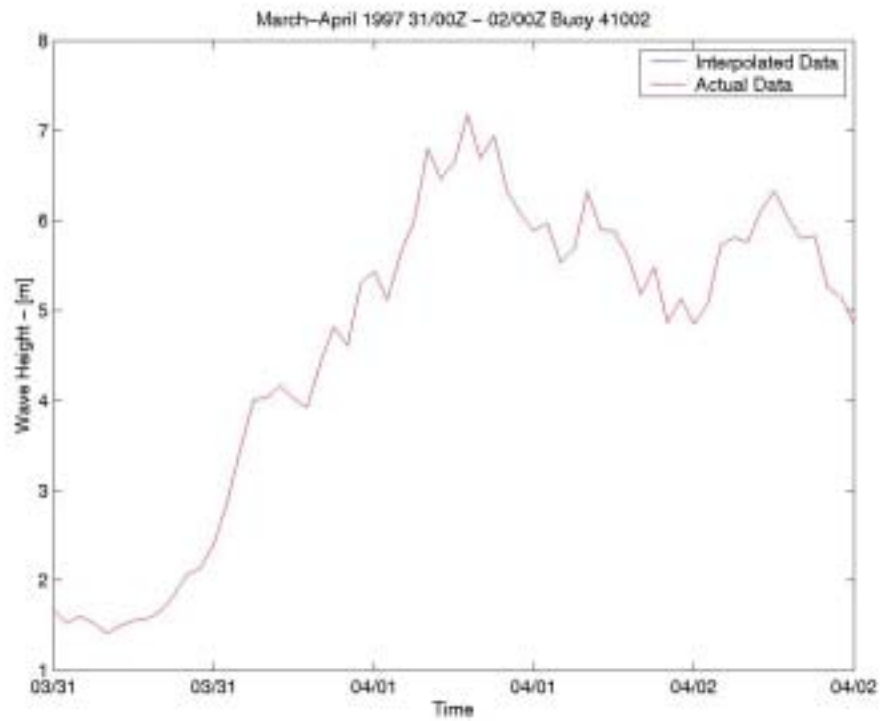
Figure 82. Buoy 41002 Significant Wave Height (March-April 1997 31/00Z-03/00Z)
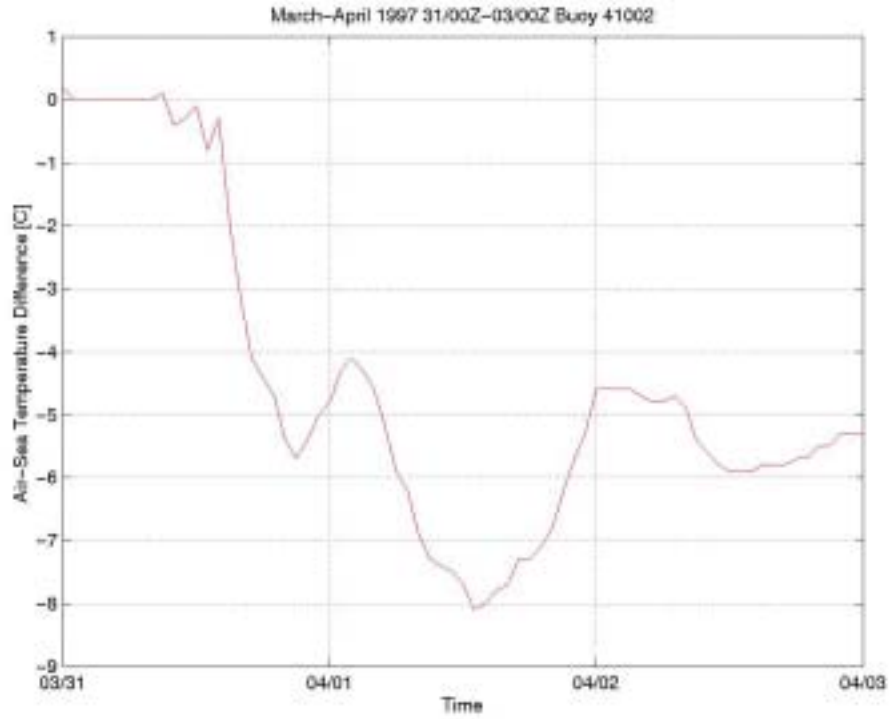
Figure 83. Buoy 41002 Air-Sea Temperature Difference
(March-April 1997 31/00Z-03/00Z)
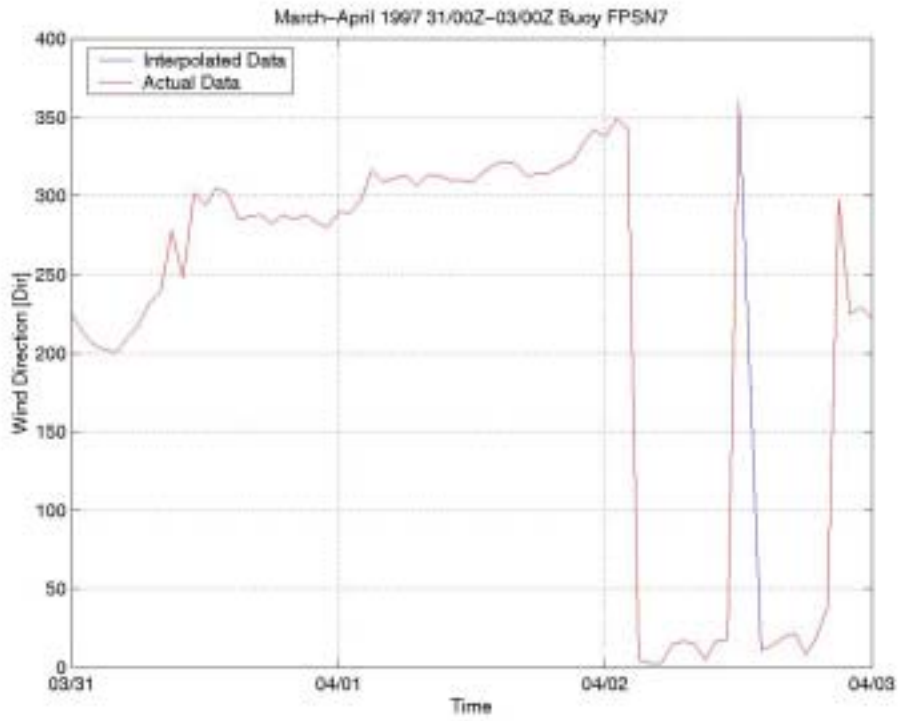
Figure 84. Buoy FPSN7 Wind Direction (March-April 1997 31/00Z-03/00Z)
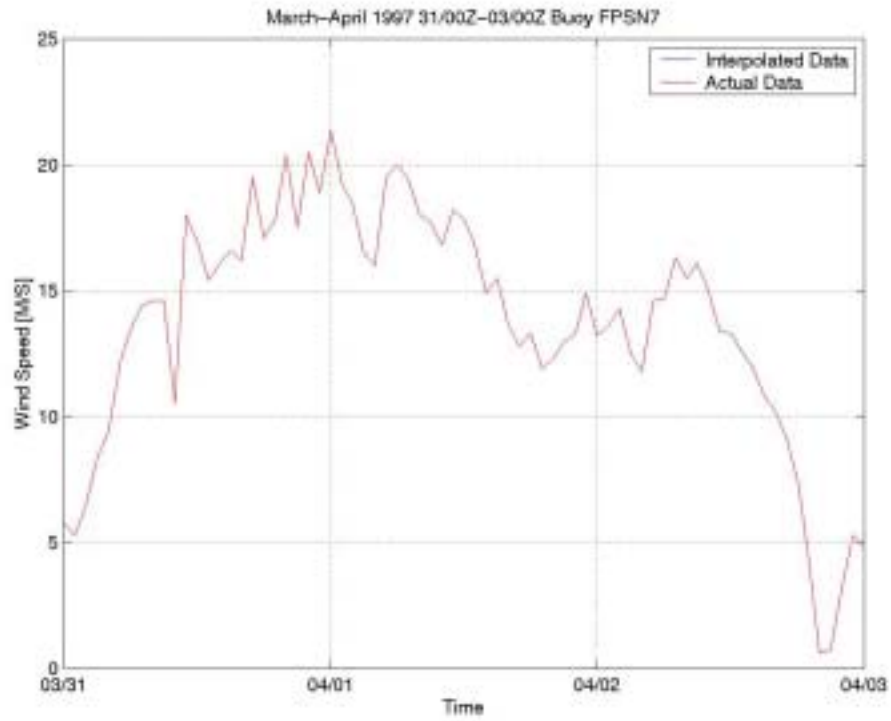
Figure 85. Buoy FPSN7 Wind Speed (March-April 1997 31/00Z-03/00Z)
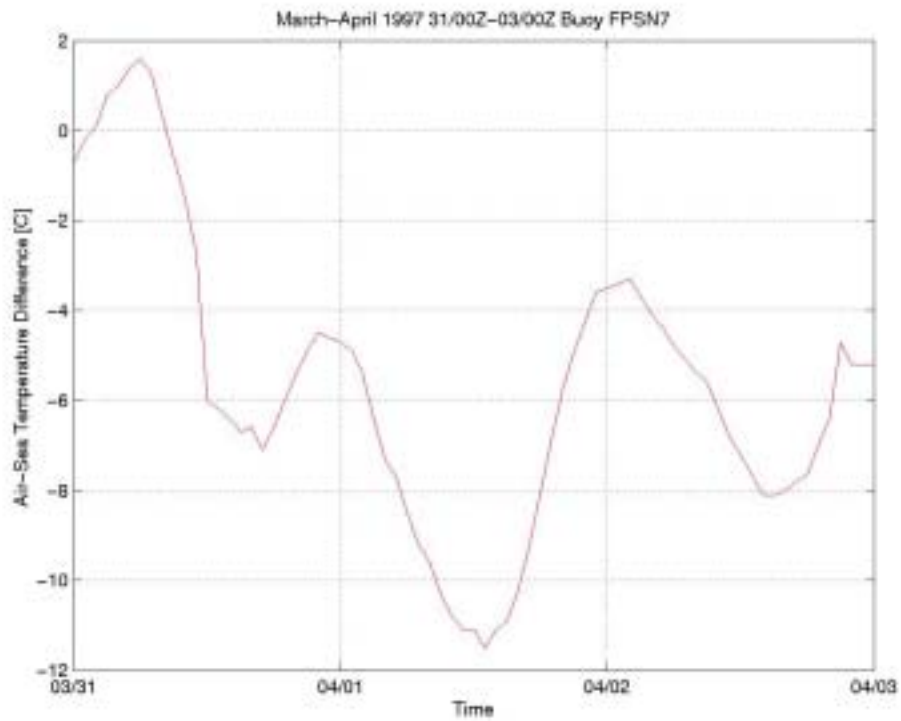
Figure 86. Buoy FPSN7 Air-Sea Temperature Difference
(March-April 1997 31/00Z-03/00Z)

86
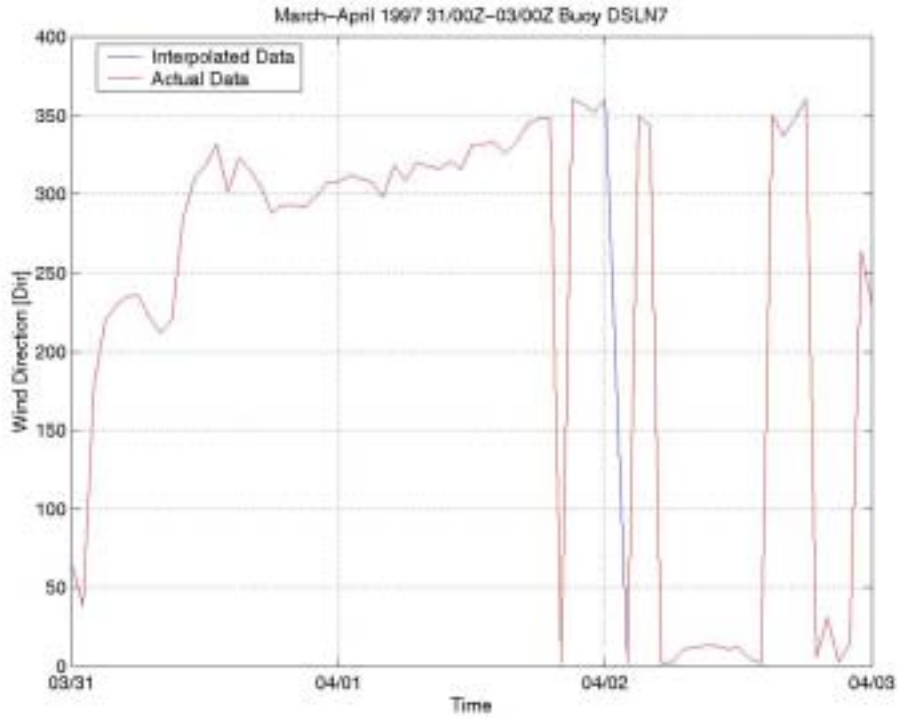
Figure 87. Buoy DSLN7 Wind Direction (March-April 1997 31/00Z-03/00Z)
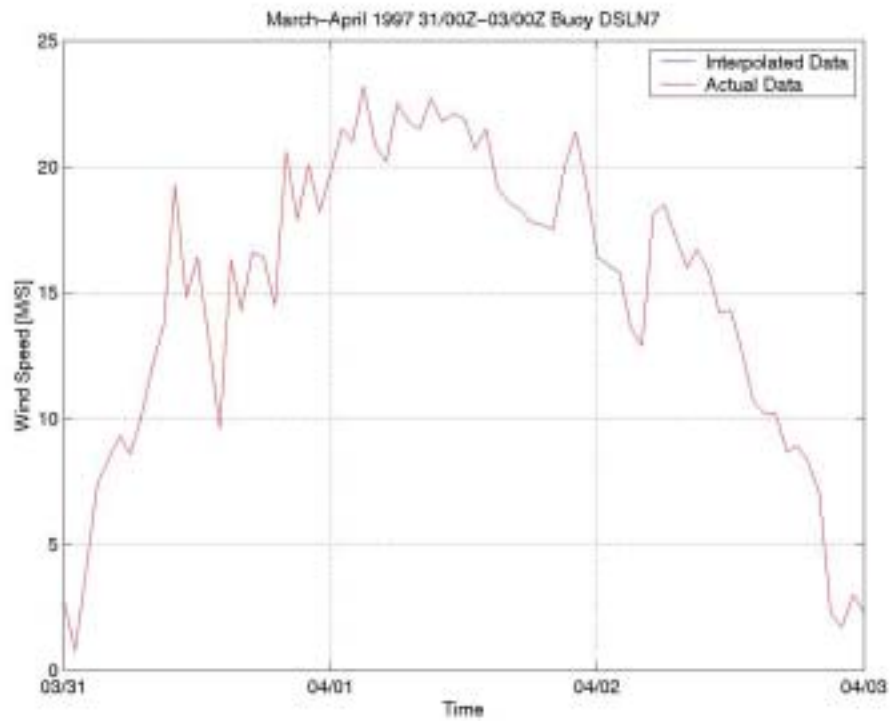
Figure 88. Buoy DSLN7 Wind Speed (March-April 1997 31/00Z-03/00Z)

87
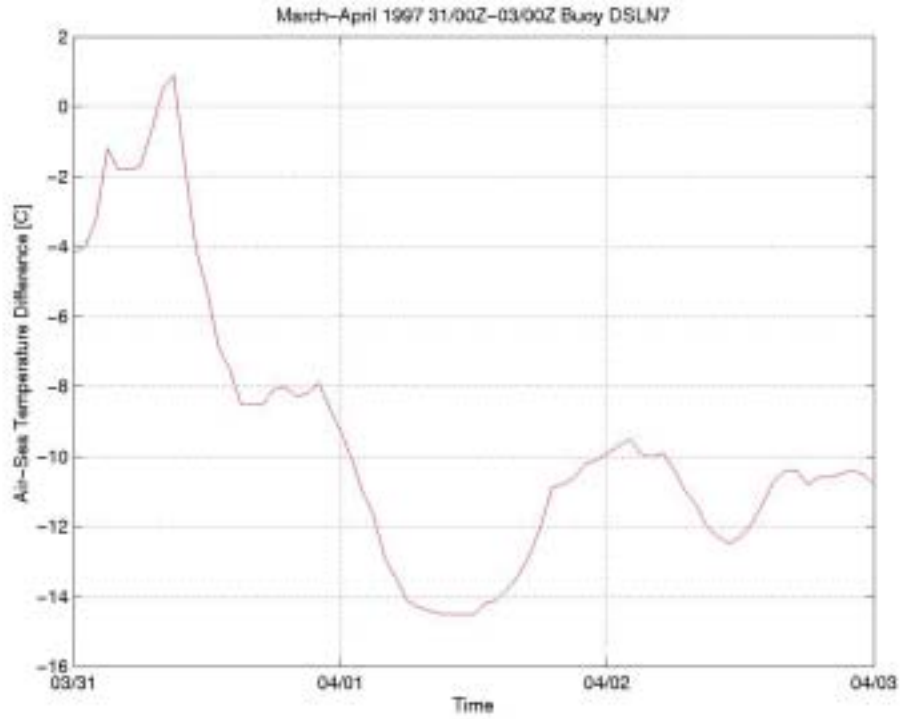
Figure 89. Buoy DSLN7 Air-Sea Temperature Difference
(March-April 1997 31/00Z-03/00Z)
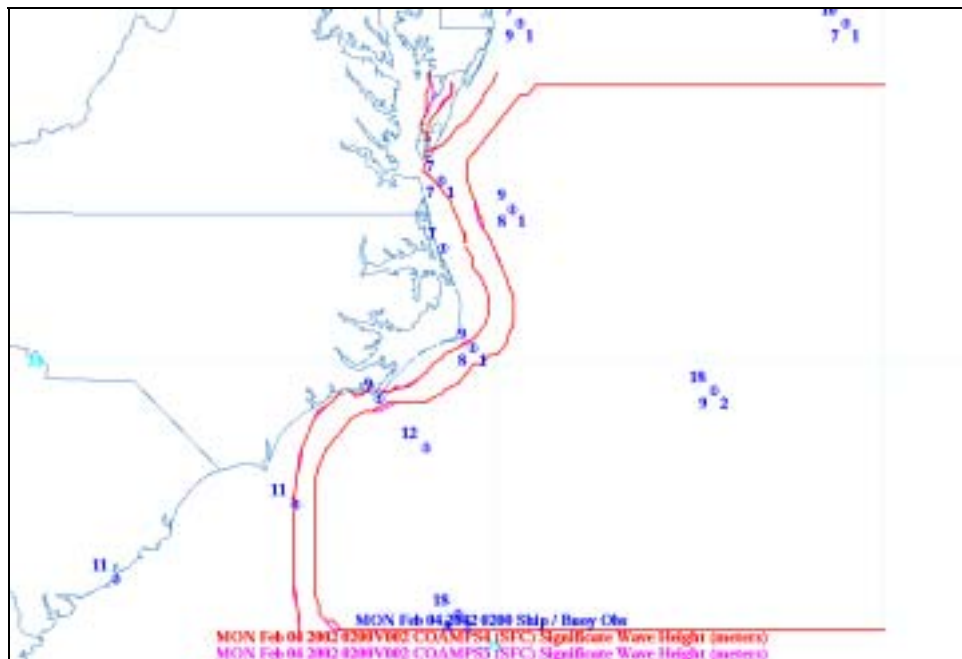
Figure 90. WWIII Significant Wave Height and Observations (February 2002 04/02Z)

88
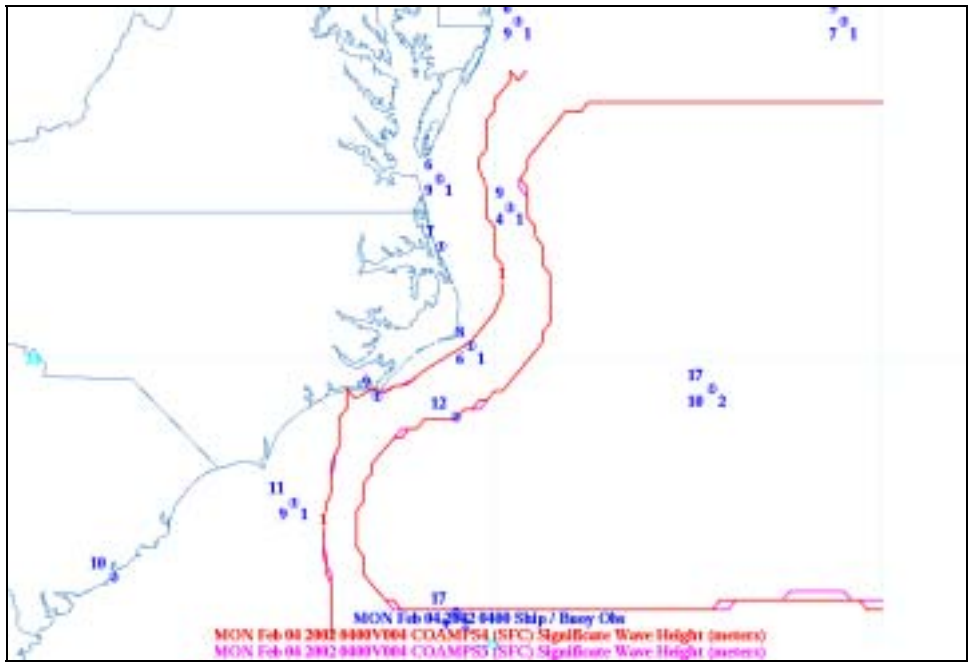
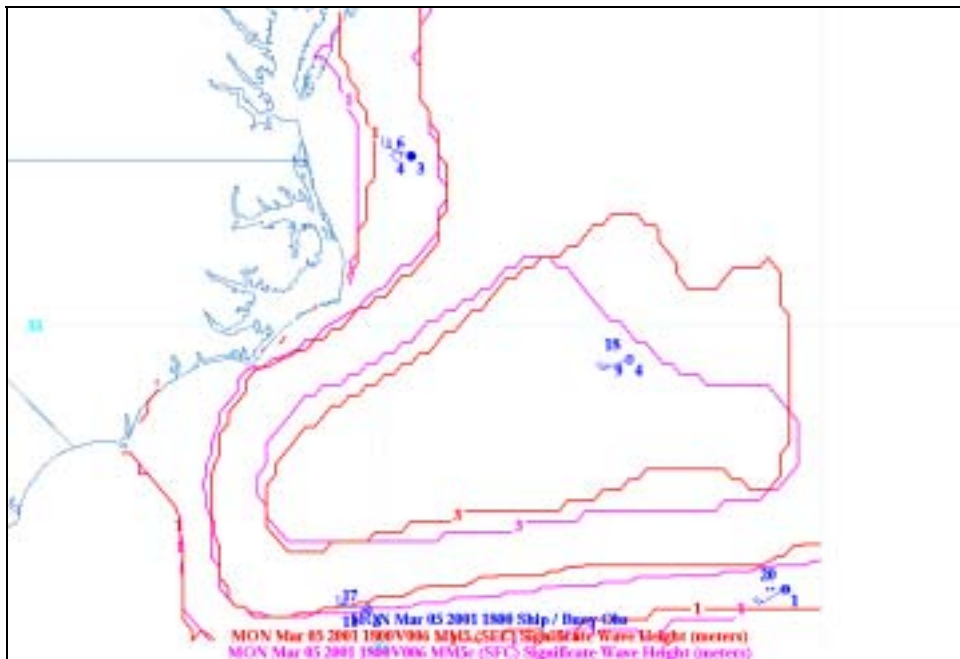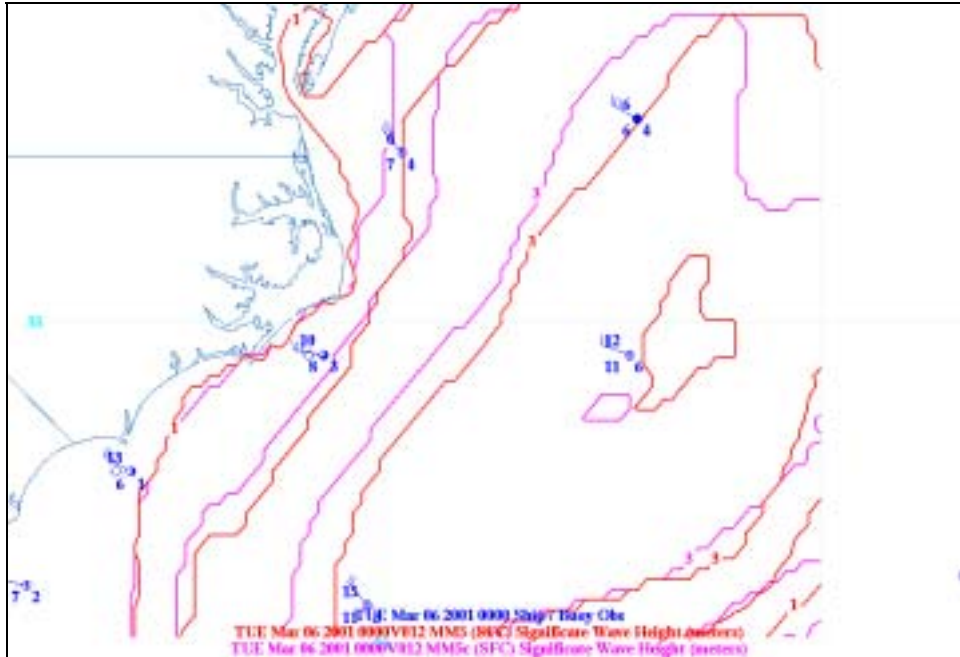Figure 91. WWIII Significant Wave Height and Observations (February 2002 04/04Z)
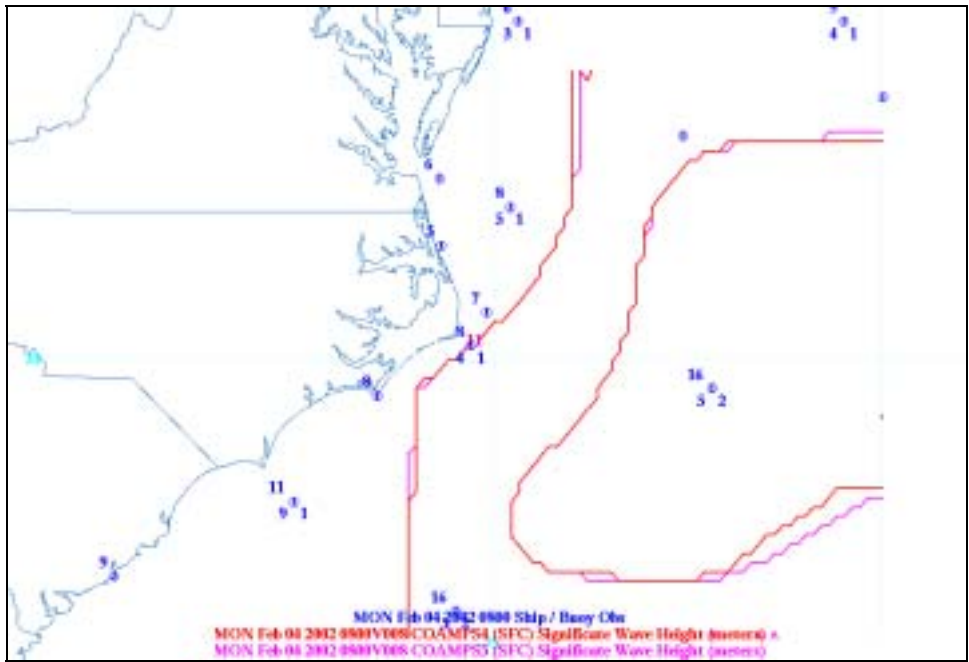
Figure 92. WWIII Significant Wave Height and Observations (February 2002 04/08Z)
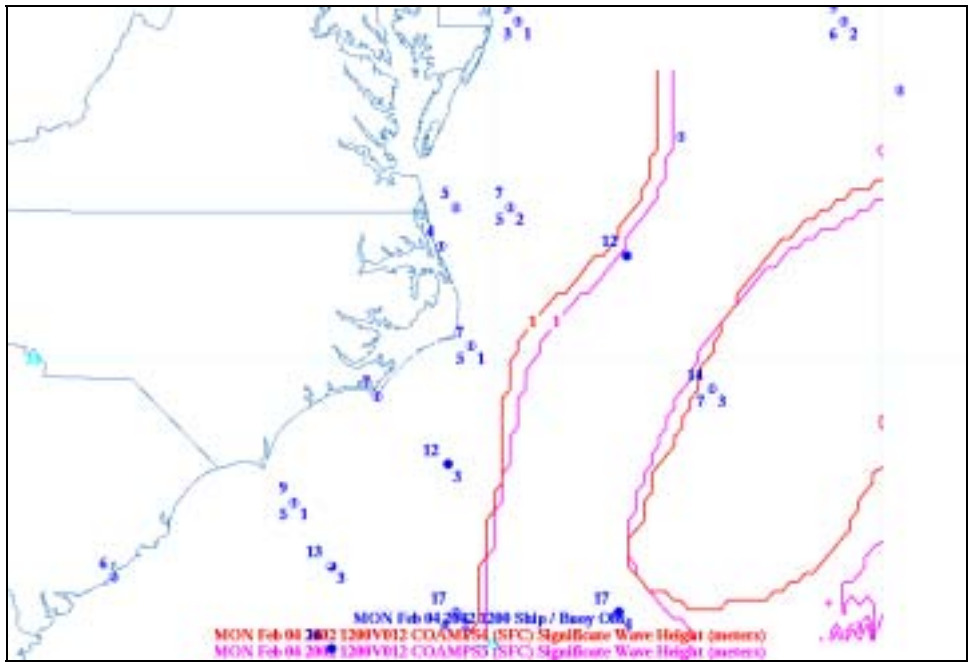
Figure 93. WWIII Significant Wave Height and Observations (February 2002 04/12Z)
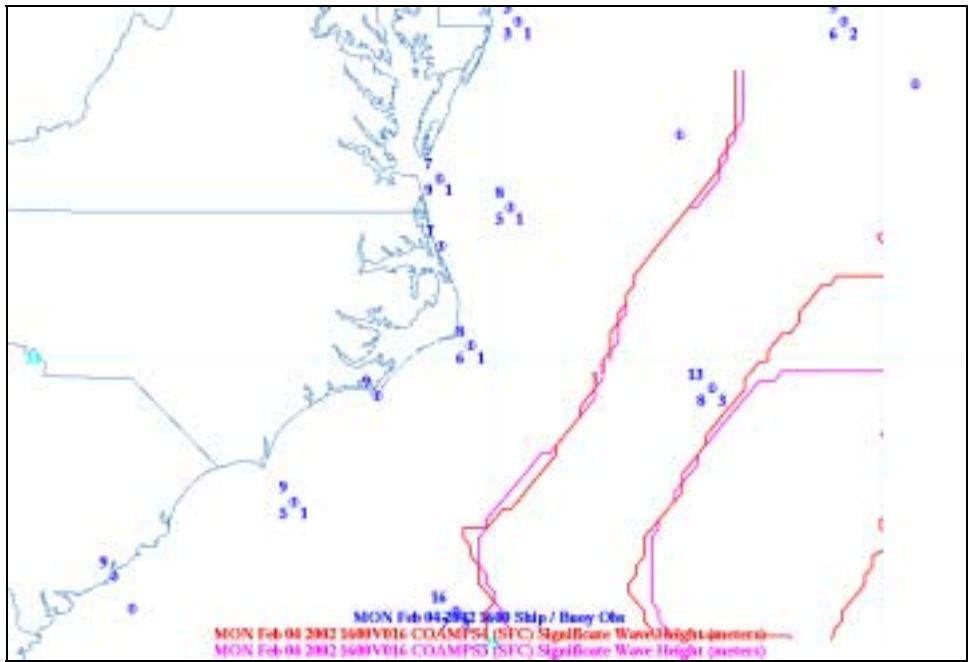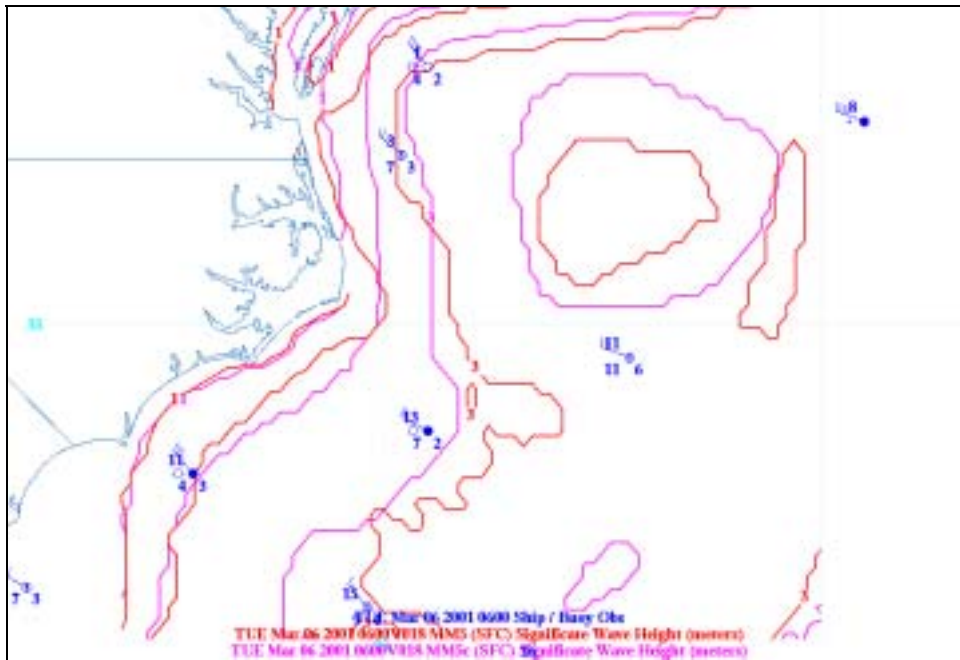

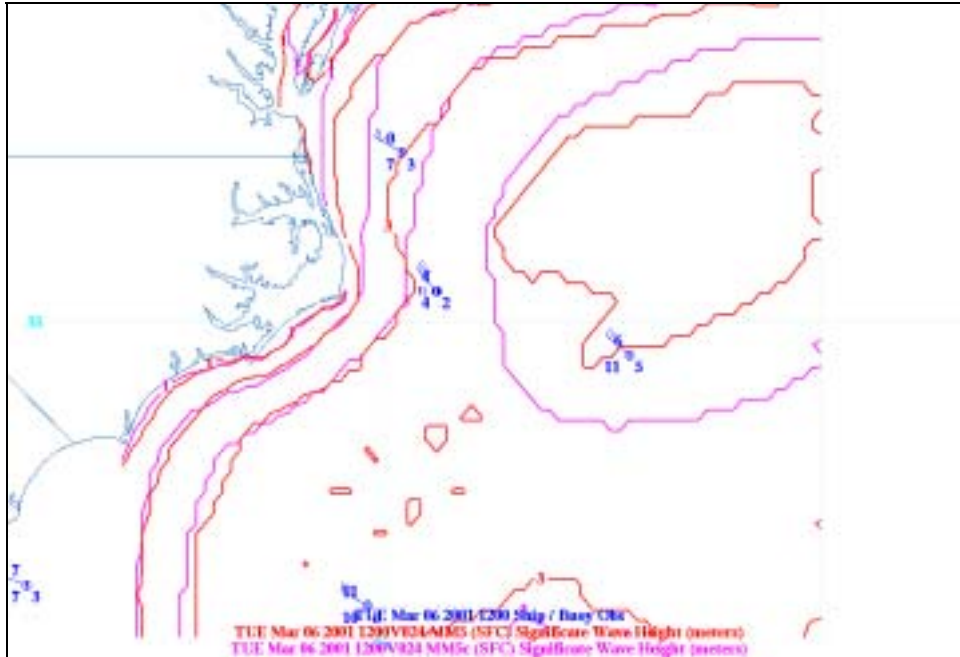Figure 94. WWIII Significant Wave Height and Observations (February 2002 04/16Z)
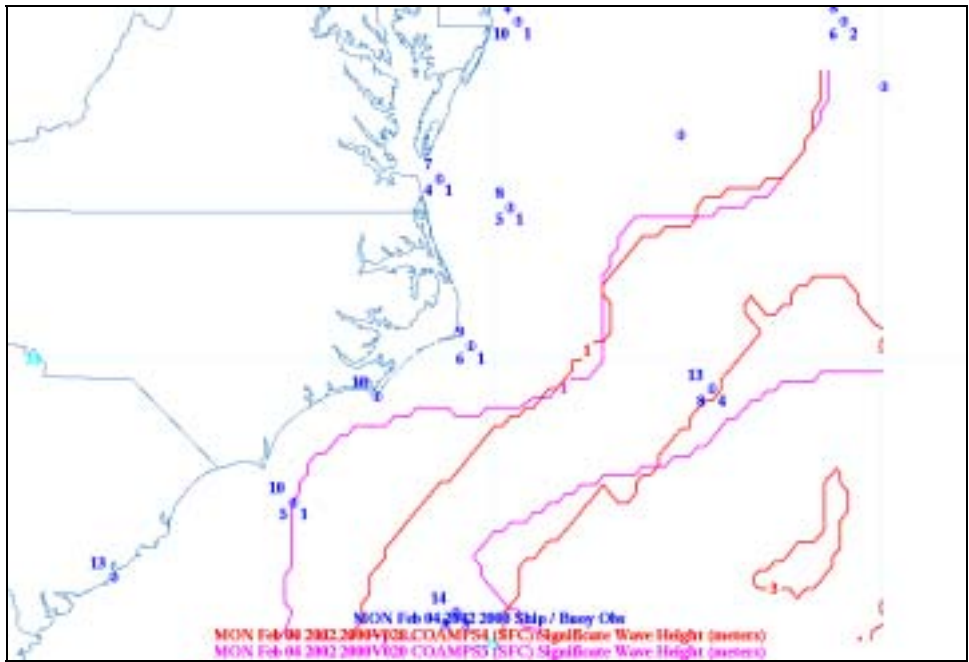
Figure 95. WWIII Significant Wave Height and Observations (February 2002 04/20Z)
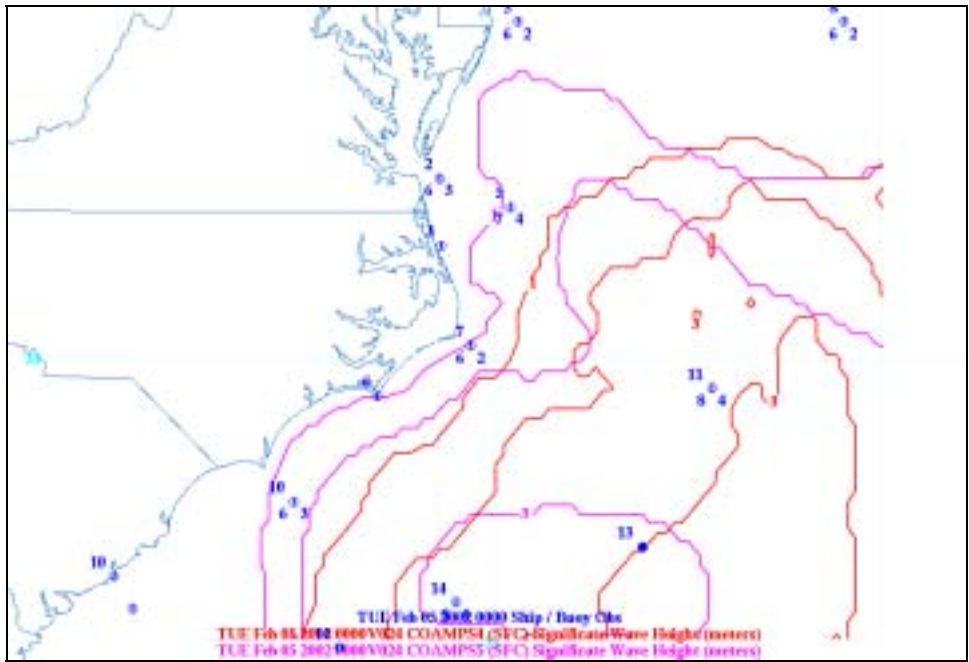
Figure 96. WWIII Significant Wave Height and Observations (February 2002 05/00Z)
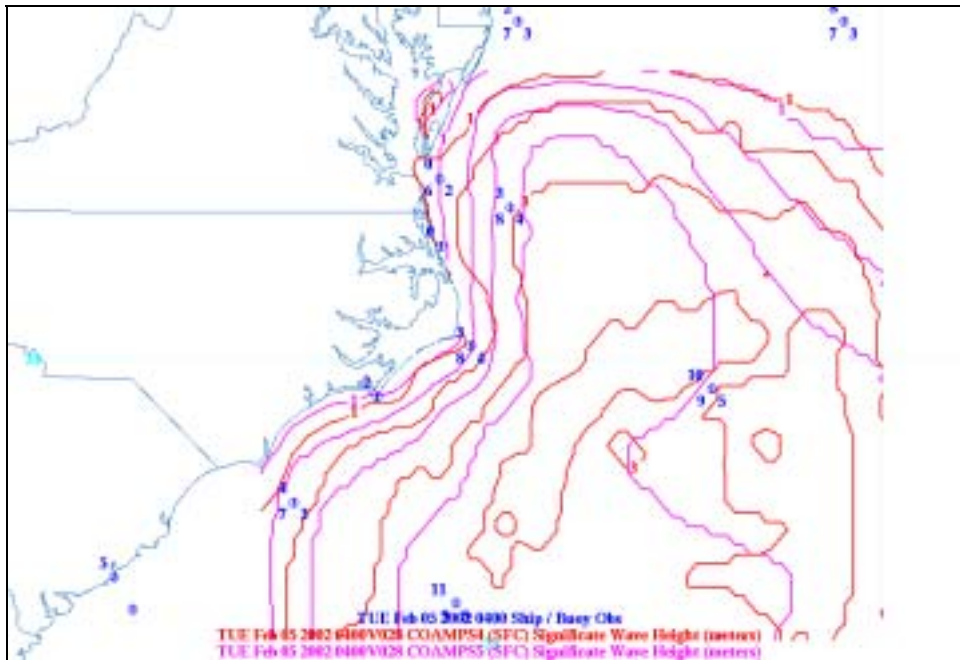
Figure 97. WWIII Significant Wave Height and Observations (February 2002 05/04Z)
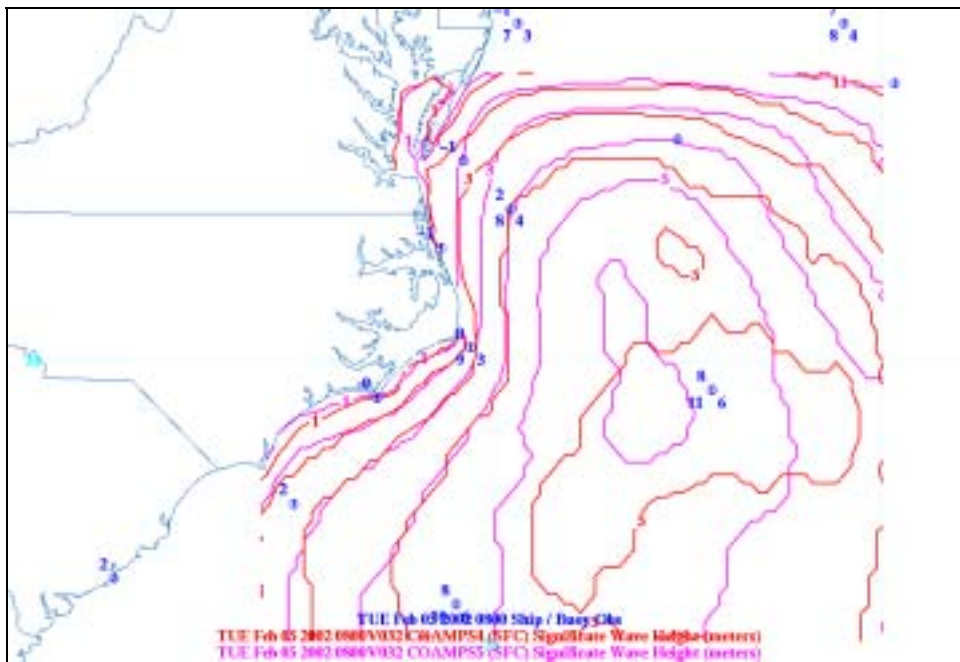
Figure 98. WWIII Significant Wave Height and Observations (February 2002 05/06Z)
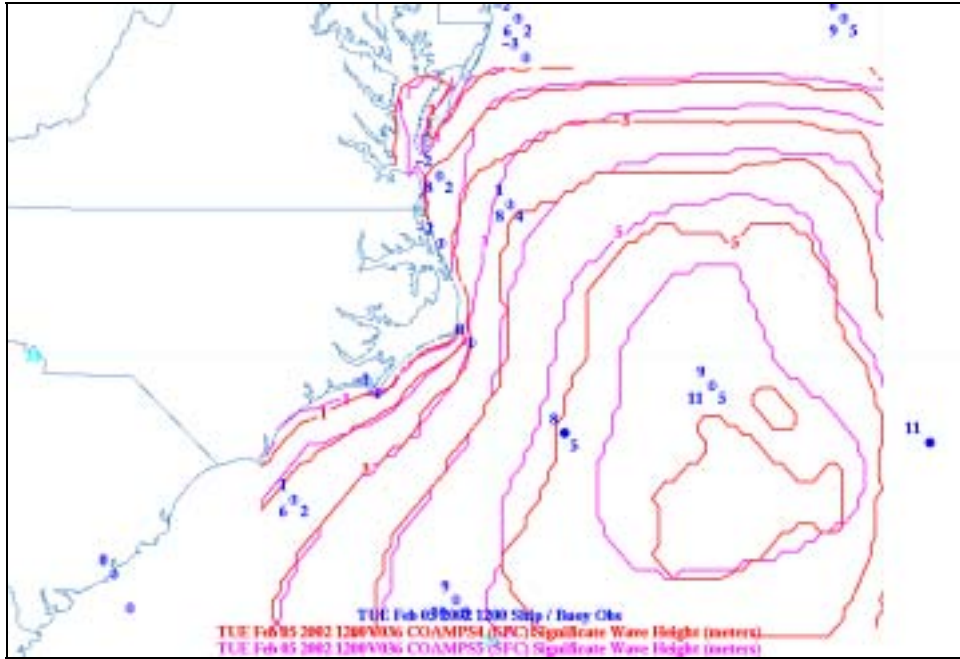
Figure 99. WWIII Significant Wave Height and Observations (February 2002 05/12Z)
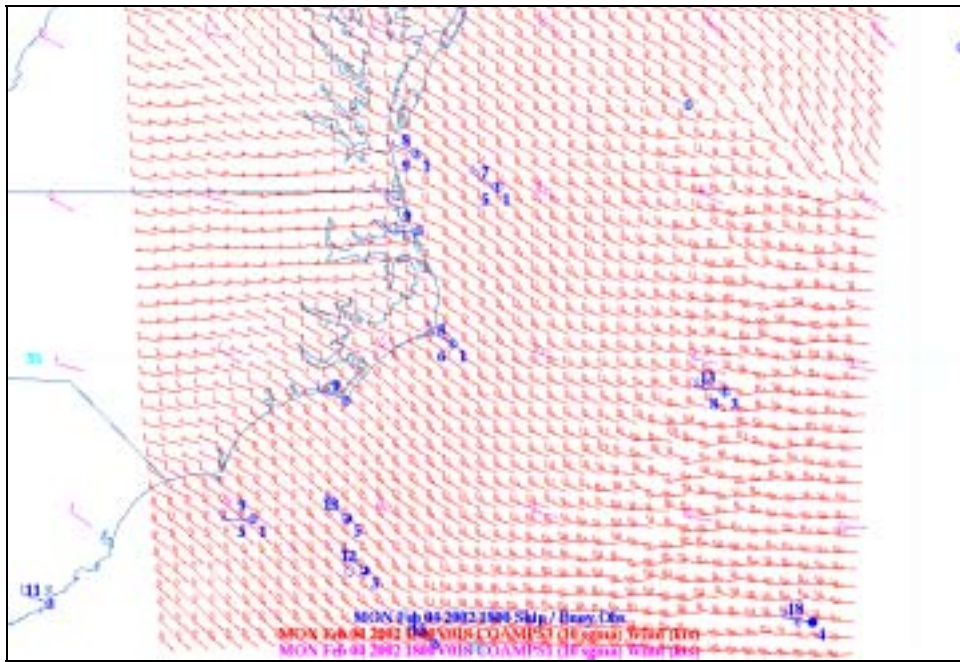
Figure 100. COAMPS 10 Meter Winds and Observations (February 2002 04/18Z)
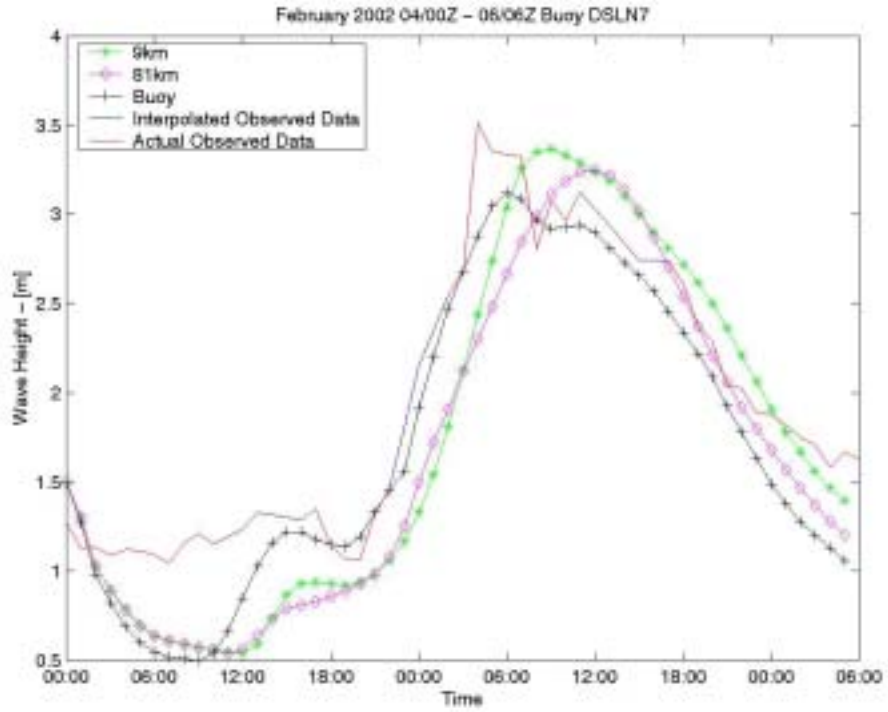
Figure 101. DSLN7 Observed and WWII Significant Wave Height Time Series
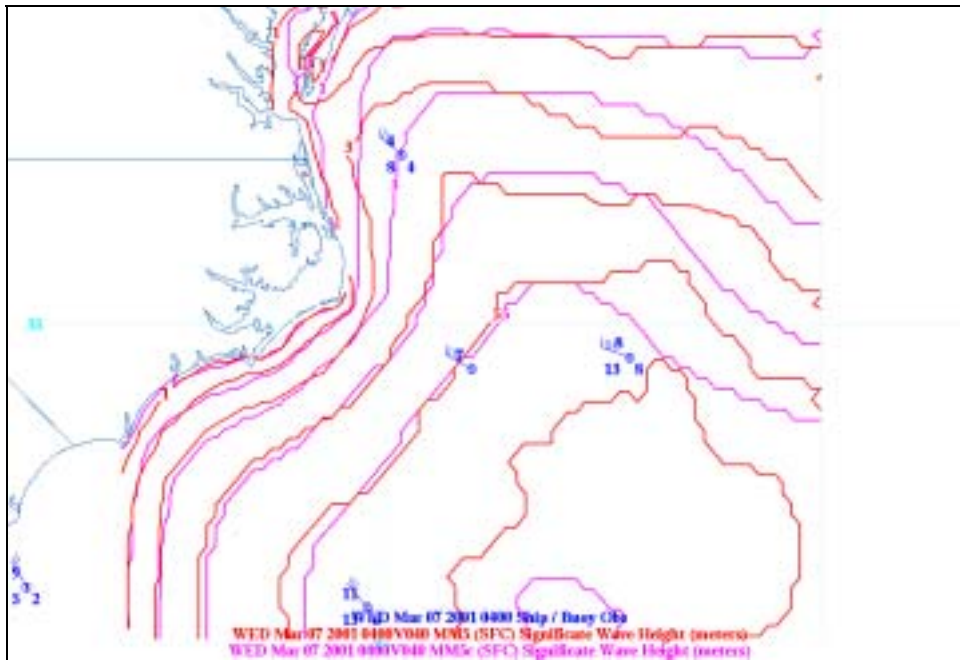(February 2002)

Figure 102. WWIII Significant Wave Height and Observations (March 2001 05/18Z)

94

Figure 103. WWIII Significant Wave Height and Observations (March 2001 06/00Z)

Figure 104. WWIII Significant Wave Height and Observations (March 2001 06/06Z)

Figure 105. WWIII Significant Wave Height and Observations (March 2001 06/12Z)

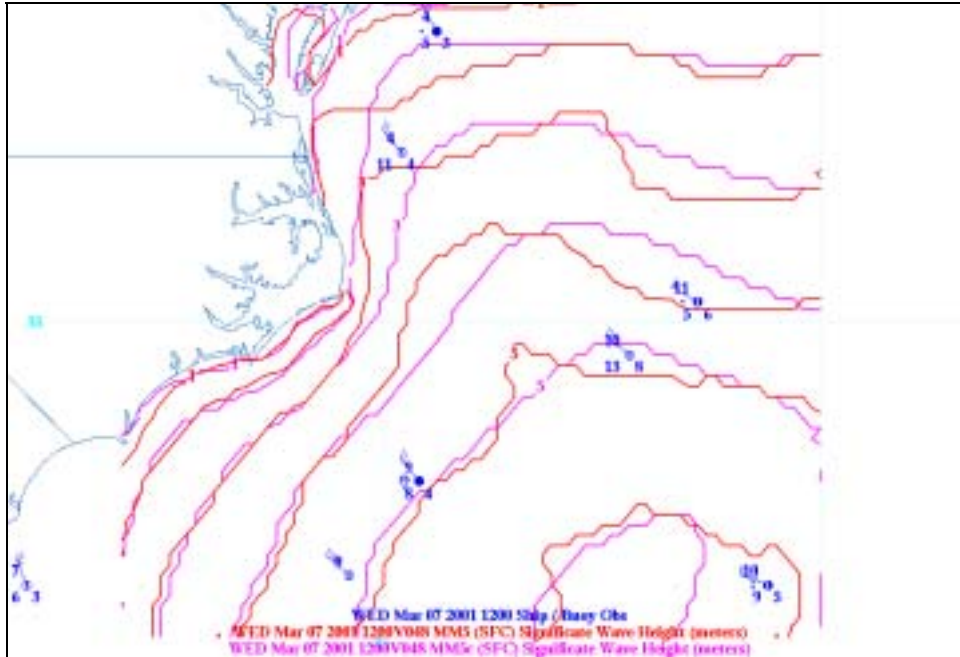Figure 106. WWIII Significant Wave Height and Observations (March 2001 07/04Z)

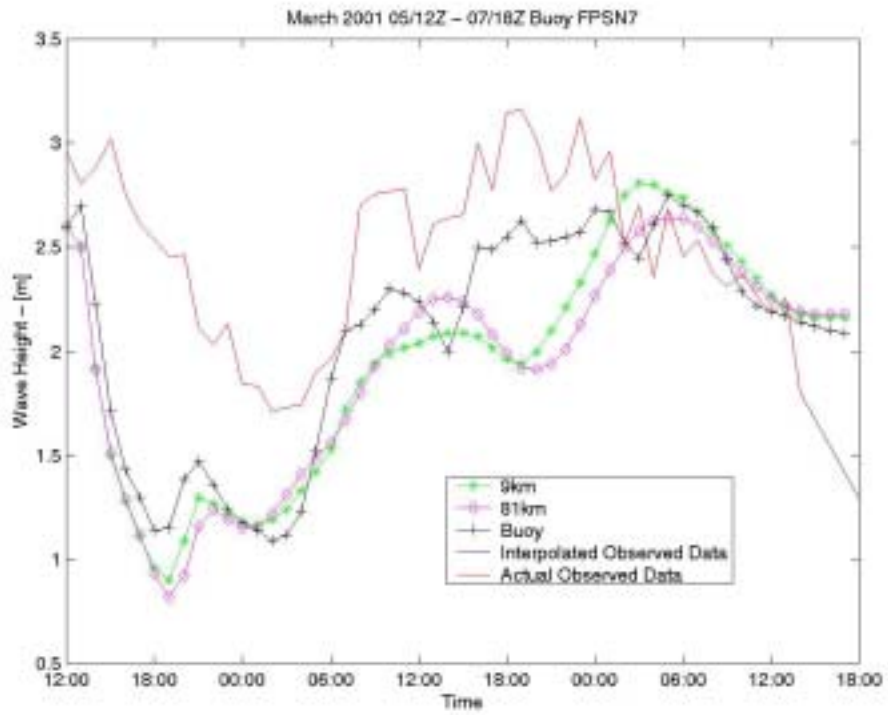Figure 107. WWIII Significant Wave Height and Observations (March 2001 07/12Z)

Figure 108. FPSN7 Observed and WWII Significant Wave Height Time Series
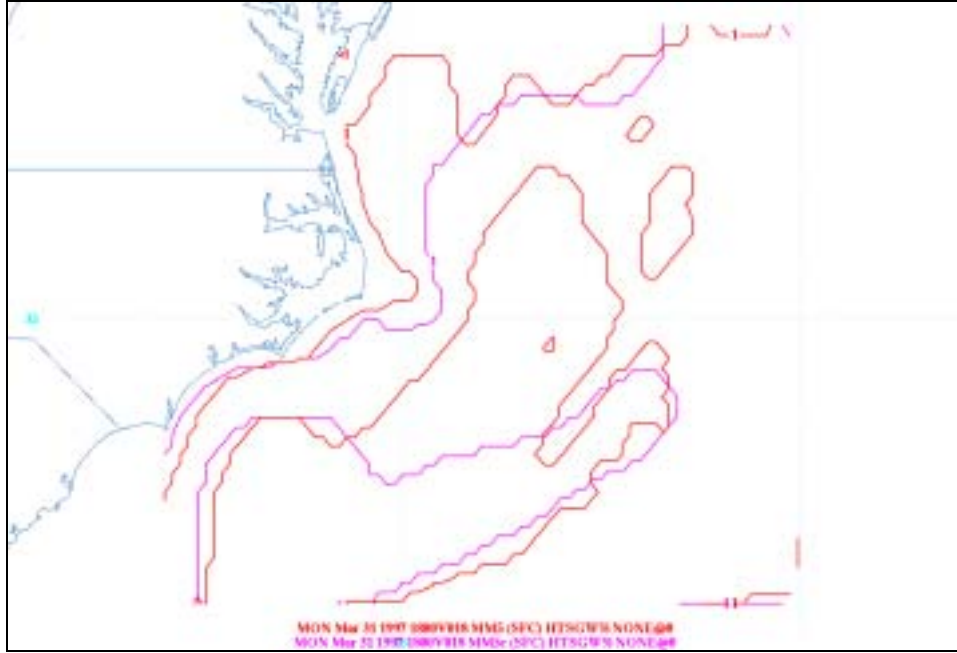(March 2001)

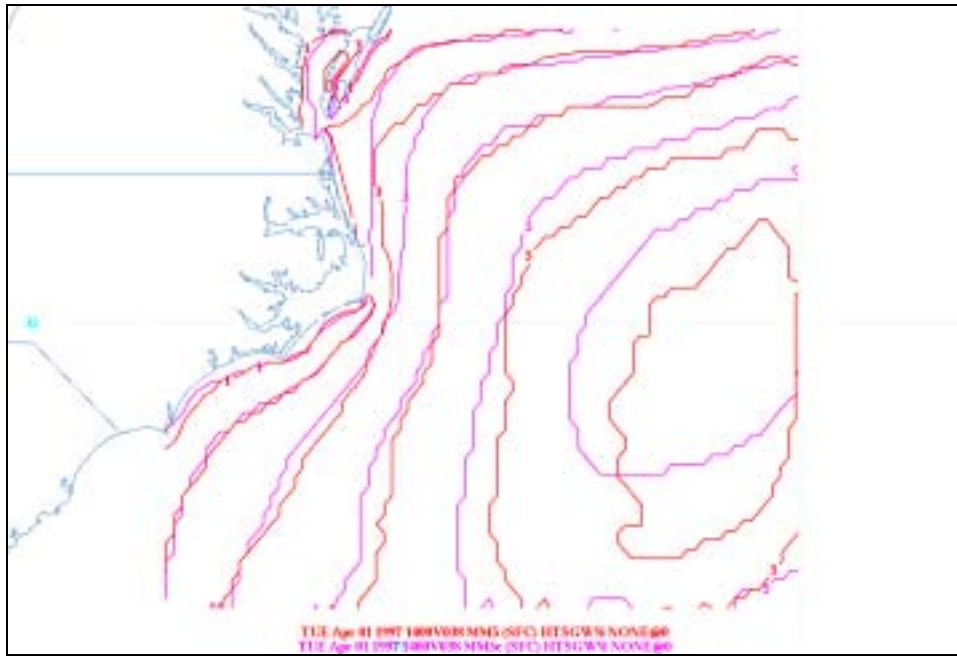Figure 109. WWIII Significant Wave Height and Observations (March 1997 31/18Z)

Figure 110. WWIII Significant Wave Height and Observations (April 1997 01/14Z)
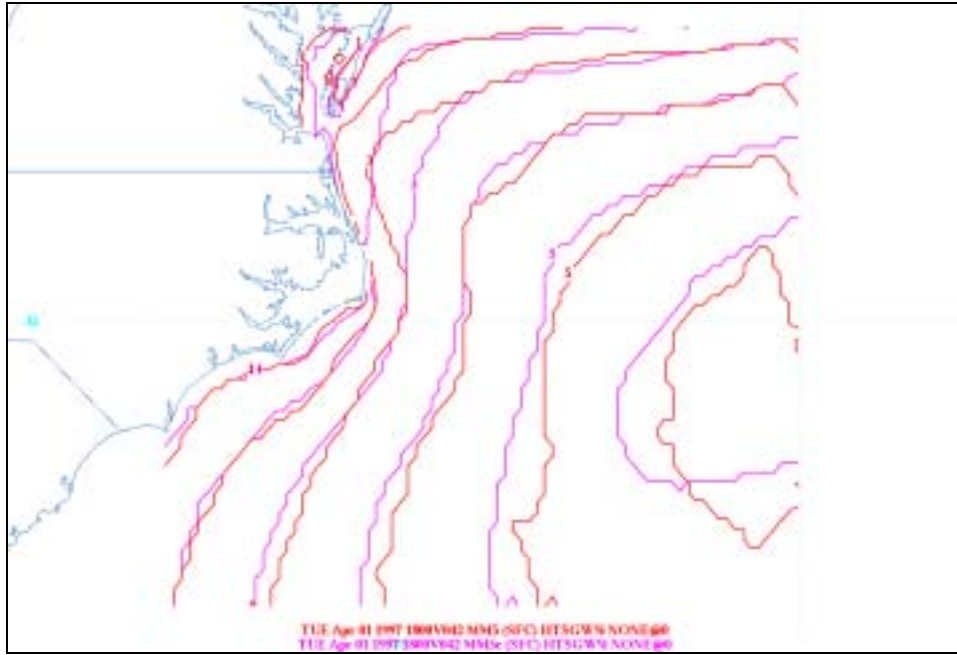
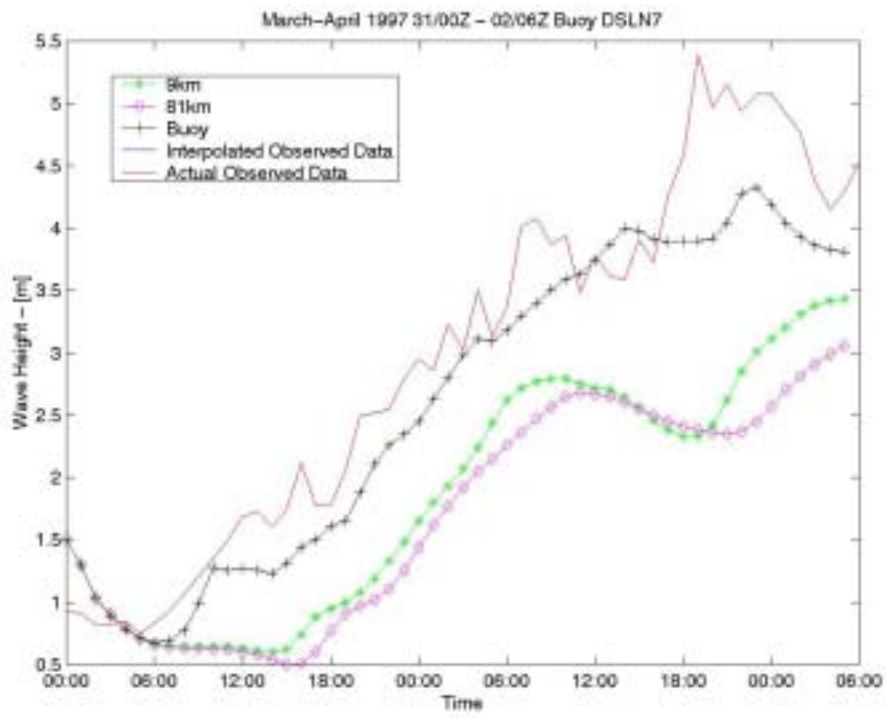Figure 111. WWIII Significant Wave Height and Observations (April 1997 01/18Z)

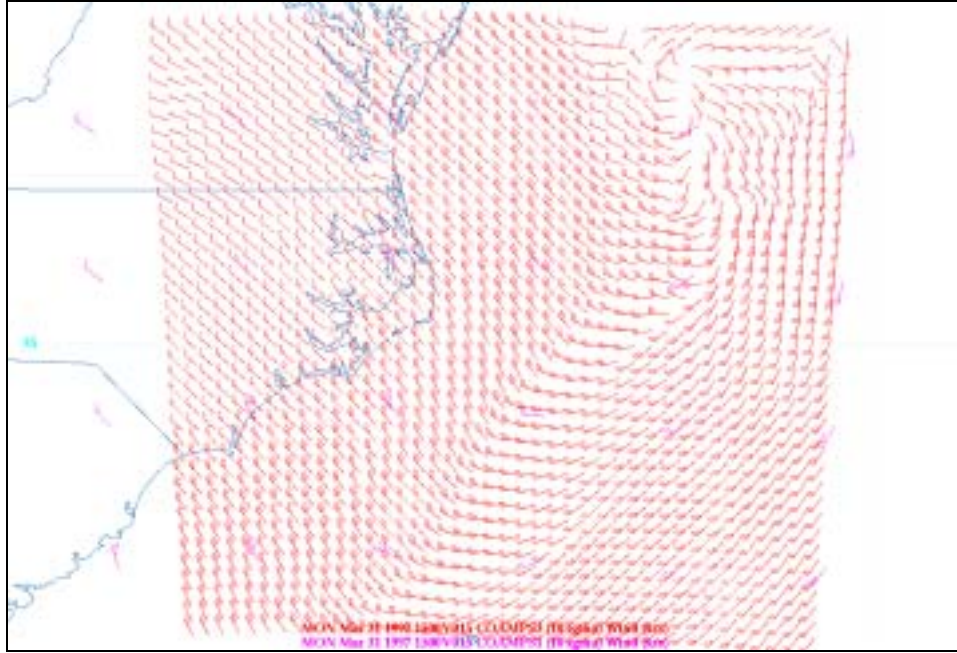Figure 112. DSLN7 Observed and WWII Significant Wave Height Time Series
(March-April 1997)

Figure 113. COAMPS 10 Meter Winds and Observations (March 1997 31/15Z)

LIST OF REFERENCES

Bane, J.M. Jr. and K.E. Osgood: "Wintertime Air-Sea Interaction Processes Across the Gulf Stream". *Journal of Geophysical Research*, v. 94, pp.10, 755-10,772, 15 August 1989.

Grossman, R.L., A.K. Betts, "Air-Sea Interaction during and Extreme Cold Air Outbreak from the Eastern Coast of the United States", *Monthly Weather Review*, v. 118, pp. 324-342, February 1990.

Konrad, C.E. II, S.J. Colucci, "An Examination of Extreme Cold Air Outbreaks over Eastern North America", *Monthly Weather Review*, v. 117, pp. 2687-2700, December 1989.

Vukovich, F.M., J.W. Dunn, and Crissman, B.W., "Aspects of the Evolution of the Marine Boundary Layer during Cold-Air Outbreaks off the Southeast Coast of the United States", *Monthly Weather Review*, v. 119, pp. 2252-2279, September 1991.

THIS PAGE INTENTIONALLY LEFT BLANK

INITIAL DISTRIBUTION LIST

1.   Defense Technical Information Center
        Ft. Belvoir, Virginia

2.   Dudley Knox Library
        Naval Postgraduate School
        Monterey, California

3.   Chairman
        Meteorology Department
        Naval Post Graduate School
        Monterey, California

4.   Dr. Wendell A. Nuss
        Code MR/Nu
        Naval Post Graduate School
        Monterey, California

5.   LCDR David S. Brown
        Code MR/Bd
        Naval Post Graduate School
        Monterey, California

6.   Mr. Robert Creasey
        Code MR/Cy
        Naval Post Graduate School
        Monterey, California

7.   Commanding Officer
        Naval Atlantic Meteorology and Oceanography Command
        Norfolk, Virginia

8.   Commander
        Naval Meteorology and Oceanography Command
        Stennis Space Center, Mississippi

9.   LCDR John A. Okon
        Chesapeake, Virginia